TH Delft

Delft University of Technology

Department of Civil Engineering

EXPERIMENTS ON UNSTEADY SEPARATING FLOW IN AN OPEN CHANNEL

T. Koppel

Report no. 3-81

EXPERIMENTS ON UNSTEADY SEPARATING FLOW IN AN OPEN CHANNEL

T. Koppel *)

*) Tallinn Technical University, U.S.S.R.

Internal Report No. 3-81
Laboratory of Fluid Mechanics
Department of Civil Engineering
Delft University of Technology
Delft, The Netherlands

CONTENTS

		Page
List of symbols		
Summary		
1.	Introduction	1
1.1.	Description of investigation	1
1.2.	Short literature review	3
2.	Experimental Installation and Measuring Technique	4
2.1.	Experimental installation	4
2.2.	Measuring technique	8
2.2.1.	Laser-Doppler measurements	8
2.2.2.	Visualization of the separated flow with dye	14
2.2.3.	Visualization of the flow with small floats	16
2.2.4.	Measurements of the changes in water level	16
3.	Analysis of the Measurements on the Computer	17
3.1.	General aspects of unsteady-flow measurements	17
3.2.	Spectral estimates of turbulence energy	23
3.3.	Statistical distributions	27
3.4.	Calculation of Reynolds stresses	27
3.5.	Computer programs for data processing	28
4.	Results of the Investigation	30
4.1.	Main characteristics of the unsteady separated flow	30
4.1.1.	Visualization of the flow	30
4.1.2.	Float trajectories	39
4.1.3.	Velocity distributions obtained from LDV-measurements	44
4.2.	Turbulence measurements	65
4.3.	Spectral analysis and statistical distributions	86
5.	Conclusions	95
Acknowledgements		95
References		96

List of symbols

A - Cross-sectional area of the flow

E - Turbulence energy

D - Width of the flume

G_u, G_v - Power spectra of the velocities

H - Depth of the flow

F - Focus distance of front lense

L - Length of segment of recording

L_1, L_2 - Tidal length(model and prototype)

L_i - Integral time scale

L_v - Integral length scale

M - Number of recordings in ensemble

N - Number of recordings in arranged velocity arrays

R - Hydraulic radius

Re - Reynolds number

$R(t)$ - Correlation coefficient

S - Distance between laser beams

Sh - Strouhal number

Sk - Coefficient of skewness

T - Half-sine period of the flow

$\overline{U}$ - Time-averaged mean velocity

V_{out} - Tracker output voltage

V_1, V_2 - 45^o velocity components

Q - Flow rate

Q_m - Maximum flow rate

b_o - Diameter of laser beam

b_x - Width of the measuring volume

b_y - Length of the measuring volume

f - Frequency

f_d - Frequency of output of LDV

f_D - Doppler frequency

f_s - Frequency shift

k - Optical constant of the system

l - Tidal wave period

$m_x(t)$ - Time averaged mean value

$\hat{m_x}(t)$ - Ensemble averaged mean value

n - Number of intervals in discrete recordings

n_r - Refractive index of water

t - Time

u,v - Velocity components in flow-direction and in cross-direction

u_o - Instantaneous mean velocity over cross-section of the flume

u',v' - Velocity fluctuations

$\bar{u},\bar{v}$ - Mean velocity components

$\overline{u'v'}$ - Reynolds stress

$x(t)$ - Realisation of the measurements

α,β - Coefficients of linear trend

λ - Laserlight wavelength

λ_L - Micro length scale

ϕ - Angle between laser beams in air

τ - Micro time scale

σ_x^2 - Variance

σ_u,σ_v - Standard deviation of the velocity components

ω - Angular frequency

Summary

Experiments on unsteady separating flow past a sudden expansion in an open channel are described. To simulate tidal flow the flow rate in the approach channel varied as a half-sine with time. Different visualization techniques to obtain an insight into the behaviour of the separating vortex in time and space were used. Laser-Doppler velocimetry (LDV) was employed to measure velocities and turbulence characteristics.

The data obtained from the LDV-measurements was processed on a computer using the ensemble-averaging technique.

Results at different flow rates of the visualization experiments, measured mean-velocity fields, and characteristics of the turbulence - such as intensities, Reynolds stresses and turbulence energy - are shown. Some examples of velocity power-spectra and statistical distributions are presented also. The experiments also provide information about the generation of turbulence related to the separation mechanism and that owing to boundary-layer instability.

1. Introduction

1.1. Description of investigation

The experiments to be described are concerned with unsteady separating flow at a sudden expansion in an open channel. The flow started from rest and then varied as a half-sine with time to simulate a tidal flow (see figs. 2.3 and 2.4). From the literature various investigations related to steady separated flow in an open channel are known, but not too many deal with unsteady separating flow. Mostly unsteady separation investigations are carried out with a solid body moving in a fluid, or with a flow past a solid body.

The experiments were carried out mainly to obtain
- some ideas about what is happening during unsteady separation;
- quantitative information about important flow characteristics for future comparison with theoretical models. With unsteady flow methodical problems arise, especially in turbulent flows, when determining estimates of the quantities involved. One aspect of the present investigation was concerned with the question how to process the experimental results on the computer.

For the measurement of the mean-velocity distributions and various characteristics of the turbulence a two-channel Laser-Doppler velocimeter (LDV) system was used. The measurements were done such that the ensemble-averaging method could be used. To this end the experiments had to be repeated a number of times with the same boundary and initial conditions. To compute the time-dependent mean velocities and turbulence characteristics a set of computer programs was written. The repeatability of the measurements was found to be good and the obtained results should be sufficiently reliable.

Some visualization experiments with dye in the separation region and with floats in the whole channel section near the expansion were carried out also.

It is possible to draw some conclusions from the results about the processes in the flow. In unsteady separating flow we have several phenomena that affect each other in quite a complicated way. The following main features were observed.

First. When the flow starts a separating vortex develops at the protruding corner of the expansion. At small flow rates this vortex is quite stable during the development of the flow (in both accelerating and decelerating phases). When the flow rate is larger several smaller vortices develop inside the large vortex, which affect each other during the flow.
A theoretical model for the large vortex could be of potential-flow type, but modelling the transfer inside this vortex may be difficult.
Second. Generation of turbulence in the boundary layer is not very important as far as the large vortex is concerned. However, in the downstream part it should be considered, because in this part the turbulence intensity is considerable when compared with that resulting from separation. Also the influence of inertia forces on the development of the turbulence should be considered. As we know from other experiments the development of turbulence is suppressed in accelerating flows and amplified in decelerated flows. Also the circulation of the large vortex should decrease the development of turbulence.
Third. Inside the mixing-layer between main flow and separation region we can follow coherent semi-permanent structures, which are now known to be of fundamental interest to describe the turbulent motions.

Next, some critical remarks about the present research will be presented.

The experiments were conducted with a half-tidal flow period. The measurements started with still water in the flume and proceeded with a flow rate in the approach channel according to a half-sine time function until the flow rate had become zero again. After each measurement we had some circulation of the flow in the flume during several minutes. This circulation should have some influence in the next opposite tidal half-period. This effect could not be realized in the experimental set-up available. In a real tidal flow we have always turbulent flow and it is difficult to estimate how the turbulence generated during a half-tidal period influences that in the next one.

Not all experiments planned were actually carried out. Unfortunately, the spectral computations could not be finished and this must be postponed to the future. Also, insufficient information about the turbulence characteristic in some parts of the separating flow was obtained. Furthermore, not all measurement verticals were selected in the best way.

Most results in this report, which are presented in graphical form, need more careful elaboration in the future.

1.2. Short literature review

Only some references related to separated flow are given here. It is quite difficult to find literature on unsteady flow separation in an open channel. Most investigations are concerned with separation at a solid surface, in ducts etc. This kind of research is dealt with by Friehe (1980), Ta Phuoc Loc (1980), Bouard and Contanceau (1980), Bernardinis et al. (1981), Koromilas and Telionis (1980), Graham (1980), Golovkin (1979). Most experiments are carried out with air. Koromilas and Telionis (1980) did experiments also with water. Several references are connected with unsteady separation, such as Disselhorst and Wijngaarden (1979), Bernardinis et al. (1981), Bouard and Contanceau (1980), Ta Phuoc Loc (1980), Koromilas and Telionis (1980), Graham (1980), Golovkin (1980).

Investigation on flow over a step in an open channel was carried out by Restivo and Whitelaw (1978), Etheridge and Kemp (1978), Kim (1980), Mullin (1980), Atkins et al. (1980) Some works are concerned with an expansion in a channel, such as Chedron et al. (1978) and Durst et al. (1974).

2. Experimental Installation and Measuring Technique

2.1 Experimental installation

The experimental part of the investigation was done in the hydraulic set-up shown schematically in fig. 2.1.

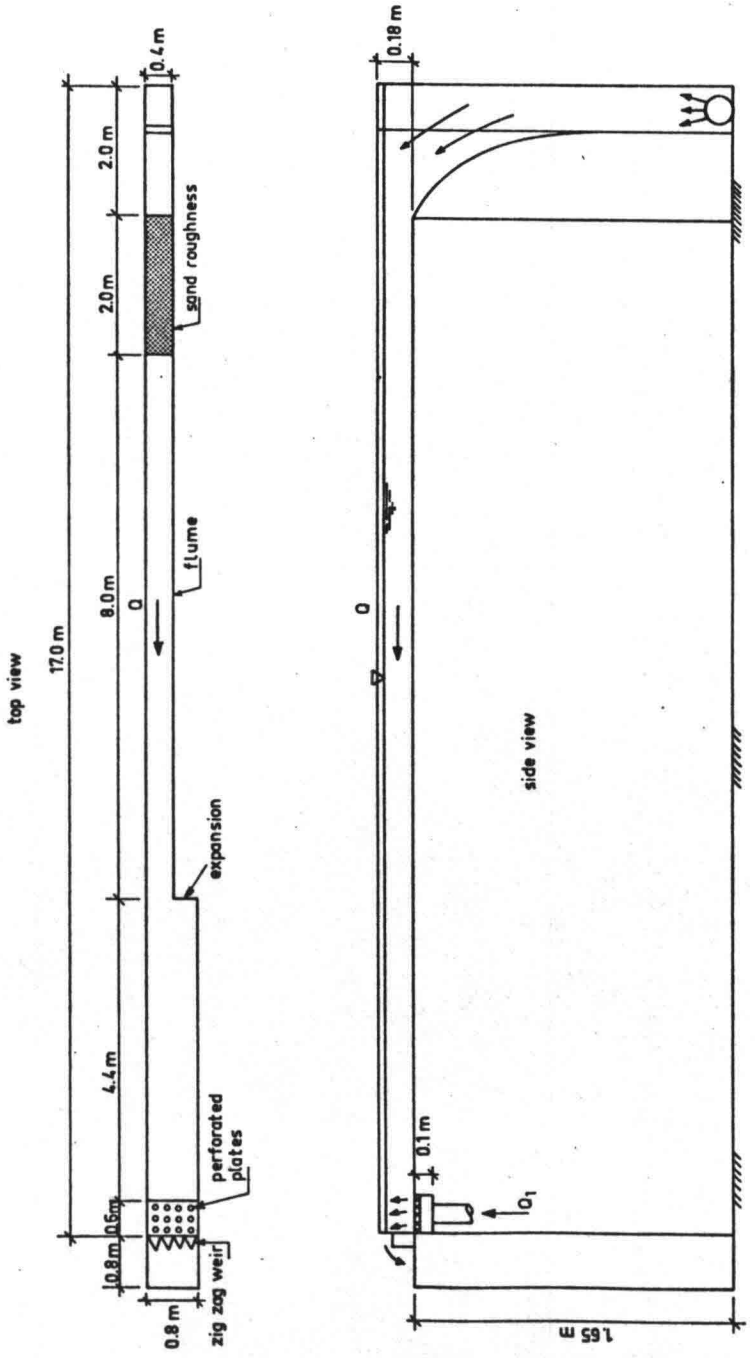

Fig. 2.1. Experimental set-up.

The set-up consists of an open transparent flume (Plexiglass) with an expansion at 10 m downstream from the entrance. Sand was glued in the first two meters of the bottom of the flume for decreasing the hydraulic inlet length of the flume. One important problem in simulating this kind of unsteady flows is the consideration of the possibility of wave reflection at the downstream end of the flume. Reflected waves would influence the velocity distribution in the flume. To avoid the reflection of these (long) waves in the flow a distributed-inflow system (Q_1 = 16 1/s) was built in the downstream end of the flume together with a weir (height 0.07 m. developed length 2.8 m).
A photo of the experimental set-up is given in the fig. 2.2.

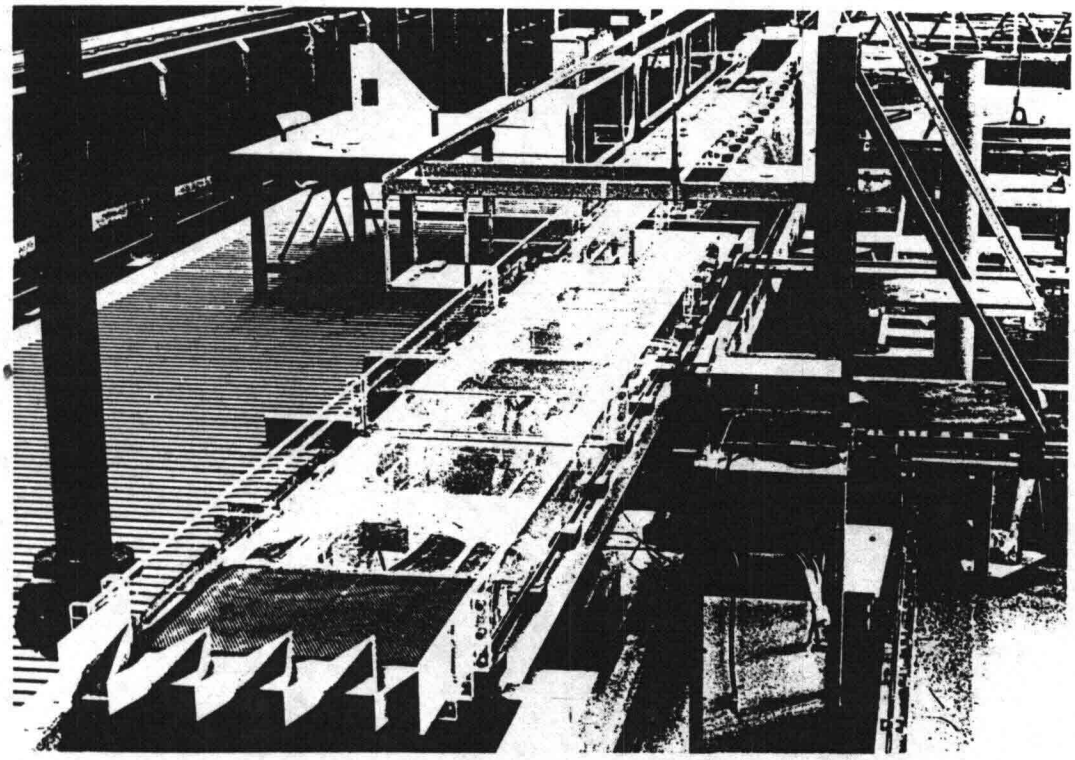

Fig. 2.2. View of the experimental set-up.

Unsteadyness of the flow was obtained by a control-system consisting of data-track programmer (R.I. Controls, U.S.A.), electromagnetical flowmeter (Fox boro model 696) and motor-driven valve. With the data-track it was possible to prescribe a desired discharge-time relationship.
Two half-sine time functions used are drawn in fig. 2.3. Some other half-sine functions were used for visualization experiments.

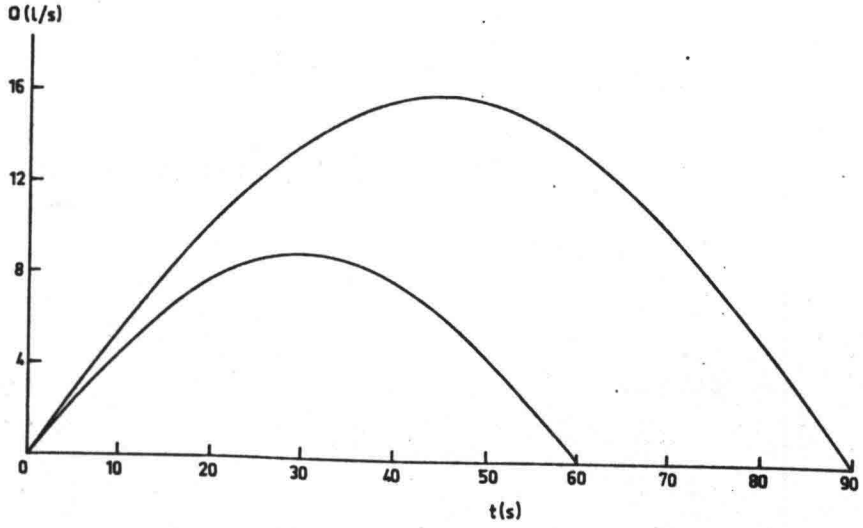

Fig. 2.3. Flow rates as functions of time measured with electromagnetical flowmeter.

The flow was measured automatically by the electromagnetical flowmeter, and a feedback system including the data-track controlled the electromotor opening or closing the valve. The flow-rates in the experiments were derived from prototype tidal flow parameters using the Strouhal criterion (fig. 2.4.):

$$Sh = \left(\frac{L_1}{U_{m_1} T_1} \right)_{model} = \left(\frac{L_2}{U_{m_2} \cdot T_2} \right)_{prototype} \qquad (2.1)$$

where prototype parameters are, for example, L_2 = 1000 m, U_{m_2} = 0.5 m/s, T_2 = 20,000 s.

In this case we have for the prototype $Sh_2 = 0.1$.

For the model L_1 = 0.4 m, and when T_1 = 60 s we have U_{m_1} = 0.07 m/s.

The Reynolds number calculated from U_{m_1} and hydraulic radius of the flume R (when H = 0.109 m, D = 0.4 m) is

$$Re_1 = \frac{U_{m_1} \cdot R}{\nu} = 4900 \qquad (2.2)$$

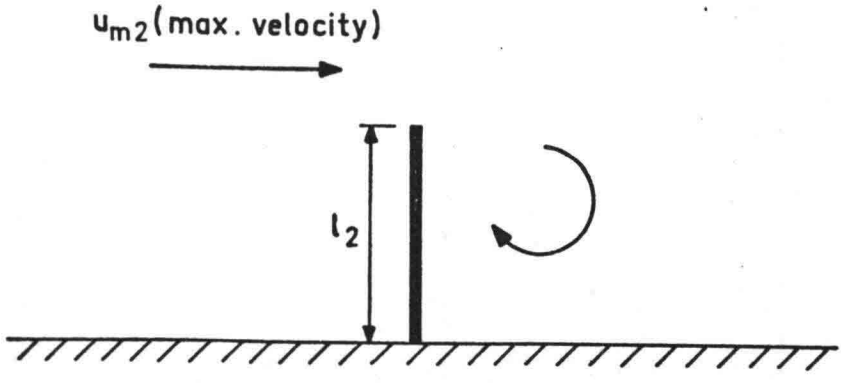

Fig. 2.4. Tidal flow separation.

For practical purposes, the transitional range of Re in steady open channel flow can be assumed to be 500 to 2000 (Ven Te Chow, 1959). It is well known that in unsteady flow the critical Reynolds number differs considerably from steady-flow values. In a hydraulically smooth pipe the critical Reynolds number for accelerated flow can be 100 times greater than the steady-flow value (Koppel and Liiv, 1977).

We should consider also the fact that in practical situations the prototype has a rough bottom generating a higher intensity of the turbulence in the boundary layer than that in a smooth-bottom model. Considering all previously mentioned facts it seems reasonable to increase the maximum velocity to have higher turbulence intensities in the flow.
The maximum flow rate was Q = 16 l/s (Re_1 = 25700, see fig. 2.3.).
The water depth in the flume before the flow started was H = 10.9 cm.

The measurements were time-consuming, because after every experiment it was necessary to wait 8 to 10 minutes to have again still water in the flume.

2.2 Measuring technique

The measurements in this work can be grouped as follows:

- measurement of the main characteristics of the flow using Laser-Doppler Velocimetry (velocities, Reynolds stresses etc.);
- visualization of the flow using dye for estimates in the separated region;
- visualization of the flow using small floats to obtain estimates of the trajectories of water particles (especially movement of vortices inside the separated region);
- measurements of the changes of the water level during unsteady flow.

A short description of these measurements will be given in the following sections.

2.2.1. Laser-Doppler measurements

In recent years the Laser-Doppler Velocimeter (LDV) has become a frequently used measurement system in experimental fluid mechanics. LDV has several advantages when compared with thermoanemometer systems:

- probes disturbing the flow are absent;
- temperature effects are absent;
- contamination problems do not exist.

These advantages are important in various fluid mechanics measurements. Nowadays several LDV systems have been developed to measure the Doppler frequency from moving particles in the flow. Different systems are described by Godefroy (1978), Durst et al.(1976), Jönsson (1974) and in DFC Proceedings (1978). The choice between the different systems depends on the type of measurements.

When applying LDV to the measurement of the velocity field in unsteady flow several problems arise. In some reports in Dynamic Flow Conference (1978), such as (Orloff, 1978) and (Buchhave,1978) only some difficulties which can arise in unsteady flow measurements are considered (required seed-particle density, particle flow tracing fidelity, optical diffraction limitations etc..).

Buchhave (1978) gives a power spectrum measured with different instruments (fig. 2.5 : 1 - correct spectrum; 2 - LDV tracker (ambiguity noise); 3 - LDV counter analog (drop-out noise); 4 - hot-wire (wire length attenuation).

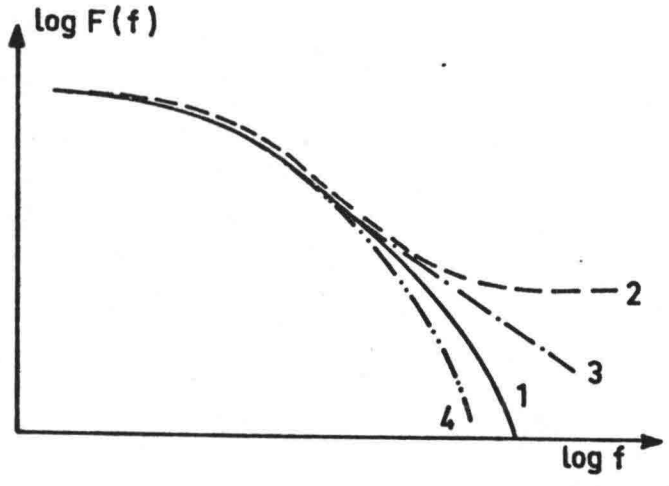

Fig. 2.5. Power spectrum measured with different instruments.

As we can see from this figure, different instruments produce different deviations from the correct spectrum at higher frequencies. In the LDV measurements these deviations are caused by ambiguity noise or drop-out noise. Ambiguity problems are considered in TPD rapport (1977) and by Berman and Dunning(1973), and Jönsson (1974) ; problems connected with particle sizing are considered by Thomson and Stevenson (1979), Orloff (1978) and Jönsson (1974).

To detect the velocity direction in unsteady flow measurements, optical frequency shifting is used. This implies addition of the carrier frequency f_s to the Doppler shift: $f_d = f_D + f_s$. The shift allows detection of the flow direction and increases the measurement dynamic range of the velocity fluctuations (Edwards et al, 1968). For the generation of the frequency shift the Brag cell is most suitable, because in this case no change occurs in the basic optical parameters of the laser beam.
The Brag cell allows stable, controlled, variable shift of the Doppler frequency over a wide range of frequencies.
In the present research the main characteristics of the flow were measured with the TPD-1077/2M LDV. It is a two-channel tracker type anemometer. For generating the frequency shift a grating disk is used (also as a beam splitter), which does not have a very stable shift mainly because the speed of the driving motor is not stable. During the experiments it was therefore necessary to check the frequency shift and to correct the calibration line.

As all flow parameters were changing in time, it was impossible to use time averaging. Therefore the experimental data concerning turbulence estimates was recorded to be processed afterwards on the computer. A block-scheme of the LDV - measurements is given in fig. 2.6.

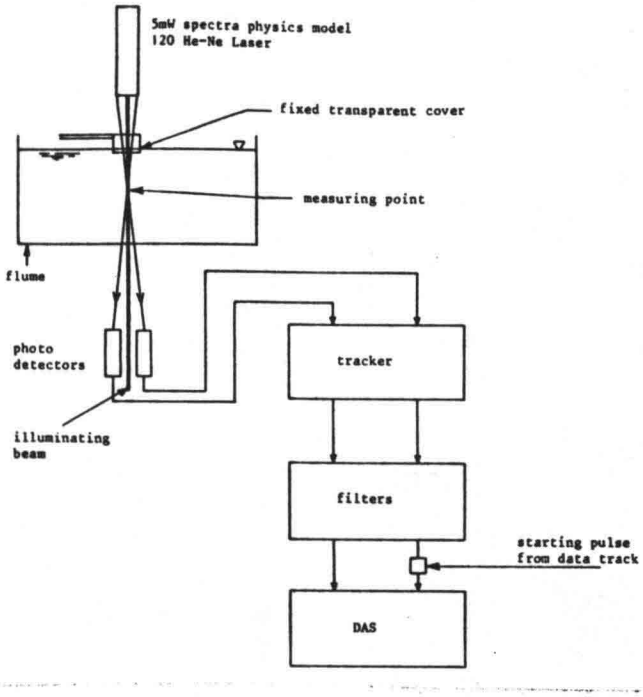

Fig. 2.6. Block-scheme of LDV-measurements.

The arrangement shown is a forward-scatter orthogonal two-component reference-beam mode. Using this configuration of the system two orthogonal horizontal components of the velocity can be measured. Photodetectors are used to collect the light of the reference beams.
Estimates of the energy spectrum of the turbulence by discrete sampling of the data is possible provided aliasing effects are avoided by pre-filtering the signals. To cut off the frequencies above the Nyquist frequency, Butterworth type filters from Rockland Systems Corporation (model 452 Dual HI/LO Filters) were used. Before unsteady-flow measurements were done, some preliminary steady-flow measurements were carried out to have some idea about dominating turbulence frequencies and to fix the sampling frequency. The spectra were estimated using a spectrum analyser. Dominating frequencies were less than 20 Hz. To avoid aliasing effects unsteady-flow recordings were done with a frequency of 50 Hz. The filters were used as low-pass filters with a cut off frequency of 25 Hz. Most of the measurements were recorded on magnetic tape using a Data Acquisition System (DAS).

A starting pulse from the data-track was added to one channel signal at the moment when the electromagnetical flowmeter was registering the start of the flow. This pulse was necessary in the computer processing of the results as a starting point in the ensemble-averaging process.
To make use of the great accuracy of DAS, signals were amplified up to 50 times before recording. DAS has 16383 quantization levels (plus the same for negative signals) which gives the one side recording accuracy as 0.0061 %.
The transparent cover (fig. 2.6.) was needed to avoid deflexion of the laser beams at the fluctuating free surface. The cover has some influence on the velocity distribution near the free surface, especially because the water level was varying during the unsteady flow. This imposes some restrictions to the velocity measurements close to the free surface.

Measurements were done with the reference-beam mode, which is convenient for two-dimensional turbulent-flow measurements (TPD Rapport, 1977; Chatterton, 1969). Two beam configurations for turbulence measurements are recommended (TPD Rapport, 1977), direct and indirect 45^{o} velocity components measurements. The advantage of 45^{o} measurements is that drop-out mistakes are reduced (especially for $\overline{uv}$ determinations).
The direct measurement gives correct results only if the drop-outs in both channels are fully correlated. The indirect 45^{o} method is also useful in the following situations:

- two-component measurements near a flow boundary;
- if the optical frequency cannot be used;
- if no correlator or computer is available to determine the cross product $\overline{uv}$ directly. The following relations between V_1, V_2 and u and v hold (fig. 2.7.) (TPD Rapport, 1977):

$$V_1 = (u + v) / \sqrt{2} \qquad (2.3)$$

$$V_2 = (u - v) / \sqrt{2} \qquad (2.4)$$

$$u = (V_1 + V_2) / \sqrt{2} \qquad (2.5)$$

$$v = (V_1 - V_2) / \sqrt{2} \qquad (2.6)$$

$$2\overline{uv} = (V_1 - V_2)(V_1 + V_2) \qquad (2.7)$$

$$2\overline{uv} = \overline{V_1^2} - \overline{V_2^2} \qquad (2.8)$$

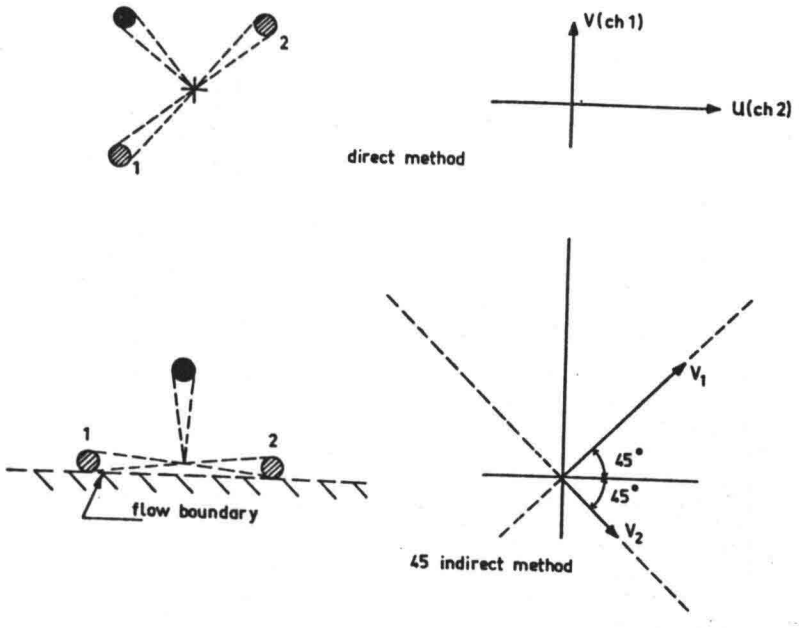

Fig. 2.7. Beam configurations in direct and indirect 45° measurements.

In the present experiments the beam configuration for direct velocity component measurements was chosen to reduce the number of calculation steps. In the 45° indirect measurements, the velocity components u and v will be computed from nearly equal values of V_1 and V_2. Subtracting these values can introduce relatively large errors. In the first measurements carried out to check the programs, some recordings also with the 45° method were done.

The calibration line is calculated from the following parameters (one optical system):

- focus distance of front lense — F = 242.5 mm
- distance between laser beams — S = 29,6 mm
- laser light wavelength — λ = 632.8 nm
- angle between laser beams in air

  $\tan \phi/2 = \frac{1}{2} S/F = 0.061$ rad ($\phi = 6.985^{\circ}$) (2.9)
- optical constant of the system

  $K = \frac{2 \sin (\phi/2)}{\lambda} = 192.5$ kHz/ m s^{-1} (2.10)
- the tracker constant = $\frac{1}{200 \text{ kHz}}$

- frequency tracker output voltage

$$V_{out} = \frac{1\ V}{200\ kHz} \times \frac{192.5\ kHz}{1\ m\ s^{-1}} = 0.9625\ {}^{V}/_{m\ s^{-1}} = 9.625\ {}^{mV}/_{cm\ s^{-1}} \qquad (2.11)$$

The relation between tracker output and velocity is

$$1\ mV = 0.1039\ cm/s$$

The calibration line is given in fig. 2.8.

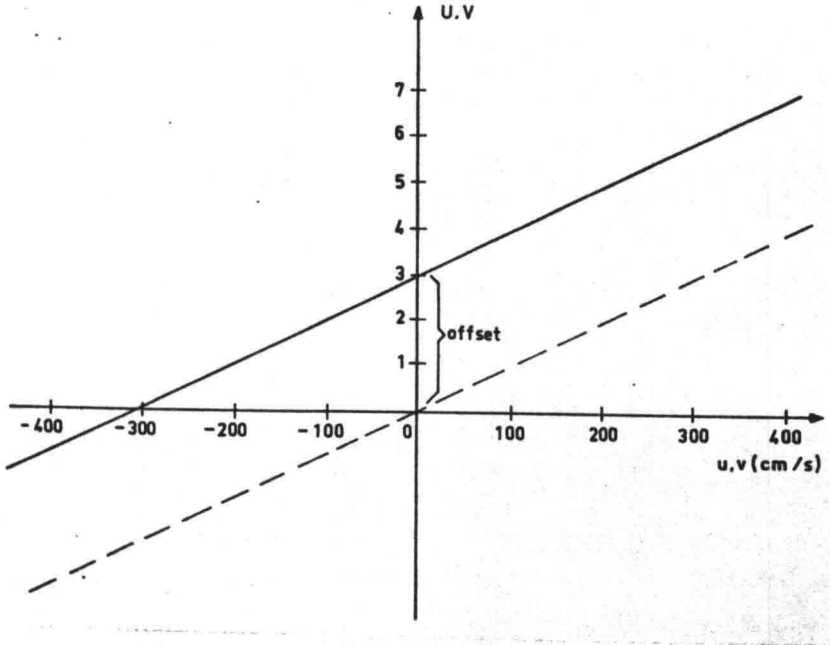

Fig. 2.8. LDV calibration line.

Using an offset the calibration line was shifted during the experiments through the origin (to remove the frequency shift). This procedure was convenient when checking the stability of the reversing grating disk and for later computations. When the motor had 50 revolution per second, the tracker output from the frequency shift was ~ 3 V.

The bias frequency-shift at zero velocity was measured by moving the measuring volume to the bottom of the flume. The motor speed was measured using a Newport Counter, Model 730.

The size of the measuring volume can be computed in the following way:

- width of the measuring volume

$$b_x = 4\lambda F/\pi\, b_o \cos \tfrac{1}{2}\phi \qquad (2.12)$$

- length of the measuring volume

$$b_y = n\, b_x / \tan \tfrac{1}{2}\phi \qquad (2.13)$$

where: b_o = ($1/e^2$ intensity limited) diameter of the laser beam originating from the laser (b_o = 1 mm); n_r = ref ractive index of the fluid medium (n_r = 1.33).

In our situation we have
b_x = 0.196 mm and b_y = 4.268 mm.

The measuring volume is quite long in the case of boundary layer measurements with the vertical-beam configuration (fig. 2.6). A horizontal-beam configuration is necessary in this case.

2.2.2. Visualization of the separated flow with dye

Several flow visualization techniques are used for integral and local measurements in fluid mechanics (Flow Visualization, Int.Symp.,1977). Flow visualization is very practical, especially during the first steps of an investigation, to obtain some ideas about the structure of the flow and to select dominating phenomena to be examined in future experiments. Flow visualization techniques are used quite often in investigations concerning different kinds of separated flows (Karahan and Peterson, 1980; Pullin and Perry, 1980; Chedron et al., 1978; Bonard and Contanceau, 1980; Bearman and Graham, 1980), to measure the coherent turbulent structures (Hussain and Clark, 1981) and to examine boundary layers (Grass, 1971).

Application of the visualization technique can be found also in complex turbulent flows (Lee and Clark, 1980). Marking materials used are, for example, dye (Pullin and Perry, 1980), smoke (Chedron et al.,1978) hydrogen bubbles (Grass, 1971), streaming birefringence of dilute colloidal suspension of birefringent materials (Karahan and Peterson, 1980), oil fog (Falco, 1980). Visualization techniques are useful for qualitative investigations, they are very tedious and time-consuming for quantitative computations, however. In the present investigation potassium permanganate was used to visualize the separated flow. The dye inflow was placed at half depth at the protruding corner of the expansion in the flume (fig. 2.9).

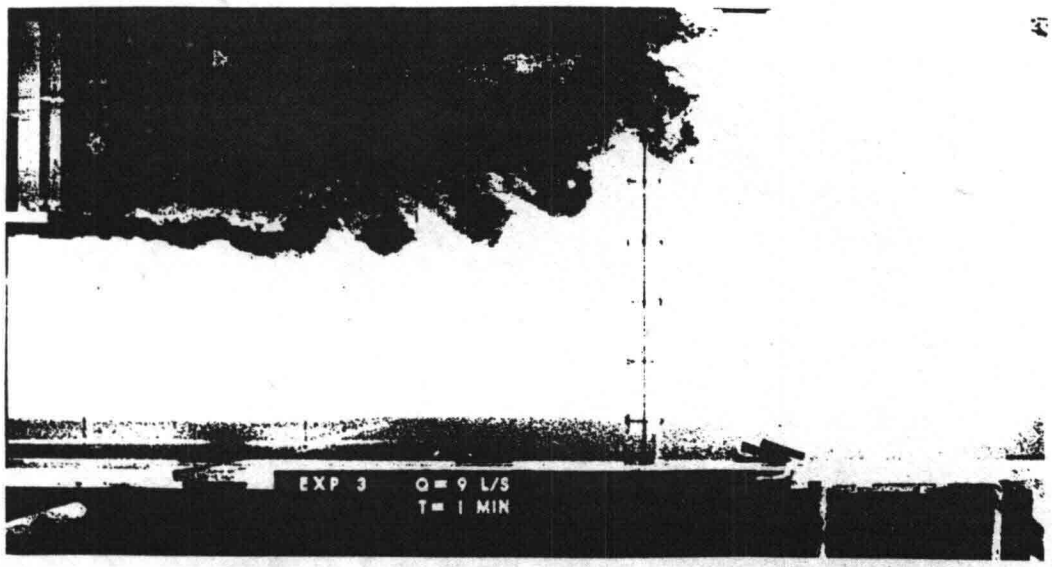

Fig. 2.9. Photo of the visualization of the separating flow.

During the experiments dye was injected continuously. Photographs of the separation region were made with time intervals of two or three seconds. These photographs give good qualitative information about the large vortices inside the separated region and also about the behaviour of the separated region in course of time(accelerating and decelerating phases of the flow). In some experiments dye was injected at different places in the flume, but these experiments did not give substantially new information.

2.2.3. Visualization of the flow with small floats

The turbulent motions inside the separated region are very complicated. We can see vortices with different scales in time and space. To have estimates about the motion of vortices and eddies inside the separation region experiments with small floats were carried out. These measurements produce approximate trajectories of water particles and also the possibility to calculate velocities of the float. The motions of the floats were registered by making photographs and also by making movies with ten frames per second. Interpretation of the photographs was difficult, because the time intervals between two photographs were not constant. Furthermore it was difficult to follow a single float among many other floats.

The trajectories of the floats could be easily determined from the movies. Coordinates of the floats as function of time determined from the movie at fixed time intervals (one second) were fed to the computer. Next, computed trajectories were plotted. The float velocities averaged over one second time interval were calculated also.

2.2.4. Measurements of the changes in water level

The unsteady flow produces long waves in the flume, and consequently the water level also varies. To have estimates about the behaviour of the flow in time, water-level changes were measured at various locations in the flume. These measurements were done using a wave height meter (Delft Hydraulics Laboratory Production). Water level changes were recorded using a Hewlett Packard 7402A Recorder.

3. Analysis of the Experimental Results on the Computer

3.1 General aspects of unsteady flow measurements

Measurements in unsteady flows are complicated in that realistic estimates about the nature of the flow field are difficult to obtain. We have usually two important problems. First the probes should have appropriate responses and second methodical problems have to be solved to obtain realistic data from measured signals. Some special problems arise in turbulent and transitional flows. Nowadays measurement systems with suitable response characteristics, such as LDV, are available and so it is no problem to measure velocity realisations. The second problem is usually more difficult to solve. This is a reason why methodical problems, in particular concerning signal processing, play such a great role in unsteady-flow measurements.

Turbulent flow is not a completely stochastic process; mostly we can find some regular phenomenon which is connected with the space and time coordinates. To this regular part a stochastic motion will be added. With statistical averaging it is possible to determine the regular structure of the flow. From probability theory it is known that only statistical averaging is correct. This means that true mean values can be found from averaging of a large number of different realisations. This is practically impossible to realise. In steady turbulent flows the ergodical theorem can be used to replace averaging of a large number of realisations by time averaging of one single realisation. This procedure requires a long time averaging period (T). The mean value of a time function x (t) is then given by

$$\bar{x} = {}^{1}/_{T} \int_{0}^{T} x(t)\, dt \qquad (3.1)$$

Fortunately steady turbulent flows are ergodical, and it is possible to use time averaging.

The averaging period T should be sufficiently long. To have a 1% accuracy for the average value, the time interval should be (Bartlett, 1958)

$$T \geq 200 \int_{0}^{\infty} R(\tau)\, d\tau \qquad (3.2)$$

where $R(\tau)$ = a correlation coefficient.

By using discrete sampling of a signal we usually record the signal at equal time intervals $\Delta t = T/n$, where n is the number of time intervals. According to Nyquist's theorem we should have as a minimum two recording points for the fluctuations with the highest frequencies, but for practical calculations it is better to have more points. The selection of an appropriate averaging time T involves a compromise between random and bias error.

For unsteady flow we cannot use time averaging and it is only possible to have some estimates of the characteristics of the flow using an ensemble of sample records $x_i(t)$; $0 \leq t \leq T$, $i = 1,2 \ldots M$. M = number of records in ensemble (Bendat and Piersol, 1971). The mean value at some time t is estimated from the ensemble average

$$\hat{m_x}(t) = \frac{1}{M} \sum_{i=1}^{M} x_i(t) \tag{3.3}$$

The variance of the estimate is

$$\text{Var}\left[\hat{m_x}(t)\right] = \frac{\sigma_x^2(t)}{M} \tag{3.4}$$

where $\sigma_x^2(t)$ is the variance associated with the underlying unsteady realisation $\{x(t)\}$, $\text{Var}\left[\hat{m_x}(t)\right] \to 0$ when $M \to \infty$, so $\hat{m_x}(t)$ is a consistent estimate of the mean value $m_x(t)$ for all t.

To estimate the time-varying variance of an unsteady signal also ensemble averaging can be used. Given a set of sample records as before, the estimated variance at time t follows from

$$\hat{\sigma_x^2}(t) = \frac{1}{M} \sum_{i=1}^{M} \left[x_i - \hat{m_x}(t)\right]^2 \tag{3.5}$$

Independent of M, the quantity $\hat{\sigma_x^2}(t)$ is an unbiased estimate of the true variance of the unsteady process $\{x(t)\}$ at any time t.

In practical applications the M sample records used to compute $m_x(t)$ and $\sigma_x^2(t)$ will be statistically independent.
When the random process $\{x(t)\}$ at any time t is Gaussian, these estimates are consistent. As we know usually turbulent fluctuations inside the fully developed flow are Gaussian, but in the boundary layers they are not.

It is better to use a slightly different sample variance as follows

$$\hat{\sigma_x^2}(t) = \frac{1}{M-1} \sum_{i=1}^{M} \left[x_i - \hat{m_x}(t)\right]^2 \qquad (3.6)$$

This estimate is an unbiased estimator for σ_x^2 (t), as well as an efficient and consistent estimator.
It is useful to have in this kind of unsteady records processing some 90% or 95% confidence intervals calculations giving some ideas about the accuracy of the estimates (see Bendat and Piersol, 1971).

Some practical experiences in the past (Koppel and Liiv, 1977) indicated that, in order to obtain good ensemble estimates of unsteady turbulent flows at every time moment, 50 to 100 realisations are needed as a minimum. In these realisations initial and boundary conditions should be the same.

To connect the time and space scales of the turbulence fluctuations Taylor's hypothesis is often used in steady flow. This hypothesis regards the turbulent velocity structure as frozen while it moves through the measuring point (Taylor, 1937).

$$\frac{\partial}{\partial t} = \bar{u} \frac{\partial}{\partial x} \qquad (3.7)$$

The hypothesis is correct for isotropic low-intensity turbulence ($\sigma_u/\bar{u} \ll 1$, where σ_u = standard deviation).
In certain unsteady flow cases it is also possible to use Taylor's hypothesis to obtain estimates about time-space relations.

The variance of the turbulent velocities (σ_x^2) will characterize the energy of the flow. The turbulence energy of the flow can be calculated in the following way

$$E = (1/2)\ (\sigma_u^2 + \sigma_v^2 + \sigma_w^2) \qquad (3.8)$$

In recent years conditional sampling is used to process unsteady flow results (Kovasznay (1978), Buchhave (1978), Orloff (1978), Reynolds (1974)). It is more practical to use conditional sampling in combination with ensemble averaging. If a flow has a periodic component, or if a somewhat regular eddy pattern is present, the flow is called conditionally unsteady.

In conditionally sampling an unsteady flow the total velocity field can be decomposed into several subfields (Orloff, 1978).

$$\vec{\underline{U}}\,(\vec{x},t) = \vec{U}\,(\vec{x},t) + \vec{\tilde{U}}\,(\vec{x},t) + \vec{u}'\,(\vec{x},t) \qquad (3.9)$$

with respective length scales L, $\tilde{l}$ and λ, where $L \gg \tilde{l} \gg \lambda$, and with respective time scales T, $\tilde{t}$ and τ, where $T \gg \tilde{t} \gg \tau$. The unconditional mean velocity $\vec{U}\,(\vec{x}, t)$ is the average velocity determined unconditionally over a long time interval T. Bien and Benner (1970) have used a LDV to investigate unsteady rotating flows. The characteristic decay time for their flow was $T \simeq 17$ s; the typical data acquisition time for a single velocity value was of the order of 0.3 s, during which the flow structure underwent negligible change. The flow could be treated as quasi-steady during the signal averaging process. The conditional mean velocity $\vec{\tilde{U}}\,(\vec{x},t)$ is a fluctuation whose occurence is either random, periodic, or some combination of both. The third component is a turbulent fluctuation $\vec{u}'(\vec{x},t)$, which is characterized by the smallest time and length scales, τ and λ.

To obtain estimates about turbulent fluctuations we should consider limitations of laser measurements, some of which are described in section 2.2.1 of this report.

The experimental investigation of unsteady separated flow in an open-channel requires quite a lot of measurements in different cross-sections of the flume and at various depths. Already before the measurements were started it was clear, that it was impossible to use ensemble averaging at various instants t.

It was preferred to use conditional averaging over short time intervals (segments), during which we can consider the flow as quasi-steady .The method was used before to determine spectral estimates of unsteady turbulent flow in a pipe (Ainola et al., 1979) This method requires several measurements at the same location with the same initial and boundary conditions. Two separate measurements of velocity components in flow direction (u) and in transverse direction (v) in the measurement point $B5/_3$(see fig. 4.1) with the flow rate $Q_m = 16\ ^{l}/_{s}$ are given in fig. 3.1.

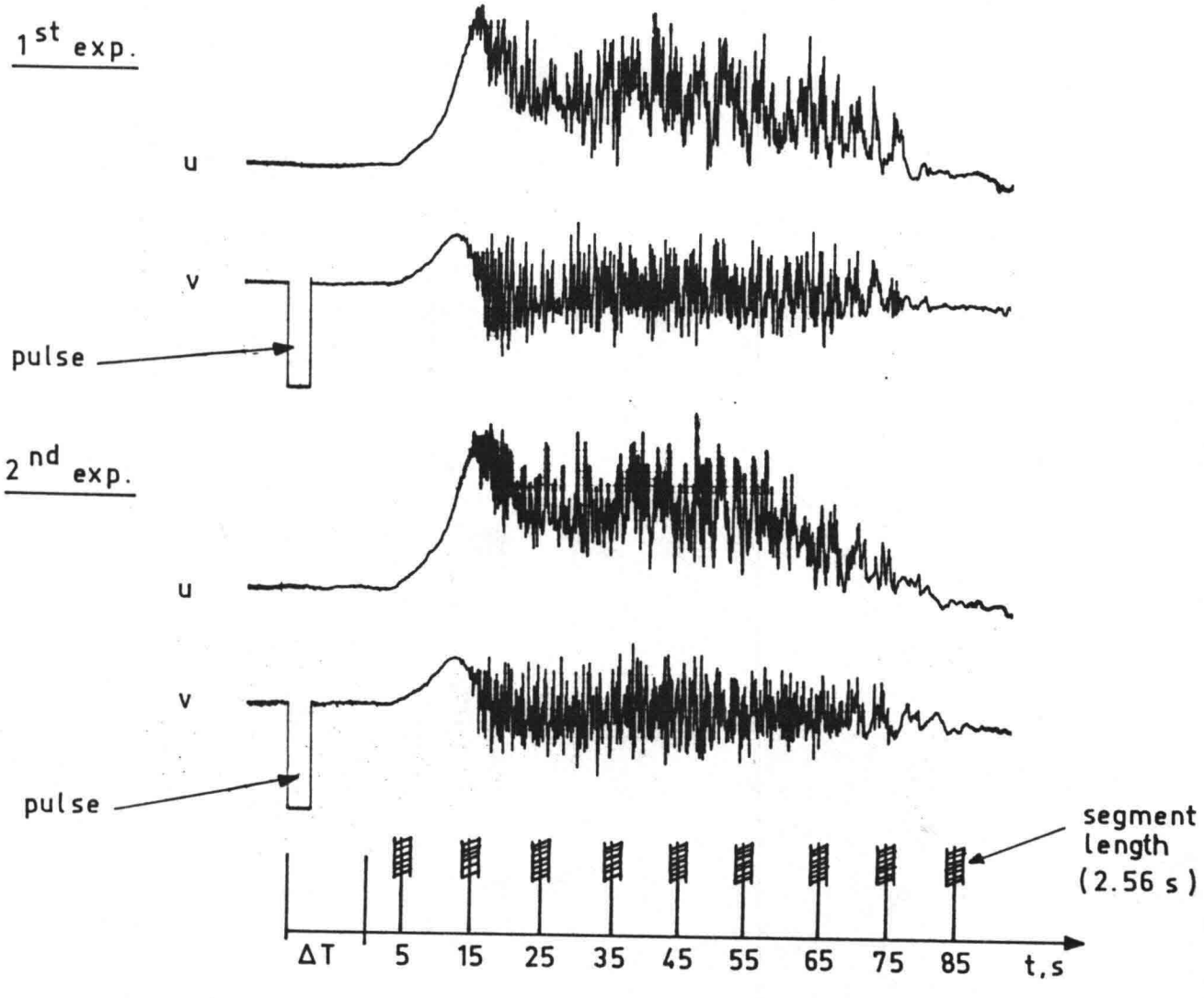

Fig. 3.1. Ensemble averaging.

In fig. 3.1 only two separate measurements are given, but usually the measurements in a single measuring point were repeated up to 15 times. As we can see the repeatability of the measurements is good. The ensemble averaging was done as follows. From each separate velocity measurement a segment at the same time interval was taken, and put into a separate data set. Mean values and turbulence characteristics of the velocities at different times were then computed from this data set. It seems that a segment length of 2.56 s or 5.12 s is sufficiently short for a quasi-steady approximation, because the durations of the experiments were 60 and 70 seconds (fig. 2.3).

The total averaging time is 15 x 2.56 s = 38.4 s or 15 x 5.12 s = 76.8 s.

To have estimates about turbulence characteristics we should remove the ensemble mean value of the velocity ($\hat{m}_x$) from the recordings. The mean value is changing in time and so the experimental velocity components can be written as

$$x(t) = \bar{x}(t) + x_c(t) \tag{3.10}$$

For a short time period $\bar{x}(t)$ can be approximated by

$$\bar{x}(t) \simeq \alpha t + \beta \tag{3.11}$$

where α and β are experimental constants; x_c can be considered as a quasi-steady turbulent realisation. Henceforth the velocity components u and v will be assumed to be quasi-steady flow realisations with a linear trend resulting from the unsteadyness of the flow. Here we have two points which should be taken into consideration:

- the time interval should be sufficiently short for the turbulence intensity to be constant, and
- the calculation of the trend is not straight forward because the deterministic component of the velocity is not exactly known beforehand.

In the present research a linear trend was used for all time intervals in the ensemble averaging procedure.
The coefficients of the linear trend were calculated using the least-squares method:

$$\int_0^T (x - \alpha t - \beta)\, dt = 0, \qquad \text{and} \tag{3.12}$$

$$\int_0^T (x - \alpha t - \beta)^2 dt = \min. \tag{3.13}$$

To calculate the linear trends the standard subroutine G02 for linear regression analysis from NAGFLIB was used. This subroutine calculates linear relationships of the form

$$x_i = \alpha t + \beta + e_i \tag{3.14}$$

where i = 1,2 .... L (L >2), L = length of segment in ensemble. The subroutine calculates the regression coefficient α , the regression constant β and various other statistical quantities by minimizing

$$\sum_{i=1}^{L} e_i^2$$

The subroutine also calculates the mean value:

$$m_x = \frac{1}{L} \sum_{i=1}^{L} x_i \tag{3.15}$$

and the standard deviation:

$$\sigma_x = \sqrt{\frac{1}{L-1} \sum_{i=1}^{L} (x_i - m_x)^2} \tag{3.16}$$

After computation of α and β the trend was subtracted from the velocity realisation in each time segment in the ensemble separately.

Measurements of the velocities and processing using the ensemble averaging procedure were performed in the more important parts of the flow, in particular in the separated region. To have mean velocities over the depth of the flow, measurements at three different depths were carried out and recorded using the HP recorder. Afterwards the calculated velocities were integrated to give the depth-averaged velocities in different locations at different time moments.

3.2. Spectral estimates of turbulence energy

To obtain estimates about kinetic energy of the different eddies in a steady turbulent flow, power spectral analysis can be used. Theoretically there are also several possibilities to obtain spectral estimates for unsteady turbulent flow characteristics, but these methods are not useful for practical calculations. Inside the separated flow, especially in the mixing layer, we can see semi-permanent coherent structures and it is interesting to estimate how the distribution of turbulent energy is changing in time.

For power spectral estimates we have the relation (Ibragimov et al., 1978)

$$G_x^* (\omega) = \left[1/T\right] \left| \int_0^T \exp(i\omega t) \left[x(t) - m_x(t)\right] dt \right|^2 \tag{3.17}$$

This kind of estimates for the power spectra is practical when we have a great number (M) of realisations of the stochastic process. It is possible to average the power spectra for each frequency:

$$G_x^* (\omega) = \left[1/M\right] \sum_{j=1}^{M} G_x^* j \ (\omega) \tag{3.18}$$

where ω = angular frequency.

In fluid mechanics the spectra are usually normalized with the variance σ_x^2:

$$G_x = \int_0^\infty \frac{G_x^*(\omega)\, d\omega}{\sigma_x^2} \tag{3.19}$$

It is possible to derive some integral scales from the spectral estimates (Ibragimov) et al., 1978):

$$\lim_{f\to 0} \left[G_u(f)/\sigma_u^2\right] = 4 \int_0^\infty R_1(\tau)d\tau = 4\, T_i \tag{3.20}$$

and

$$\lim_{f\to 0} \left[G_v(f)/\sigma_v^2\right]\bar{v} = 4 \int_0^\infty R_v(\delta)d\delta = 4\, L_v \tag{3.21}$$

where f = frequency of fluctuations (s^{-1}), $f = \omega/2\pi$.

T_i is the mean life time of the large eddies and L_v is called the integral scale or macro-scale.

To determine the micro-scales it is possible to use the following relations

$$1/\eta^2 = (2\pi^2 / \sigma_u^2) \int_0^\infty f^2\, G_u(f)df \tag{3.22}$$

$$1/\eta_u^2 = \left|2\pi^2 /(\bar{U}^2\, \sigma_u^2)\right| \int_0^\infty f^2\, G_u(f)df \tag{3.23}$$

The integral scales are proportional to the value of the power spectrum function at zero frequency.

The power spectral estimates $G_u(f)$, $G_v(f)$ and $G_w(f)$ are one-dimensional spectral functions. It is convenient to use the wave number k for the three-dimensional spectra, so for one-dimensional spectra we have

$k_1 = 2\pi f/\bar{U}$ and

$$G_u(k_1) = (\bar{U}/2\pi)G_u(f) \tag{3.25}$$

The shortcoming of one-dimensional spectra is that they do not give the precise distribution of energy as a function of the wave number. The three-dimensional spectra function is equal to zero at zero frequency, but the one-dimensional spectrum is not. One-dimensional $G_u(f)$ and three-dimensional $G(f)$ spectra are shown in fig. 3.2 (Ibragimov et al.,1978)

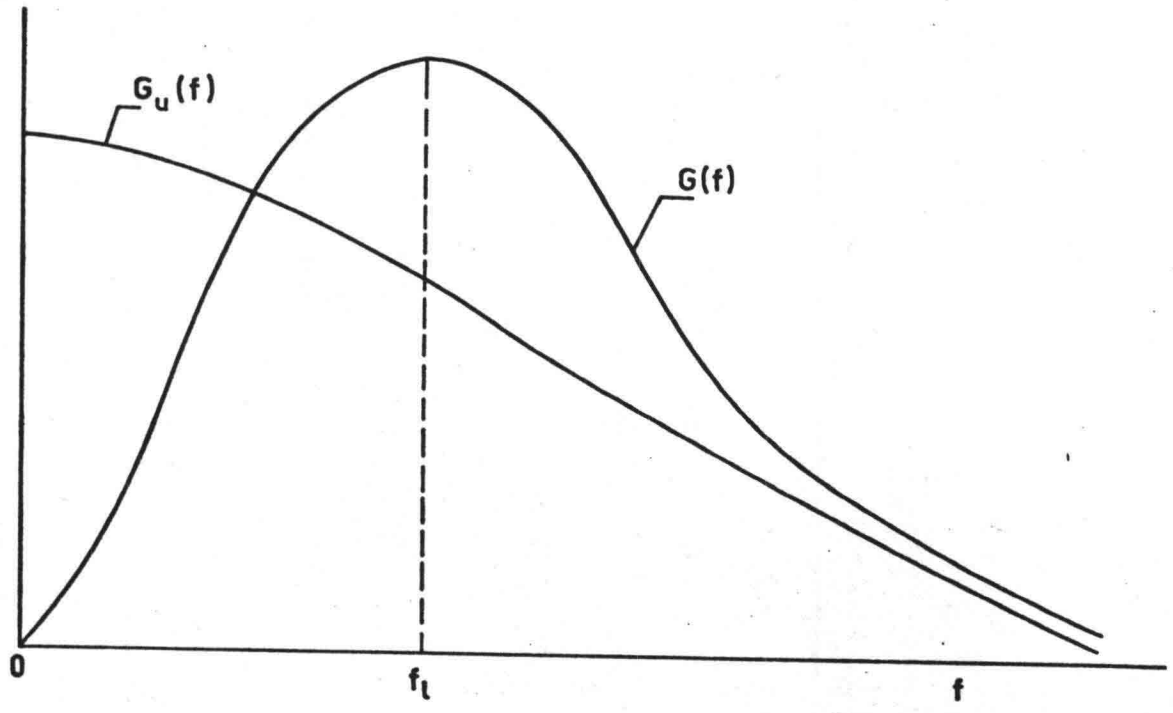

Fig. 3.2. One-dimensional ($G_u(f)$)and three-dimensional ($G(f)$)energy spectra.

We should consider also the fact that with LDV measurements of turbulence power spectra, ambiguity noise appears as a constant background spectrum. Then the noise spectrum can be subtracted from the measured spectrum and the integral of the corrected spectrum finally gives the estimate about the variance of the turbulence.

To compute power spectra of the unsteady-flow velocities, the short-time averaging operation as described in section 3.1 was used. It was used successfully before by Ainola et al. (1979). This kind of calculations can produce useful qualitative information about time-varying spectral properties of the velocities but quantitative applications of the results should be treated with caution.

For the computation of the power spectra the IMSL library subroutine named FTFPS was used. This subroutine calculates Fast Fourier Transform (FFT) estimates of power spectra and cross-spectra of the two time series. After removal of a linear trend the arranged velocities from the ensemble averaging procedure were used as input time series in the FTFPS subroutine. This subroutine is recommended when the input length N of the time series is at least 15 times longer than the length L of the segment of the time series (L must be a power of two). In the computations L was equal to 128 or 256. The ensemble consists of 15 measurements and we have N equal to 1920 or 3840. The output of the subroutine is returned in units which are squares of those of the data.

A symmetric data window is used together with theFTFPS subroutine (fig. 3.3):

$$W(j) = 1 - \left| \frac{j - \frac{L-1}{2}}{\frac{L+1}{2}} \right| , \qquad j = 0,1, \ldots \; L-1 \tag{3.26}$$

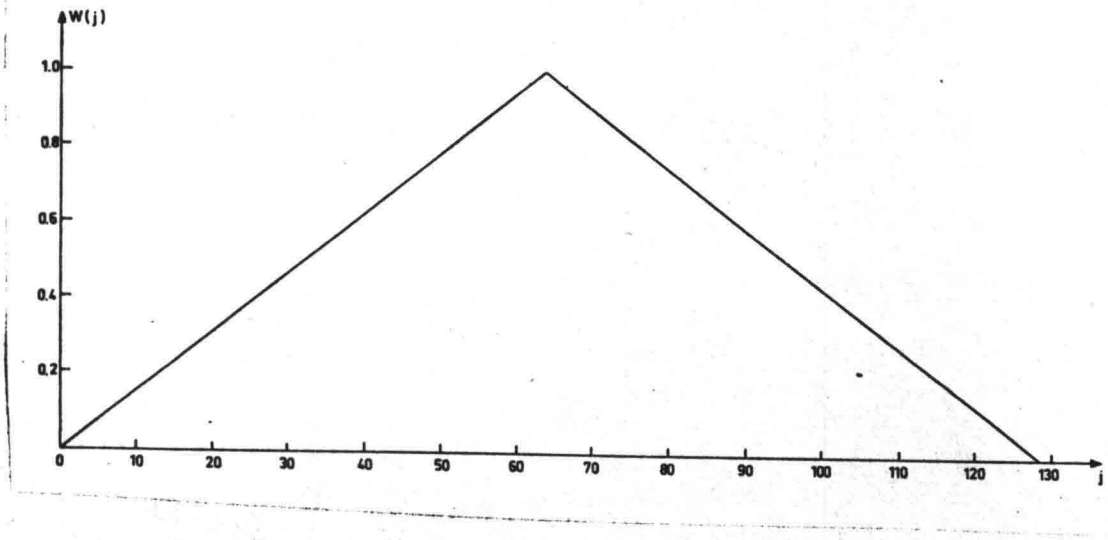

Fig. 3.3. Symmetric data window.

This is approximately the Parzen spectral window. The data window is applied to each segment of length L of the time series (see fig. 3.1). Then the IMSL routine FFTRC is called to give the FFT of the segment. The output vector is defined mathematically as

$$x_{k+1} = \sum_{j=0}^{L-1} x_{j+1} \exp(2\pi ijk/L), \tag{3.27}$$

where $k = 0,1, \ldots \; L-1$ and $i = \sqrt{-1}$.

The estimates for N/L segments are averaged and scaled. The resulting spectral estimates are given at the following frequencies

$$f_i = \frac{i-1}{L\Delta t} \tag{3.28}$$

where Δt = period of sampling of the time series. Afterwards the spectral estimates for the velocities were normalized with the variances σ_u^2 and σ_v^2.

3.3. Statistical distributions

To calculate statistical distributions of the turbulent fluctuations subroutine H I S T 2 of the Computing Centre of the Delft University of Technology was used. The subroutine was applied to arrays of segments of velocities u and v to draw out histograms and in addition it computes mean, standard deviation, the coefficient of skewness and values of the smallest and largest observations. The output of the histogram subroutine was normalized with the number of recordings in the ensembled arrays N.

The coefficient of skewness is equal to

$$Sk = \overline{(x - m_x)^3} \;/\; (\sigma_x)^3 \tag{3.29}$$

For a Gaussian distribution the skewness is equal to zero.

3.4. Calculation of Reynolds stresses

Two different ways to calculate Reynolds stresses from the indirect 45° and direct LDV measurements were described in section 2.2.1. In the present work the velocity components were measured directly. After removal of the mean velocity component (linear trend) from ensemble arrays the correlation of the velocity fluctuations $\overline{u'v'}$ was calculated directly by the computer.
Obviously it is important to have a sufficiently long averaging time to obtain stable estimates of $\overline{u'v'}$. This problem was quite difficult to solve for two contradictory reasons:

- the time interval in the ensemble averaging process should be sufficiently short to have constant properties of the turbulence, so it is impossible to use long segment lengths;
- to have long time series of the velocities after ensemble averaging we need a great number of measurements.

Used time intervals were 2.56 s and 5.12 s which gives us after ensemble averaging a length of the velocity time series 38.4 s and 76.8 s, respectively. In the mixing layer, where the properties of the turbulence are not changing

so quickly (fig. 3.1) the difference in $\overline{u'v'}$ calculations from different lengths of velocity time series was $\leq$ 5%.

3.5. Computer programs for data processing

A set of programs was compiled to process the experimental results on the computer. Several subroutines were used for some particular calculations, such as F F T, histograms, calculation of linear trend. A block-scheme of the programs is given in fig. 3.4.

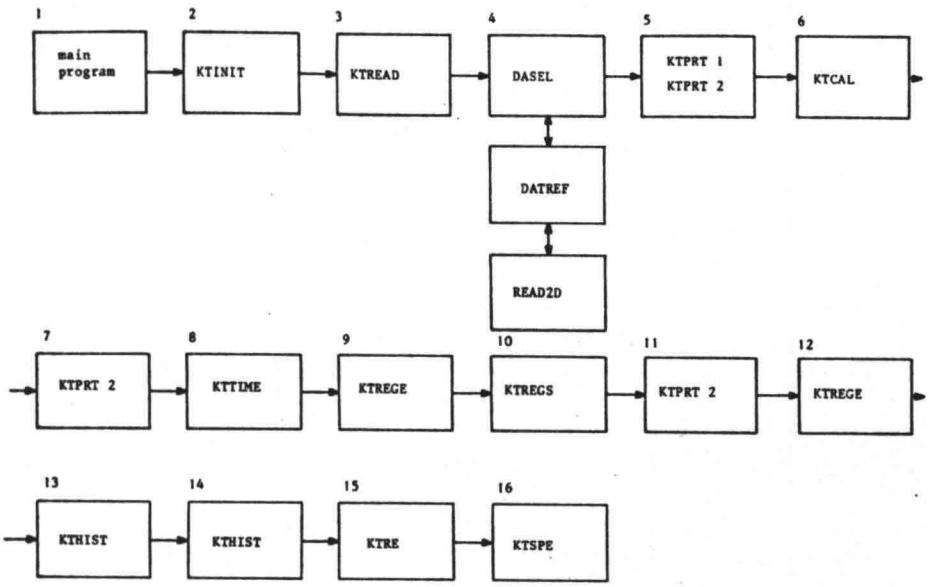

Fig. 3.4. Block-scheme of computer programs.

Next, a short description of the programs will be given:

- MAIN PROGRAM. For declaration of dimensions of used arrays and parameters, and for calling subprograms;
- K T I N I T. For declaration of several parameters used, as channel numbers, calibration coefficients, etc.;
- K T R E A D. To read input parameters which were changed more frequently, such as initial segment scan number, number of segments in ensemble averaging process etc.;
- D A S E L. To select data from several experiments according to ensemble averaging procedure and to place them sequentially into a one-dimensional array. Inside this program subprograms D A T R E F and R E A D 2 D were used. DATREF checks the pulse position in the measurements as starting point for the ensemble averaging process.

READ 2D reads a two-dimensional integer array from magnetic tape (S. de Boer, 1981);

- K T P R T 1. To print out identifications of series used;
- K T P R T 2. Print out of a segment of the composed arrays;
- K T C A L. To calibrate LDV recordings;
- K T T I M E. To calculate time scale for velocities;
- K T R E G E. For linear least-squares regression calculations of all the segments in the ensemble;
- K T R E G S. For linear least-squares regression calculations of separate segments in the ensemble and for subtracting the linear trend;
- K T H I S T. To calculate histograms and several parameters of the ensemble arrays;
- K T R E. For Reynolds stresses calculations;
- K T S P E. For Fast Fourier Transform calculations of two velocity components.

Some subroutines were used twice when processing the results, as KTHIST applies to one-dimensional arrays only. Outputs from the spectral estimates were drawn by the plotter.

4. Results of the Investigation

4.1. Main characteristics of unsteady separated flow

4.1.1. Visualization of the flow

The visualization technique is frequently used in investigations of separated flows. Mostly the main effort is concerned with the flow inside of the separated region. The possibilities to investigate the flow downstream of the separation are limited.

The first step in the present investigation was the visualization of the flow with dye. The visualizations were done with different flow rates Q_m and different time periods T (half sine). The more important aspects of the visualization experiments will be dealt with next.

In fig. 4.1. is given, as an example, the development of the separated region in time when Q_m = 9 1/s and T = 60 s. The starting time of the flow was t = 13 s. The first moments the circulation of the separated region is relatively fast and we can follow dye streaks while the centre of the vortex remains visible, It is also possible to distinguish the mixing-layer quite clearly from the main flow. From the pictures we can say also, that the exchange between separated region and the main flow is small, and that most of the water inside the separation region is coming from the protruding corner of the expansion in the flume.
Probably the turbulent mixing between the mixing-layer and the main flow is not playing an important part in the growth process of the separated region. In the photos no. 3, 4 and 5 we can follow semi-permanent coherent structures in the mixing-layer. In the accelerating phase of the flow, the separation is developing mostly in downstream direction. In the beginning of the decelerating phase the separation starts to widen also across the flume (photo no. 7) and at the end of the experiment it extends up to the opposite wall of the flume (photo no. 12). This fact indicates some influence of the opposite wall on the separating and main flows. In a real tidal-flow situation we do not have this factor. Unfortunately it is not possible to follow the downstream movement of the centre of the separating vortex on the photos.

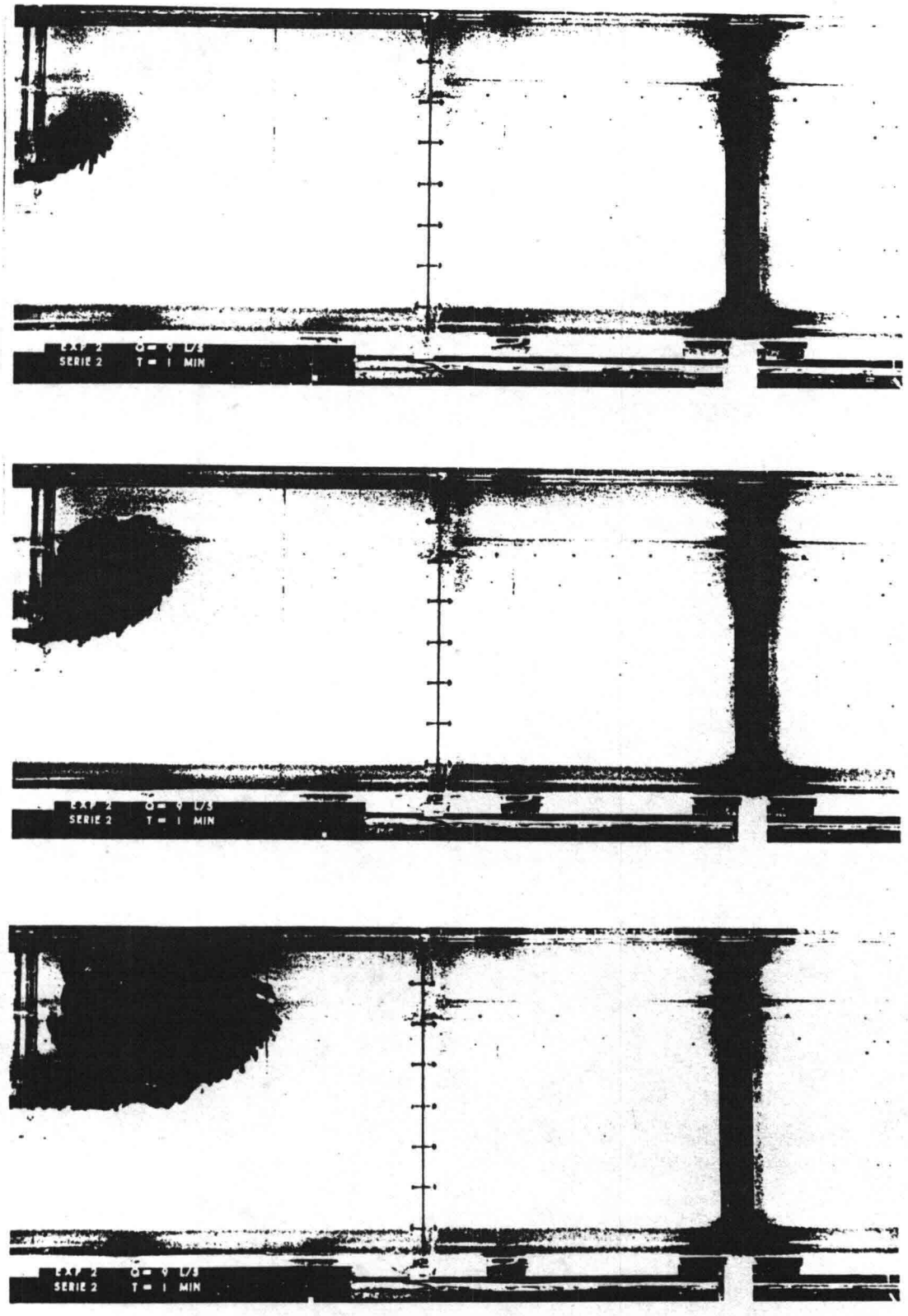

Fig. 4.1. Visualization of the separated flow with dye (Q_m = 9 l/s, T = 60 s).

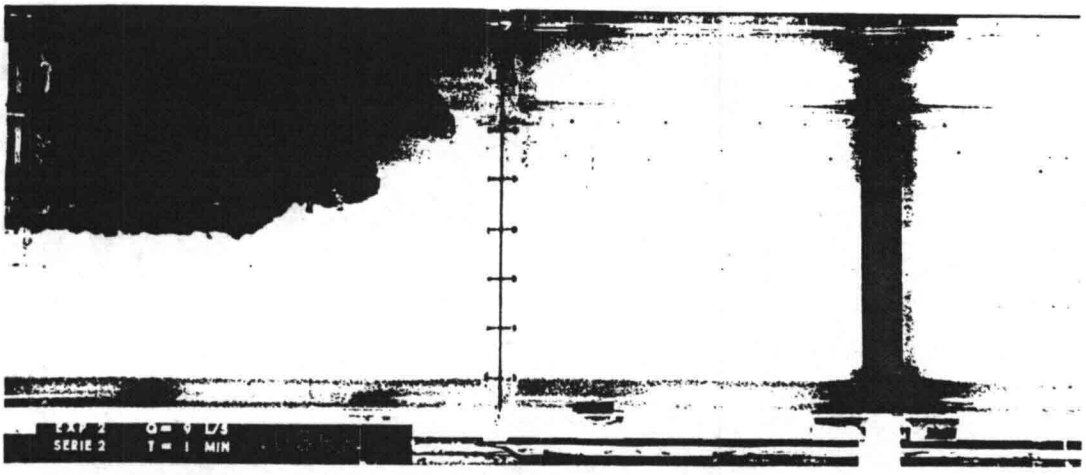

36.2 s

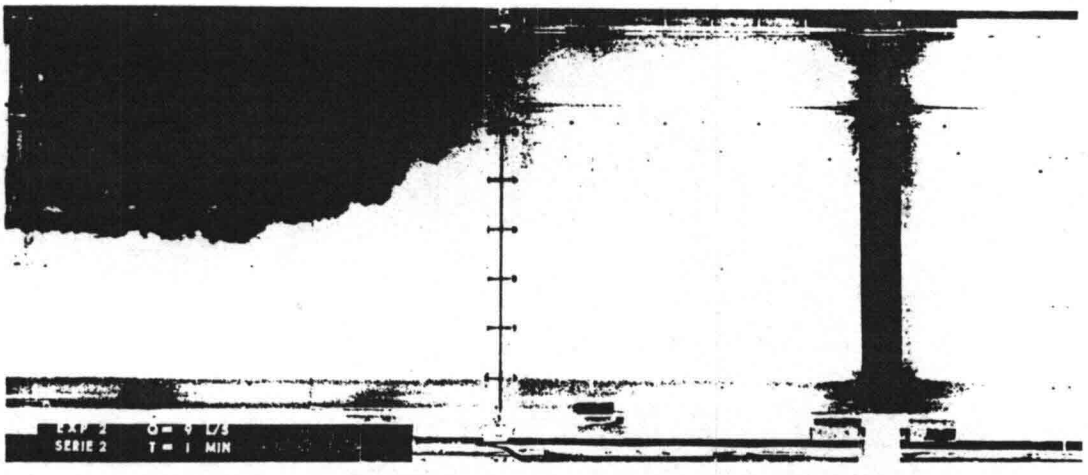

37.8 s

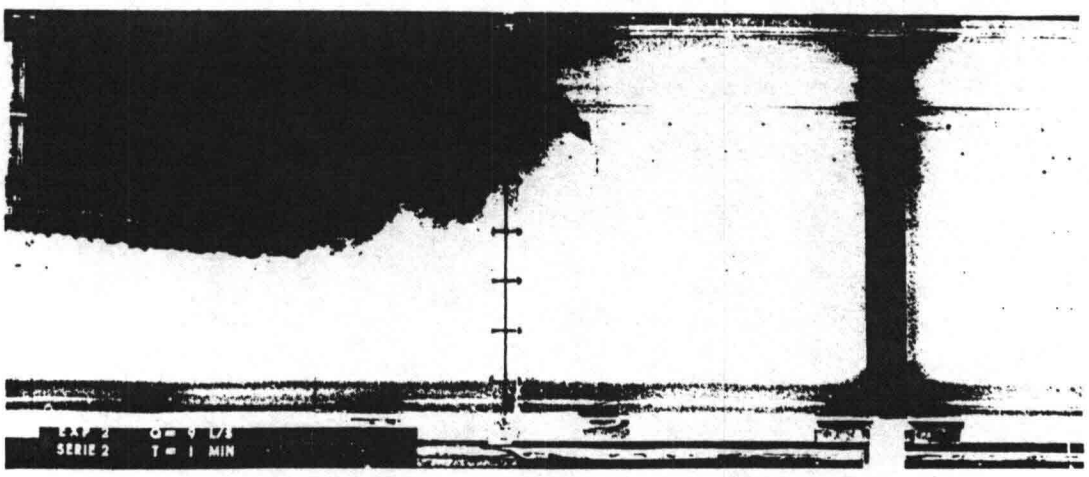

42.5 s

Fig. 4.1. (Continuation)

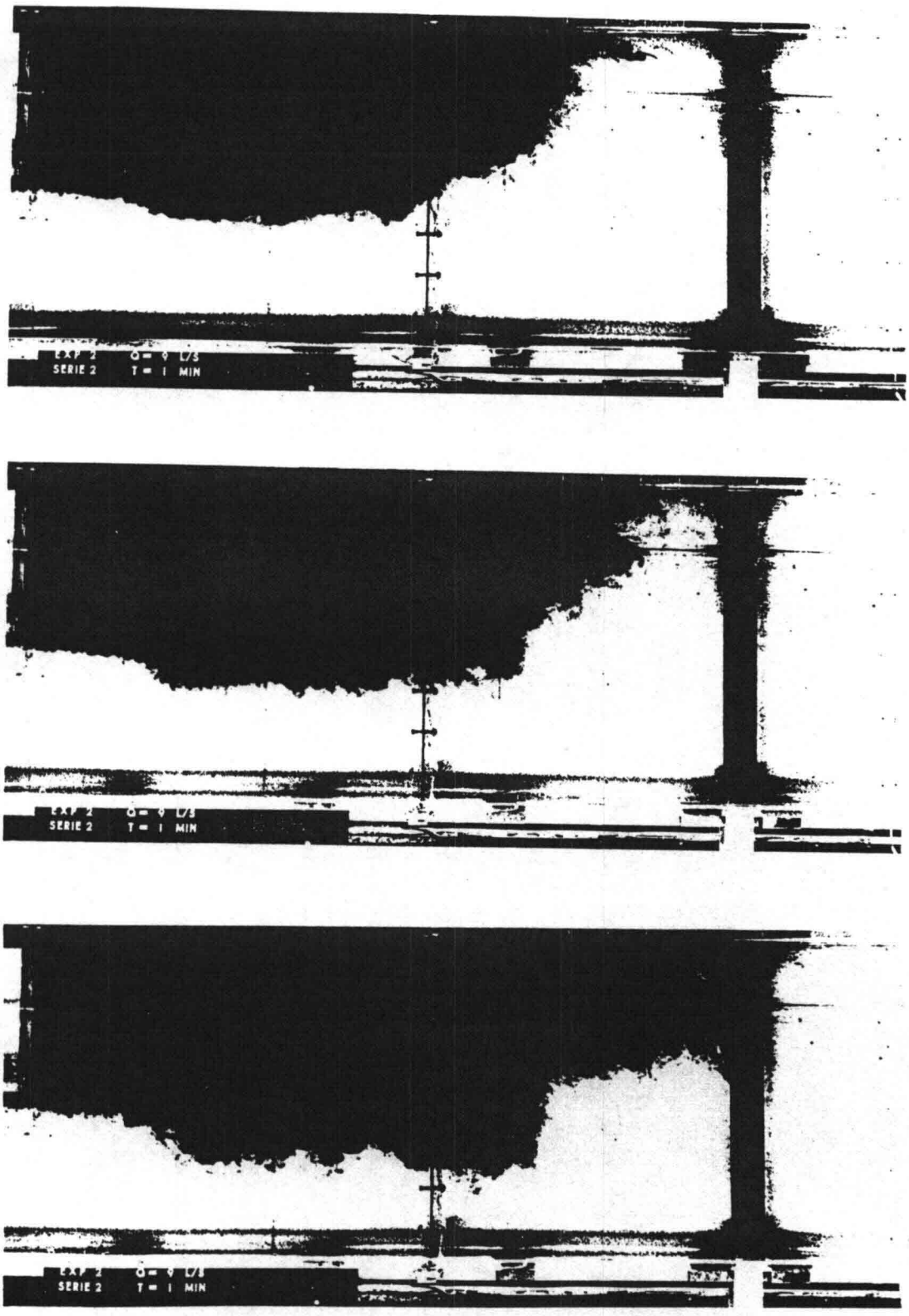

48.8 s

53.4 s

58.2 s

Fig. 4.1. (Continuation)

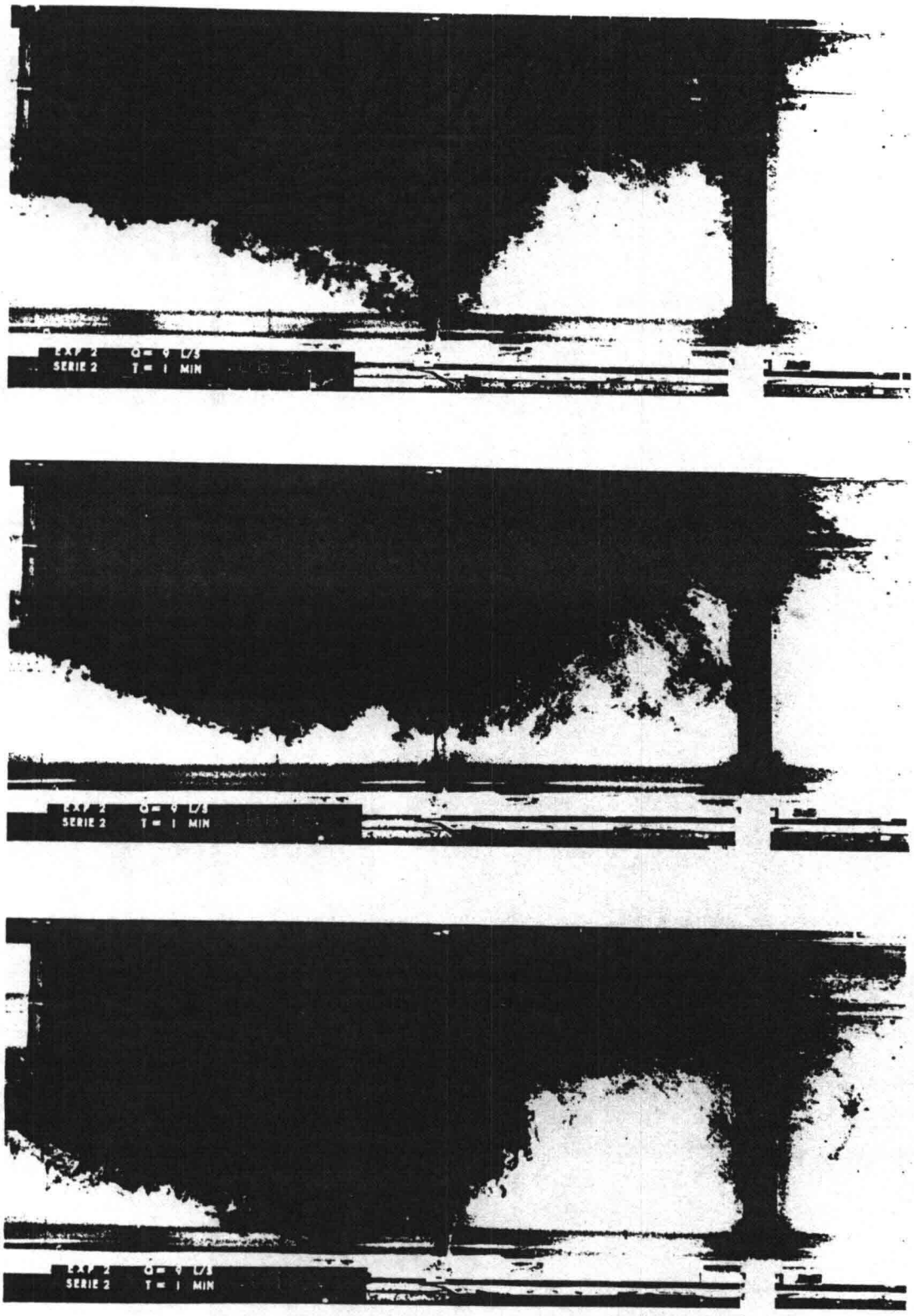

62.7 s

67.4 s

72.3 s

Fig. 4.1. (Continuation)

The development of the small coherent structures in the mixing-layer can be clearly seen on fig. 4.2.

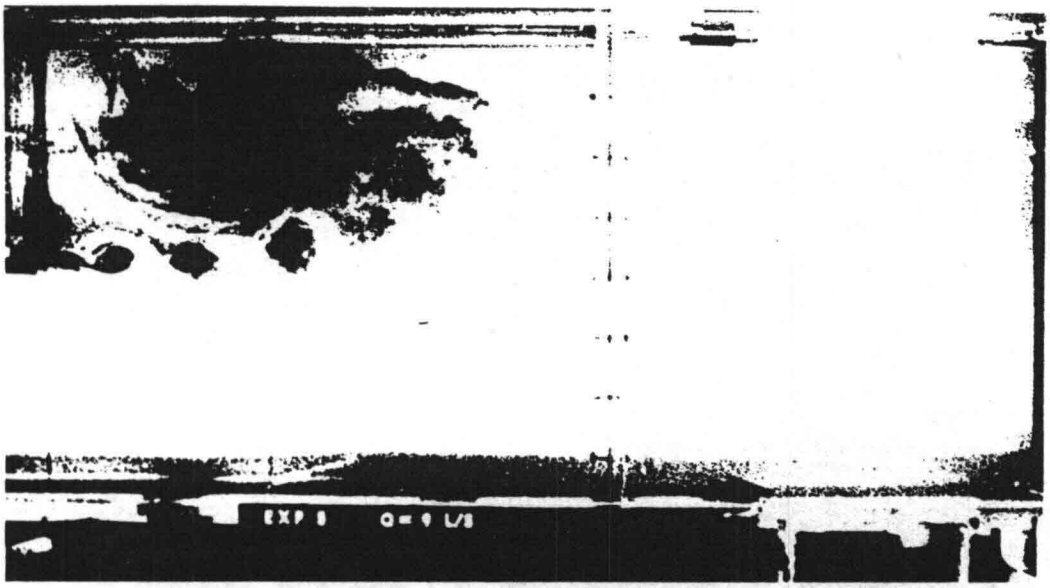

Fig. 4.2. Development of small coherent structures in the mixing-layer (Q_m = 9 l/s, T = 180 s, t = 31 s).

Not all photos obtained from visualizations of the separating flow will be reproduced here. However, the general aspects are the same at different maximum flow rates Q_m and time periods T. The boundaries of the separation region as functions of time at different flow rates Q_m and time periods T drawn from photos are given in figs. 4.3 , 4.4 , 4.5 , 4.6 , 4.7 , and 4.8.

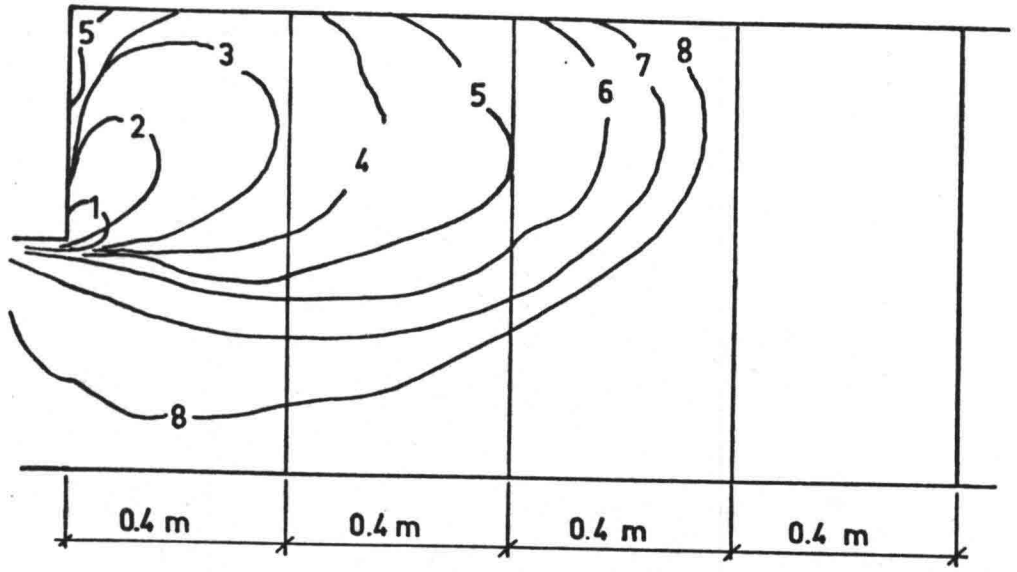

Q_m = 4.5 1/s
T = 60s

no. 1 - 1.9s 4 - 23.1s 7 - 47.6s
2 - 7.6s 5 - 31.5s 8 - 54.7s
3 - 15.3s 6 - 39.6s

Fig. 4.3. The boundaries of the separation region at various instants (Q_m = 4.5 1/s, T = 60 s).

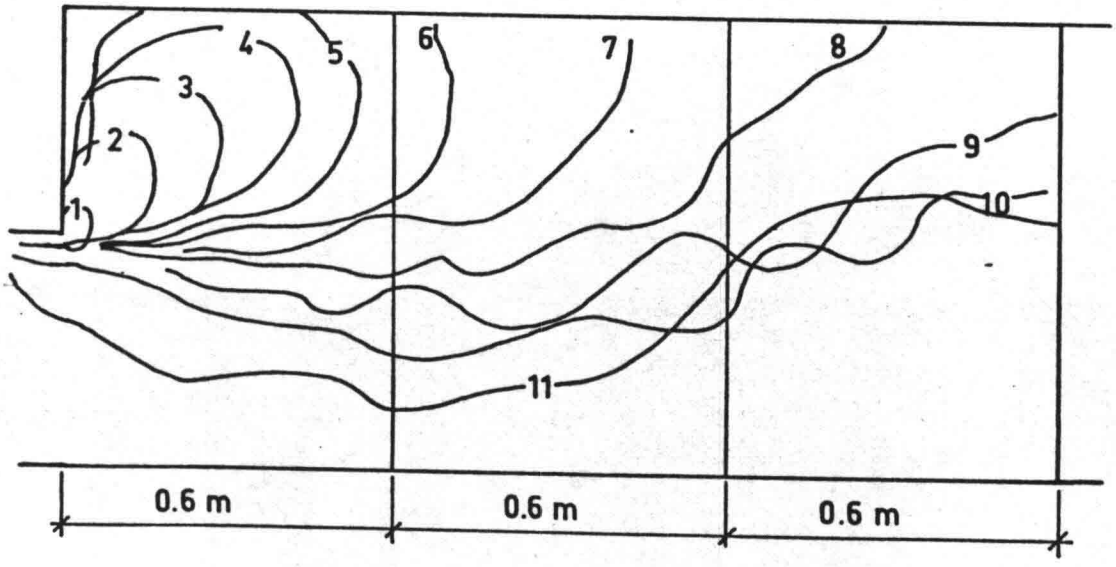

Q_m = 4.5 1/s
T = 120s

no. 1 - 3.5s 4 - 21.4s 7 - 50.4s 10 - 98.3s
2 - 9.2s 5 - 29.9s 8 - 65.4s 11 - 112.8s
3 - 15.2s 6 - 38.3s 9 - 80.4s

Fig. 4.4. The boundaries of the separation region at various instants (Q_m = 4.5 1/s, T = 120 s).

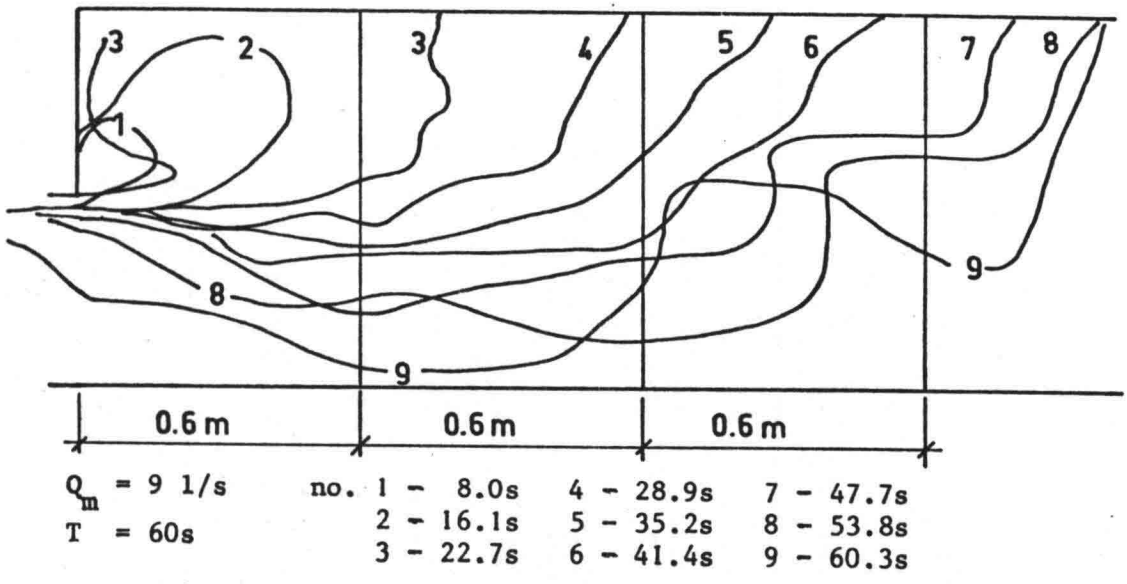

Q_m = 9 1/s
T = 60s

no. 1 - 8.0s 4 - 28.9s 7 - 47.7s
2 - 16.1s 5 - 35.2s 8 - 53.8s
3 - 22.7s 6 - 41.4s 9 - 60.3s

Fig. 4.5. The boundaries of the separation region at various instants (Q_m = 9 1/s, T = 60 s).

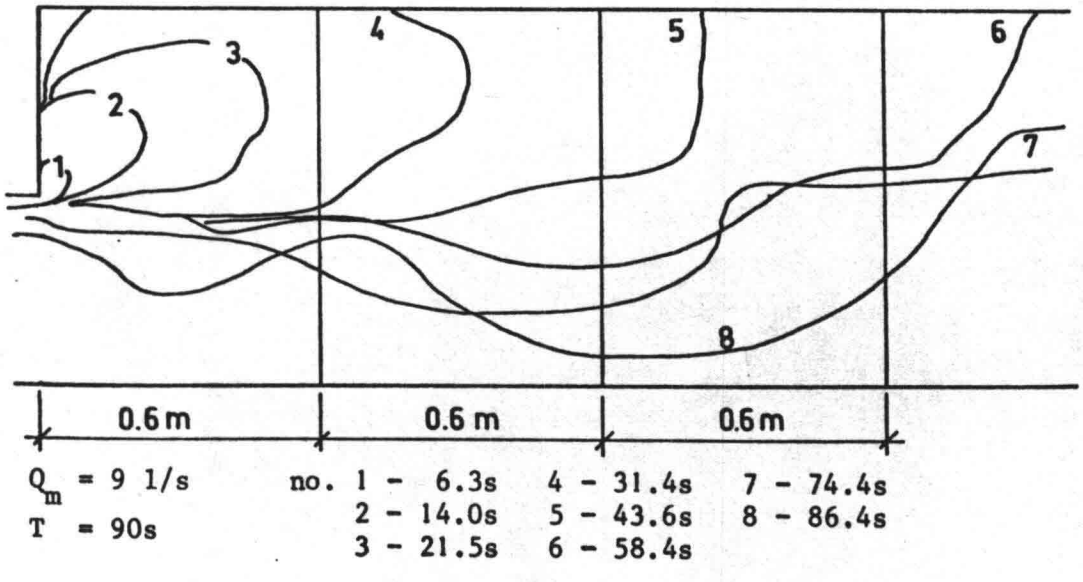

Q_m = 9 1/s
T = 90s

no. 1 - 6.3s 4 - 31.4s 7 - 74.4s
2 - 14.0s 5 - 43.6s 8 - 86.4s
3 - 21.5s 6 - 58.4s

Fig. 4.6. The boundaries of the separation region at various instants (Q_m = 9 1/s, T = 90 s).

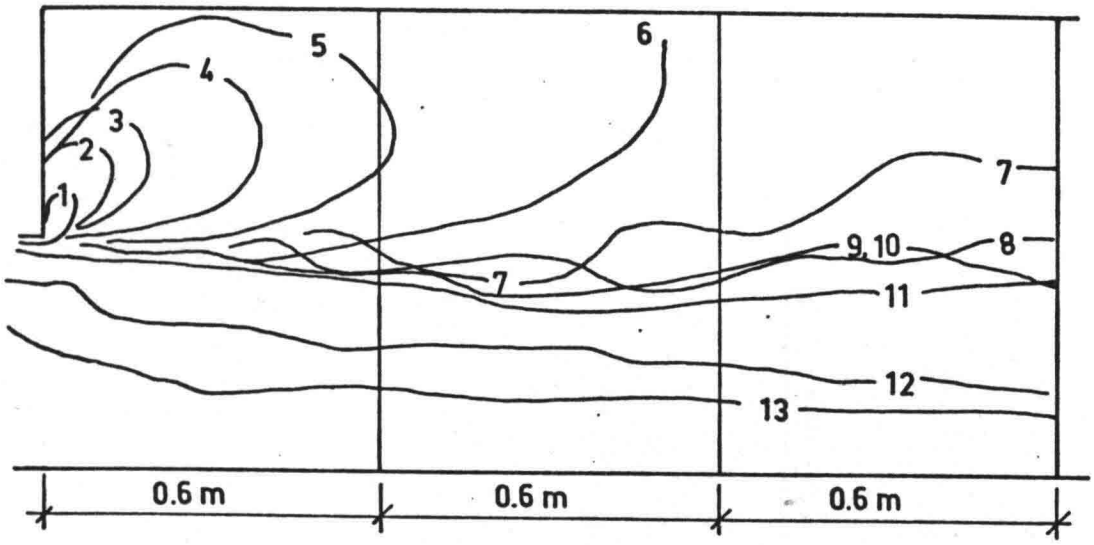

Q_m = 9 1/s
T = 180s

no. 1 - 2.4s 4 - 21.4s 7 - 58.7s 10 - 122.6s
2 - 6.7s 5 - 30.3s 8 - 76.2s 11 - 146.5s
3 - 13.8s 6 - 43.5s 9 - 98.5s 12 - 169.6s
13 - 177.9s

Fig. 4.7. The boundaries of the separation region at various instants (Q_m = 9 1/s, T = 180 s).

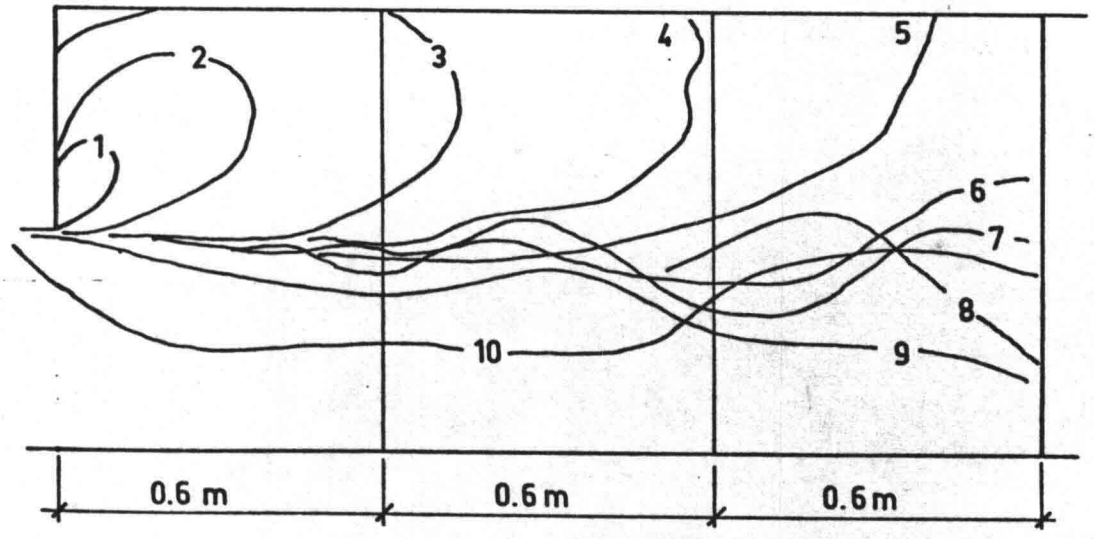

Q_m = 16 1/s
T = 90s

no. 1 - 8.6s 5 - 36.0s 9 - 82.1s
2 - 15.8s 6 - 45.8s 10 - 90.8s
3 - 22.4s 7 - 57.5s
4 - 29.2s 8 - 69.8s

Fig. 4.8. The boundaries of the separation region at various instants (Q_m = 16 1/s, T = 90 s).

In figures 4.3. to 4.8. the influence of the acceleration on the development of the separation is visible. When the acceleration of the flow is larger the separation region is more compact. Obviously, at longer time periods T the separation region will develop to a longer distance from the expansion of the flume at the same Q_m.

4.1.2. Float trajectories

The separated flow is quite independent from the main flow. It mainly consists of a large vortex with turbulent random motions inside. The motions also have some regular tendencies which are related to the boundary and initial conditions. When the maximum flow rate Q_m was smaller, such as Q_m = 4.5 1/s, the separating flow only consisted of a single large vortex (see fig. 4.3.), but the visualization experiments showed that at higher flow rates several separate vortices are generated inside the large vortex. These vortices are moving and influence each other. In order to obtain information about the depth-averaged velocities and vortex motion inside the separation region, visualization experiments with small floats were carried out (see section 2.2.3.). In figure 4.9. and 4.10. several trajectories of floats are plotted when Q_m = 4.5 1/s and T = 60 s. Starting time of the experiments was t = 13 s. Each float was placed in the flow at different time moments. The time interval between the marking symbols is one second. It is thus possible to derive velocity components and directions, which can be useful for comparison with theoretical models of separating flow. Sometimes we can see that a float carried out small circulating motions already during one second. The size of the separation region is visible on fig. 4.9. (trajectory no. 4). Inside the separation region the motions are quite complicated. From the spiraling trajectories of the particles (fig. 4.10.)we can follow the growth of the large vortex in downstream direction. Float no. 1 is in the centre of the vortex; floats no. 2 and no. 3 are affected (in the later stage) by the outer regions of the large vortex.

When the flow is higher (Q_m = 9 1/s) the flow inside the separation region is more complicated (fig. 4.11 and 4.12). The spiraling motion of the floats is again visible. Note that a secondary vortex is generated at higher flow rates. The circulation of this vortex is opposite to that of the main vortex (fig. 4.11, trajectory no. 1). This vortex develops already in the accelerating phase of the flow.

Experiment no. 2 (series 4)
Q_m = 4.5 1/s, T = 60s

——— no. 1, starting time 15.5s

——·—— no. 2, starting time 24.5s

– – – – – no. 3, starting time 32.7s

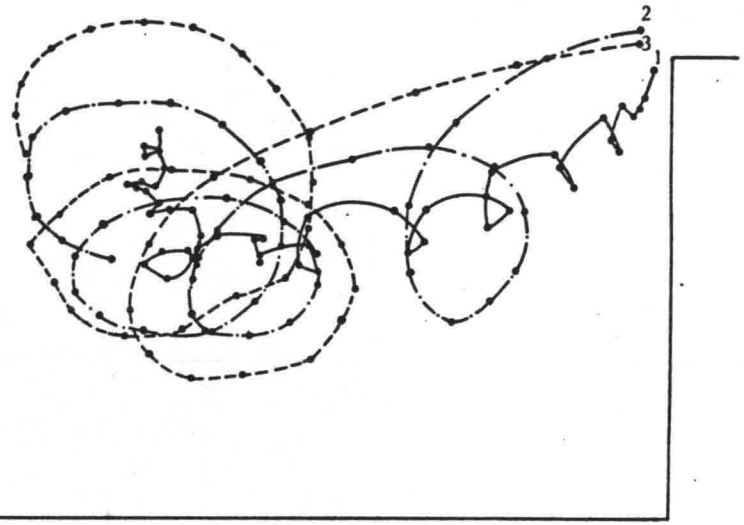

Fig. 4.9. Float trajectories (Q_m = 4.5 1/s, T = 60 s).

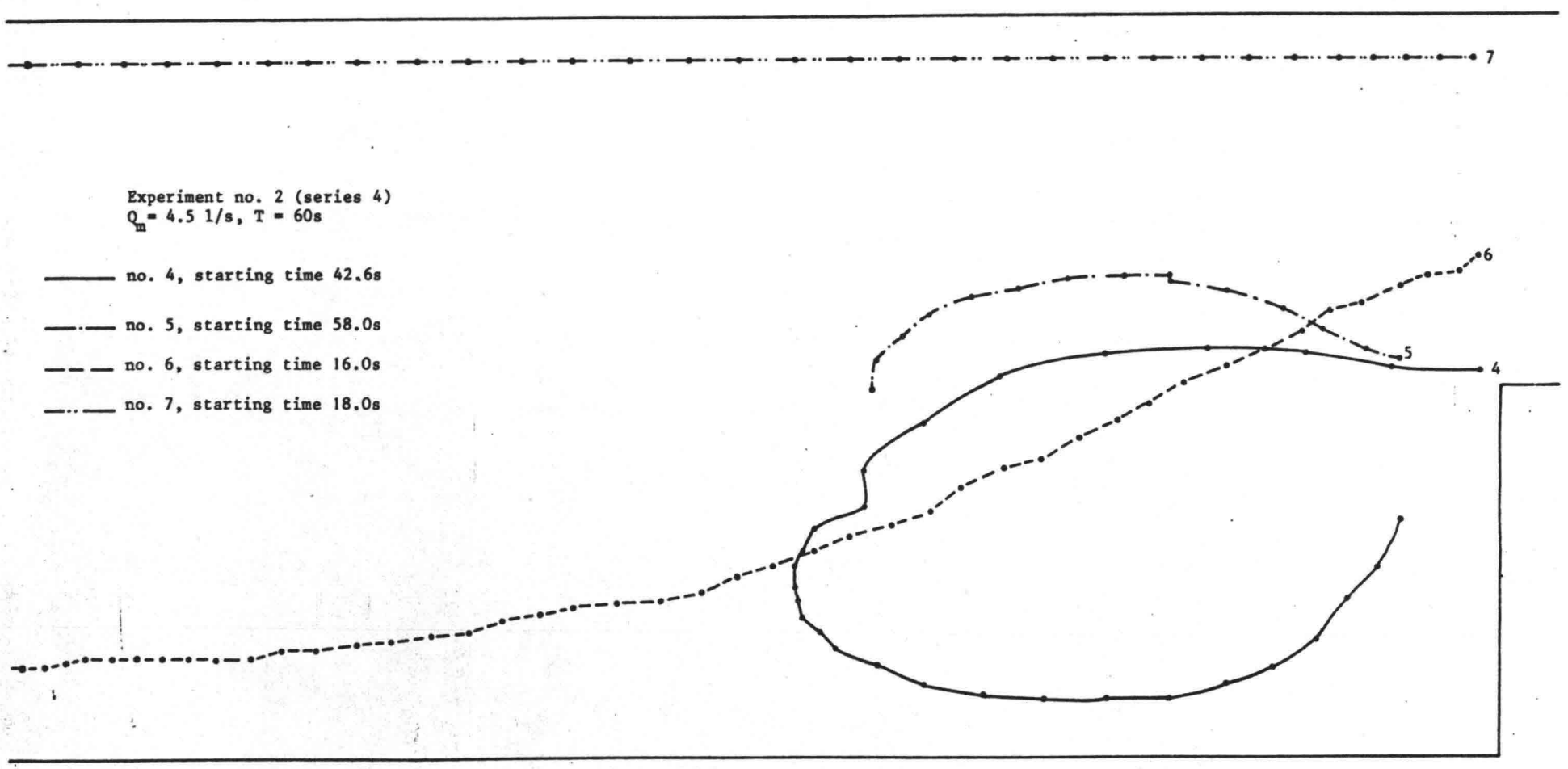

Fig. 4.10. Float trajectories (Q_m = 4.5 1/s, T = 60 s).

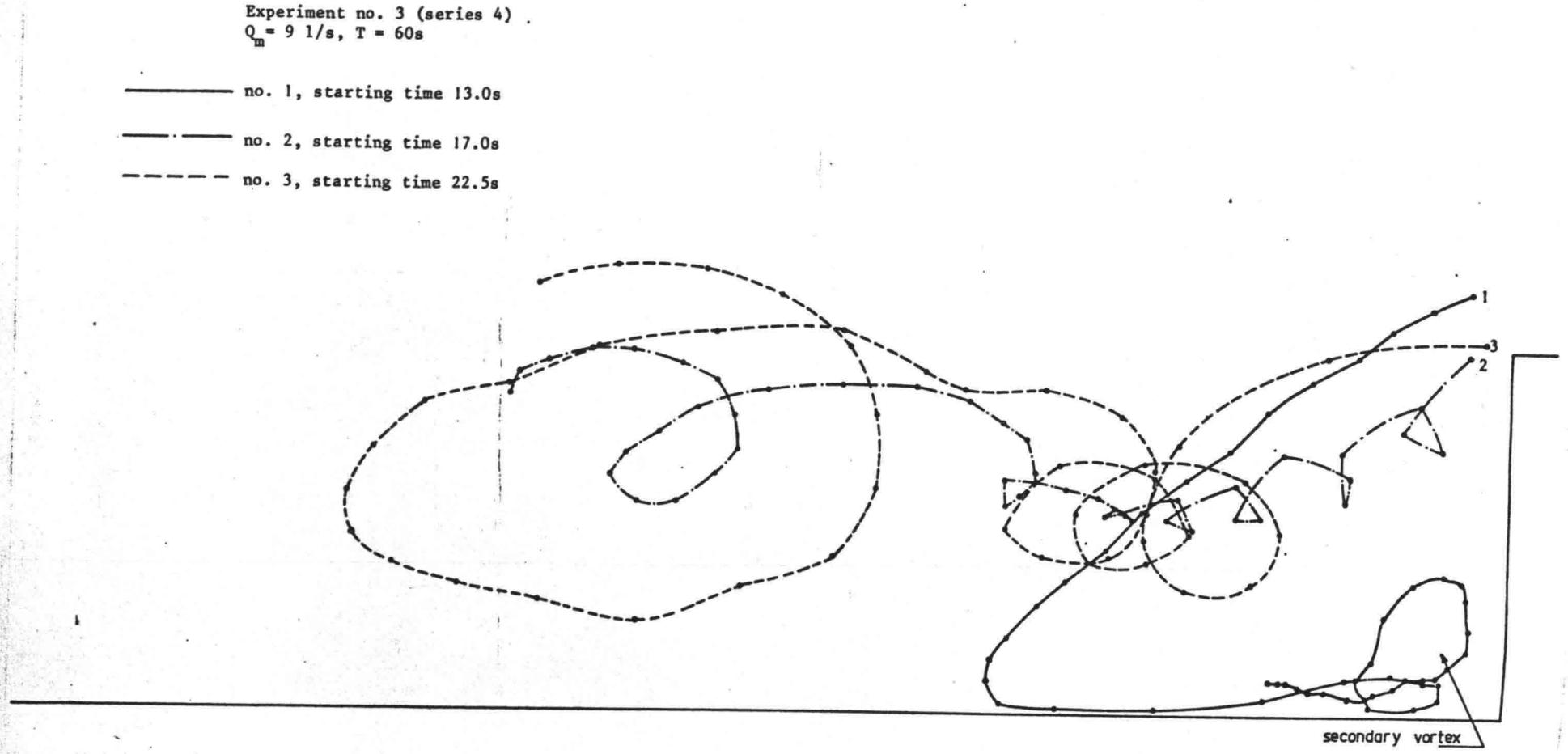

Fig. 4.11. Float trajectories (Q_m = 9 l/s, T = 60 s).

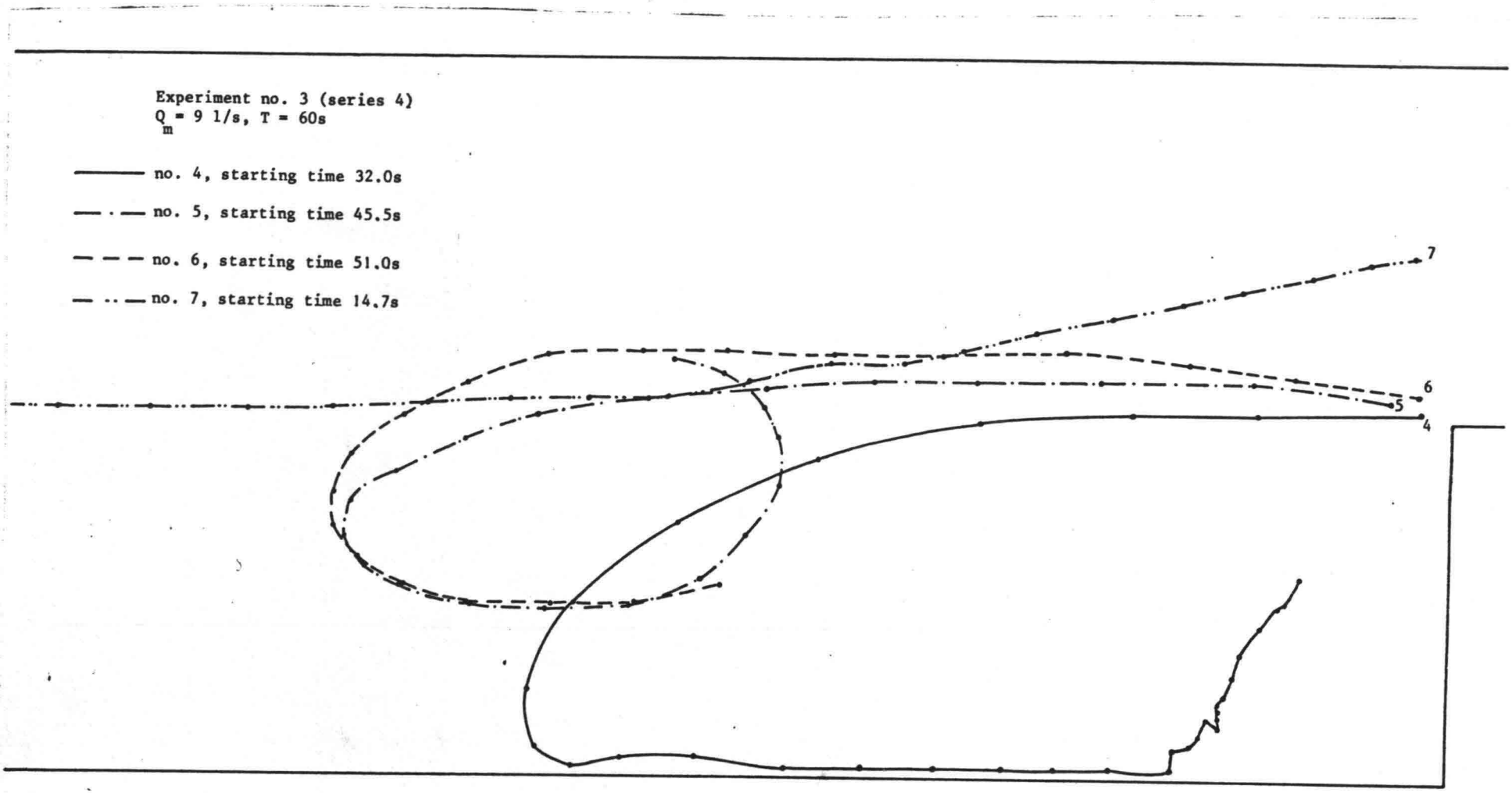

Fig. 4.12. Float trajectories (Q_m = 9 1/s, T = 60 s).

Probably trajectory no. 4 in fig. 4.12 is affected by the secondary vortex in the later phase of the experiment. It is possible to compute depth-averaged velocities from floats trajectories at different time moments. These velocities were also derived from the LDV-measurements and therefore the results obtained from the float trajectories will not be included here. It is not easy to compare the results, because in most cases the float trajectories are not going through the LDV-measurement verticals in the flume.

4.1.3. Velocity distributions obtained from LDV-measurements

The ensemble-averaging method is too laborious to obtain velocity distributions from the LDV-measurements in every profile at different depths. To obtain velocities it was therefore intended to measure only once at several depths (mostly three) and to record these measurements on the HP-recorder paper, and to integrate over the depth to determine depth-averaged velocities afterwards.

Unfortunately, it was not possible to draw velocity profiles from these recordings. The unsteadiness of the flow was very strong and the results were not sufficiently stable when considering different measurements, especially inside the separation region. Owing to the small scale (1 mm $\hat{=}$ 1.039 cm/s) the velocity computations are sensitive to small errors. However, the estimates of the average velocities from the recordings were quite acceptable. Anyway some caution should be used when interpreting these results.

The schematical representation of the measurement verticals is given in fig. 4.13. Along the flume we have identified cross sections with characters, and across the flume and in the vertical direction with numbers. The identification F 4/2, for example, means that the profile was F 4 and the measurement point was 2.6 cm above the bottom.
It was impossible to move the laser system close to the opposite wall.
In figures 4.14, 4.15, 4.16, 4.17, 4.18 and 4.19 depth-averaged velocities (in cm/s) are given at different times from the beginning of the experiment (10 s, 20 s, 30 s, 40 s and 50 s, respectively) when Q_m = 9 l/s and T = 60 s.

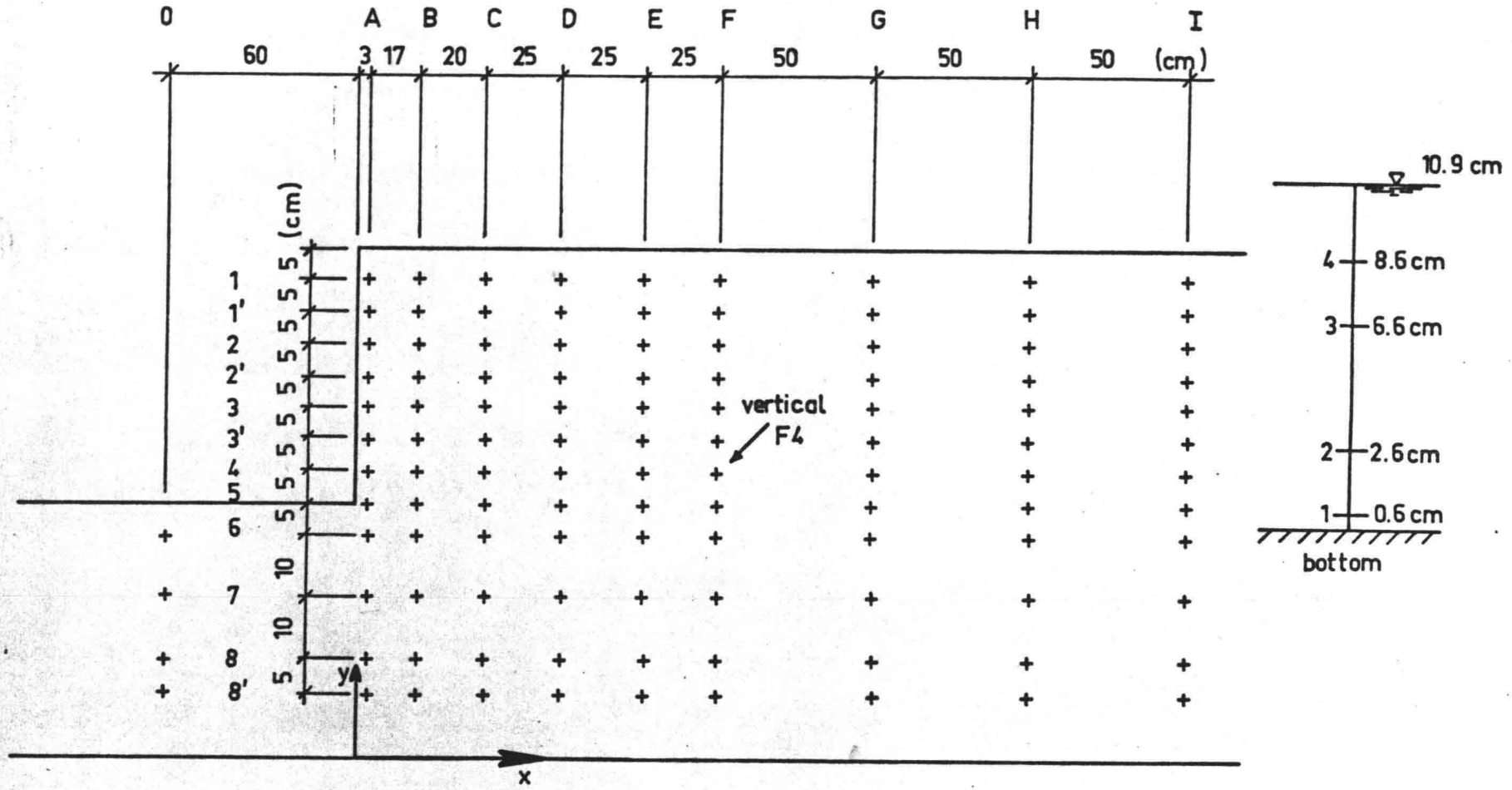

Fig. 4.13. Scheme of the measurement verticals.

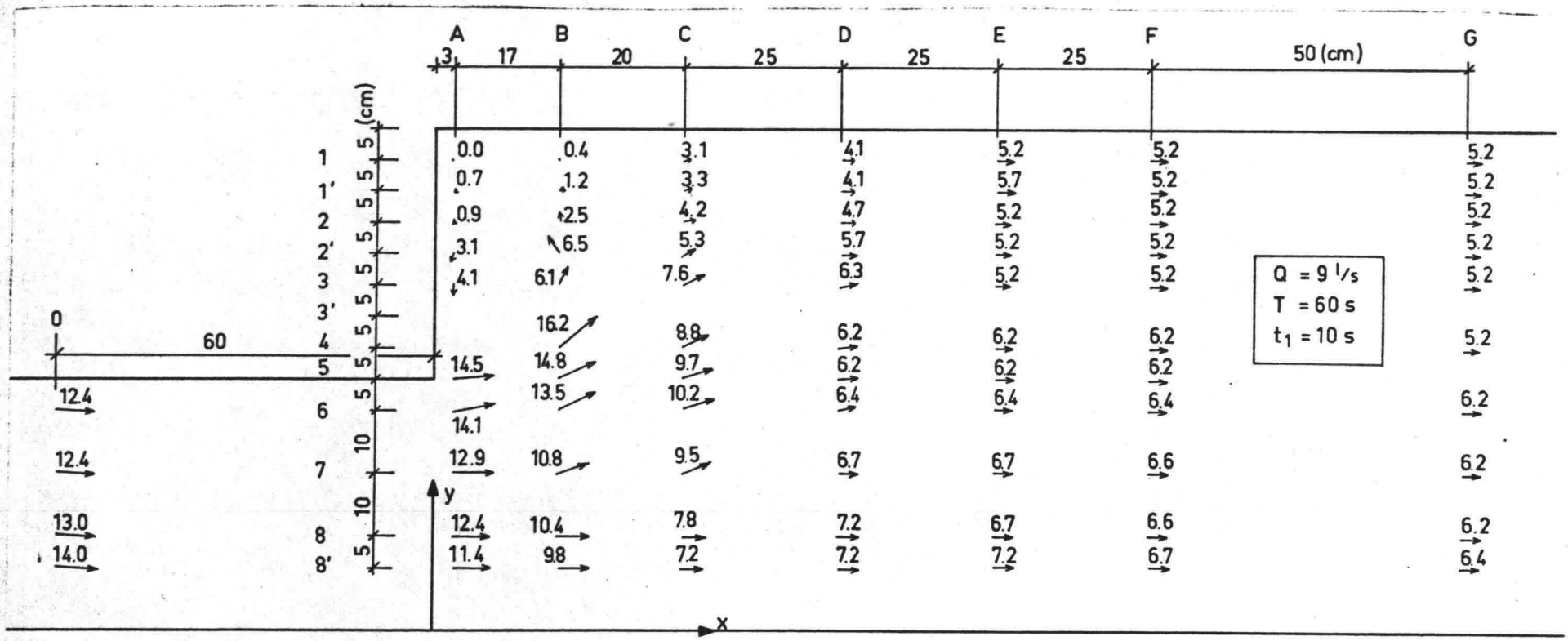

Fig. 4.14. Depth-averaged velocities (Q_m = 9 l/s, T = 60 s, t_1 = 10 s).

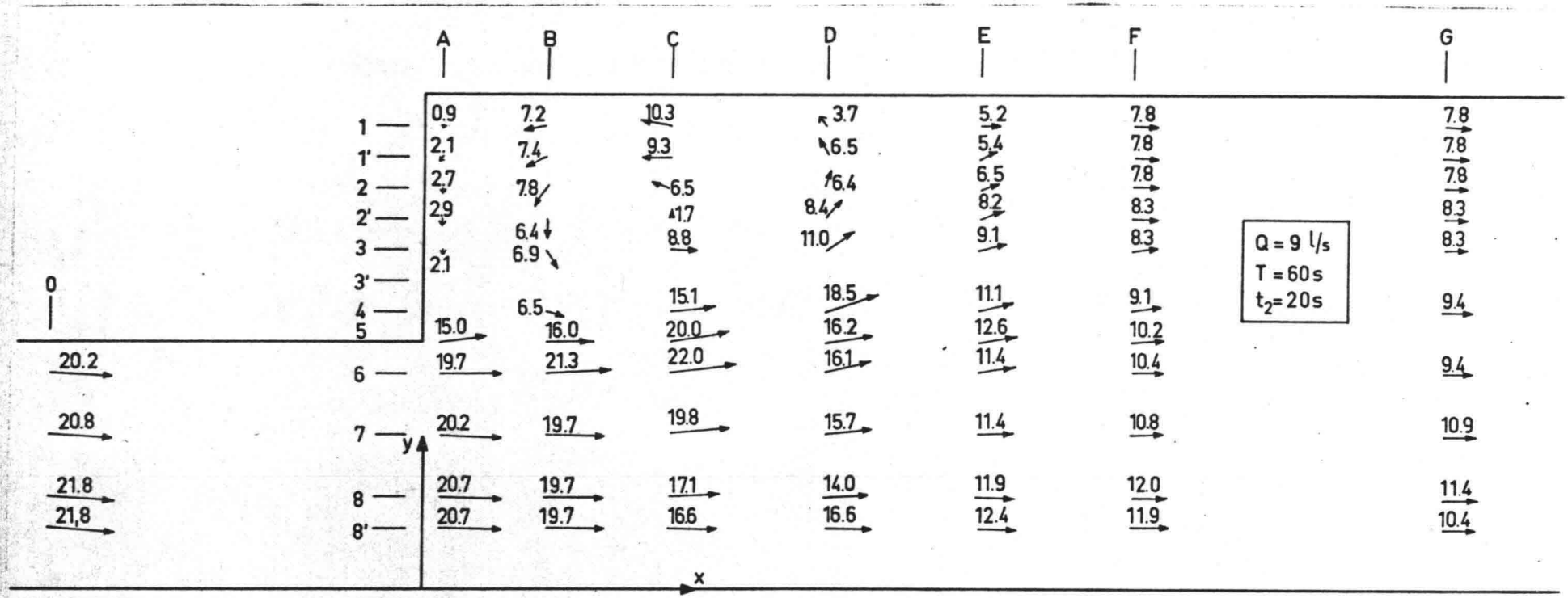

Fig. 4.15. Depth- averaged velocities (Q_m = 9 l/s, T = 60 s, t_2 = 20 s).

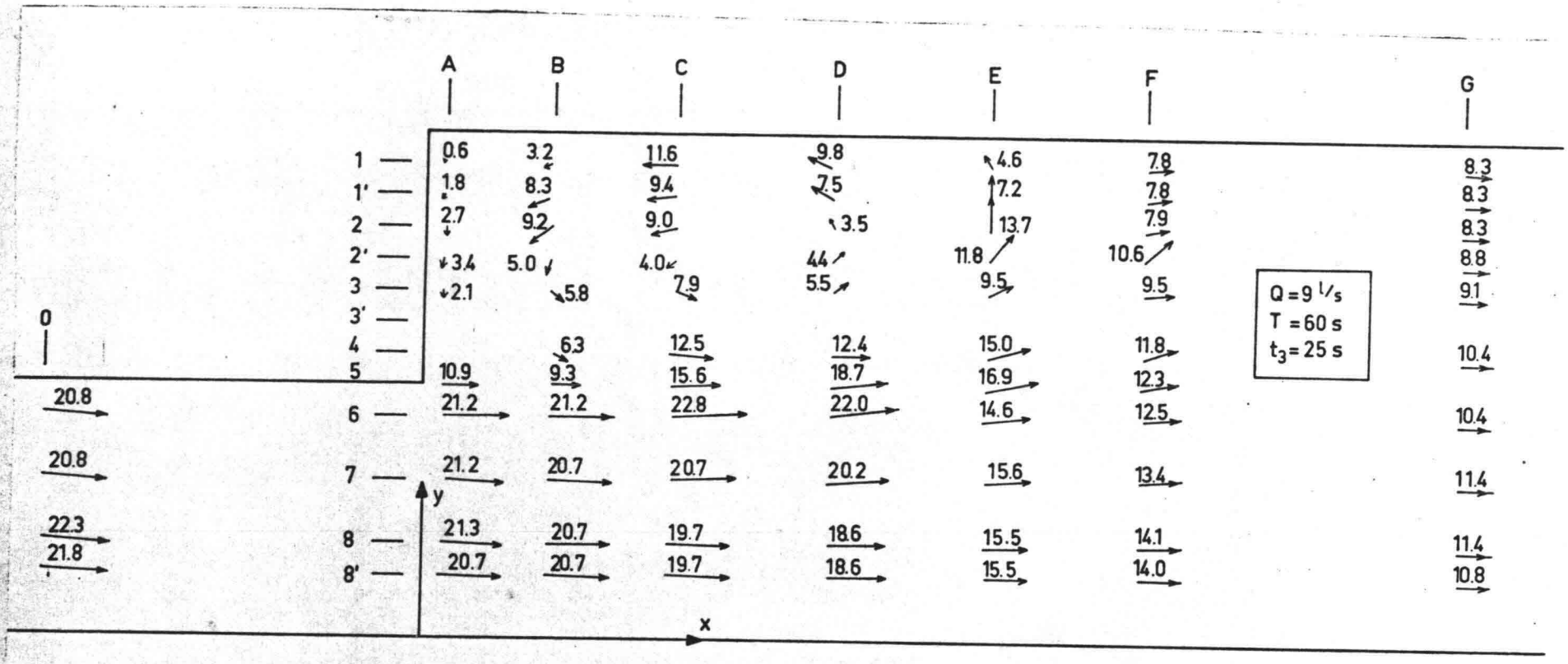

Fig. 4.16. Depth-averaged velocities (Q_m = 9 l/s, T = 60 s, t_3 = 25 s).

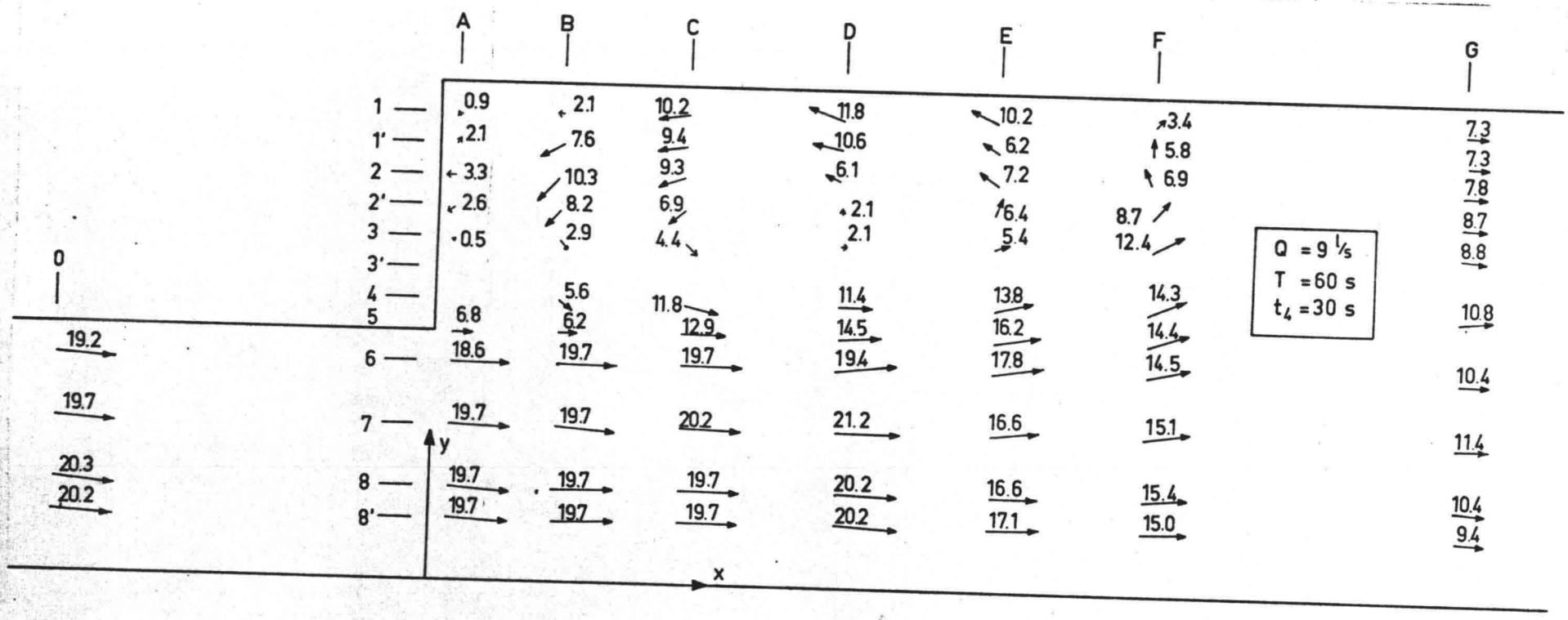

Fig. 4.17. Depth-averaged velocities (Q_m = 9 l/s, T = 60 s, t_4 = 30 s).

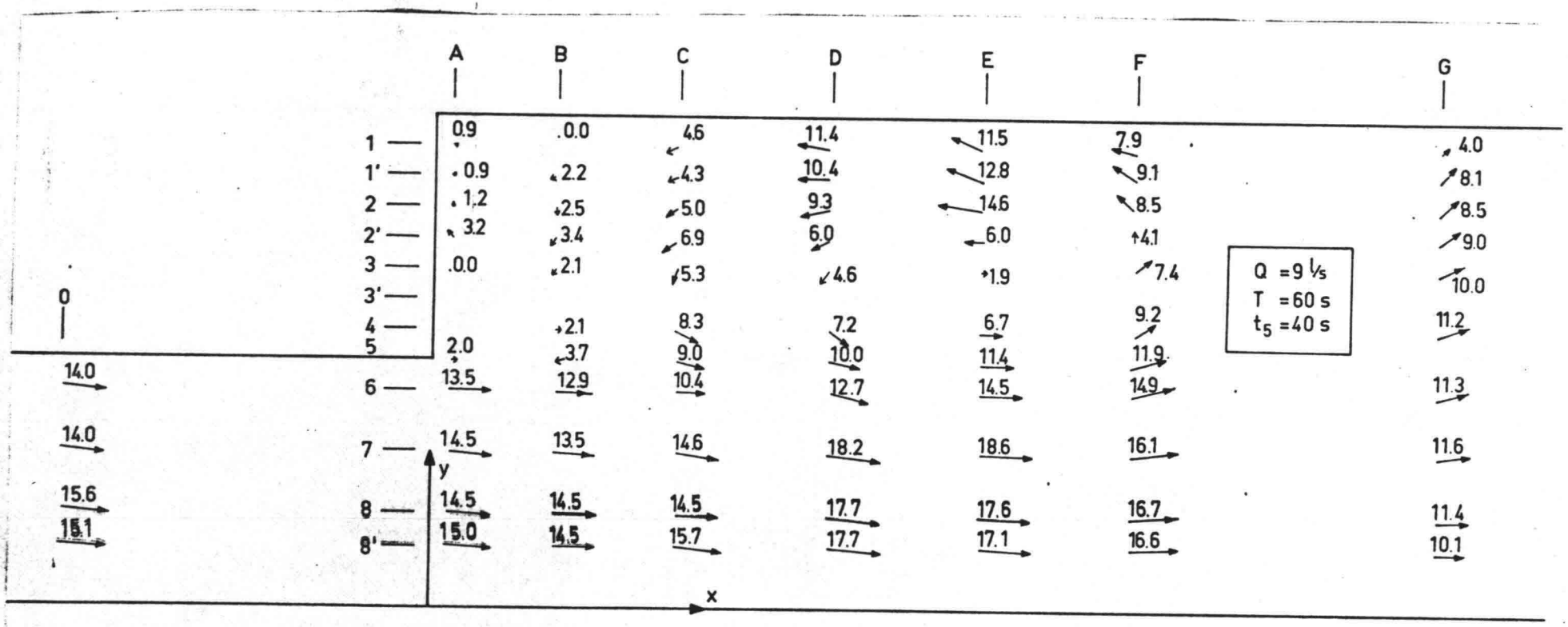

Fig. 4.18. Depth-averaged velocities (Q_m = 9 l/s, T = 60 s, t_5 = 40 s).

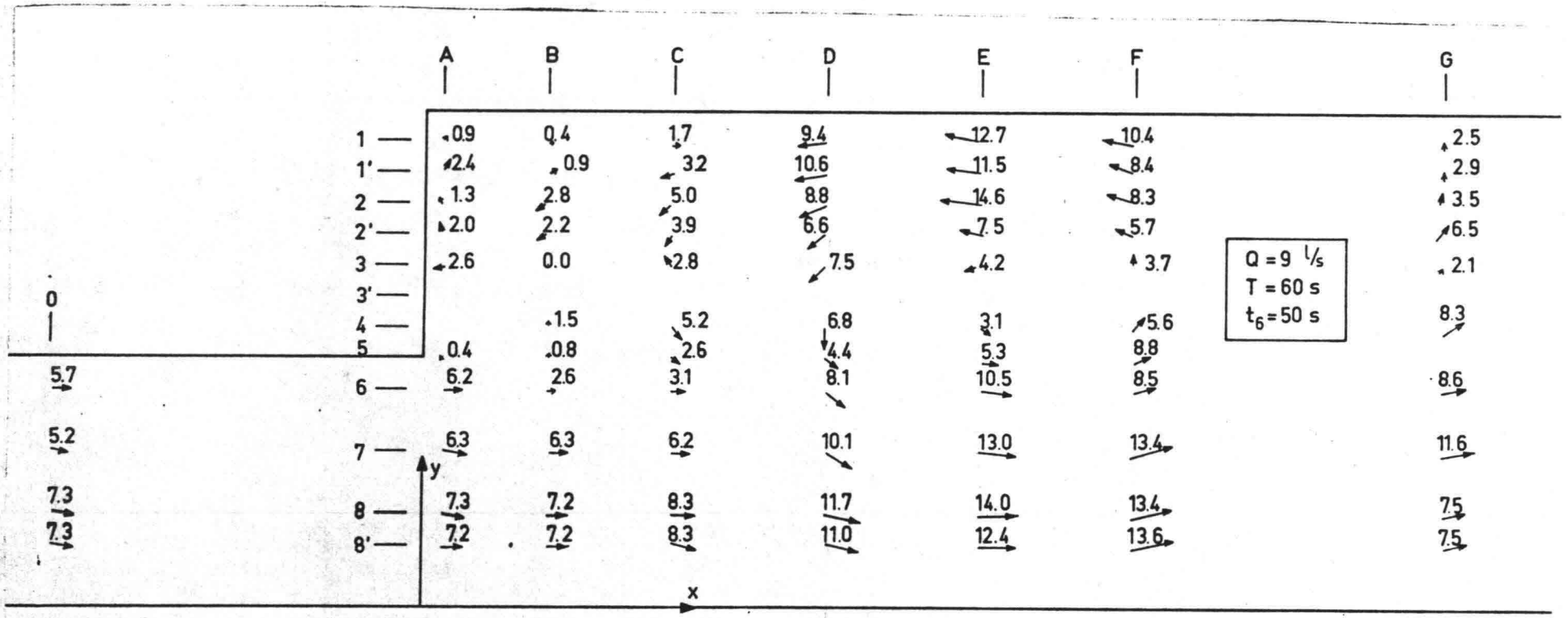

Fig. 4.19. Depth-averaged velocities (Q_m = 9 1/s, T = 60 s, t_6 = 50 s).

The velocity vectors at different time moments give a picture of the motions in the separated region, and also a possibility to calculate flow rates Q according to

$$Q = \int_A u dA \qquad (4.1)$$

Unfortunately, only rough estimates can be obtained because the depth-averaged velocities are calculated from separate single measurements. For comparison we have also the flow rate from the electromagnetic flowmeter.

The velocity vectors in figures 4.18 and 4.19 also indicate the secondary vortex in the corner of the flume.

Similar velocity distributions for Q_m = 16 1/s and T = 90 s are given in figures 4.20 to 4.27.

The secondary vortex develops faster, it can be seen already at 30 seconds after the starting of the flow. In the corner of the flume the water is hardly moving at the end of the experiment. From the velocity directions close to the opposite wall we can conclude that the presence of the wall accelerates the main flow adjacent to the separation region (fig. 4.23 and 4.24).

To obtain estimates about the flow rates in the flume it is necessary to know the water-level variations during the measurements. The water-level changes for Q_m = 9 1/s, T = 60 s in different measurement sections are given (in mm) in figs. 4.28 and 4.29, and for Q_m = 16 1/s, T = 90 s in figs. 4.30 and 4.31.

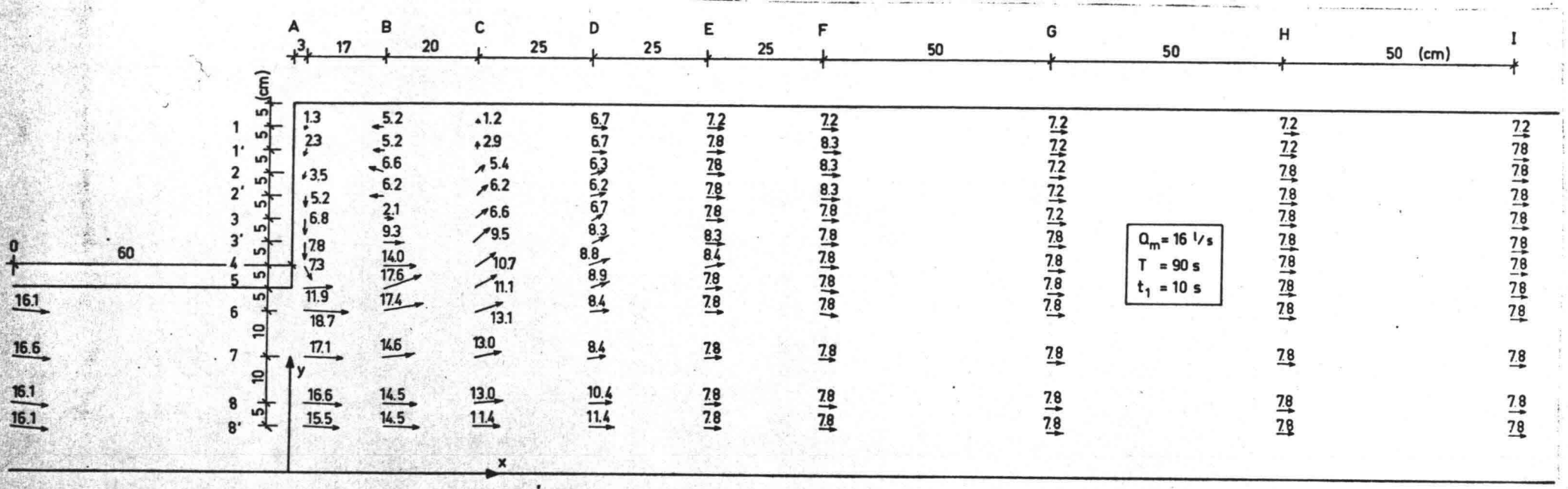

Fig. 4.20. Depth-averaged velocities (Q_m = 16 1/s, T = 90 s, t_1 = 10 s).

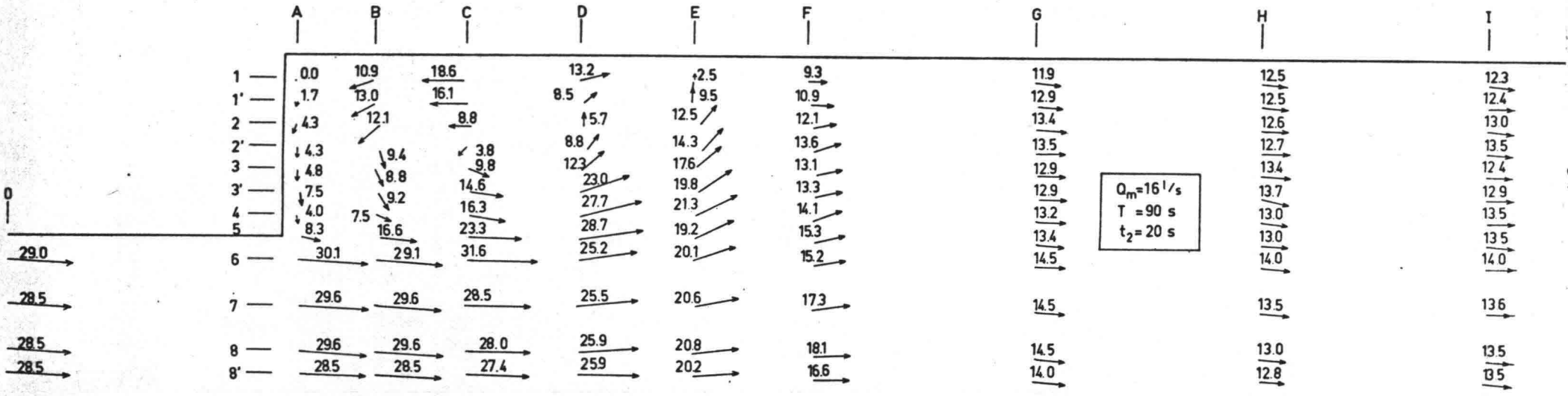

Fig. 4.21. Depth-averaged velocities (Q_m = 16 1/s, T = 90 s, t_2 = 20 s).

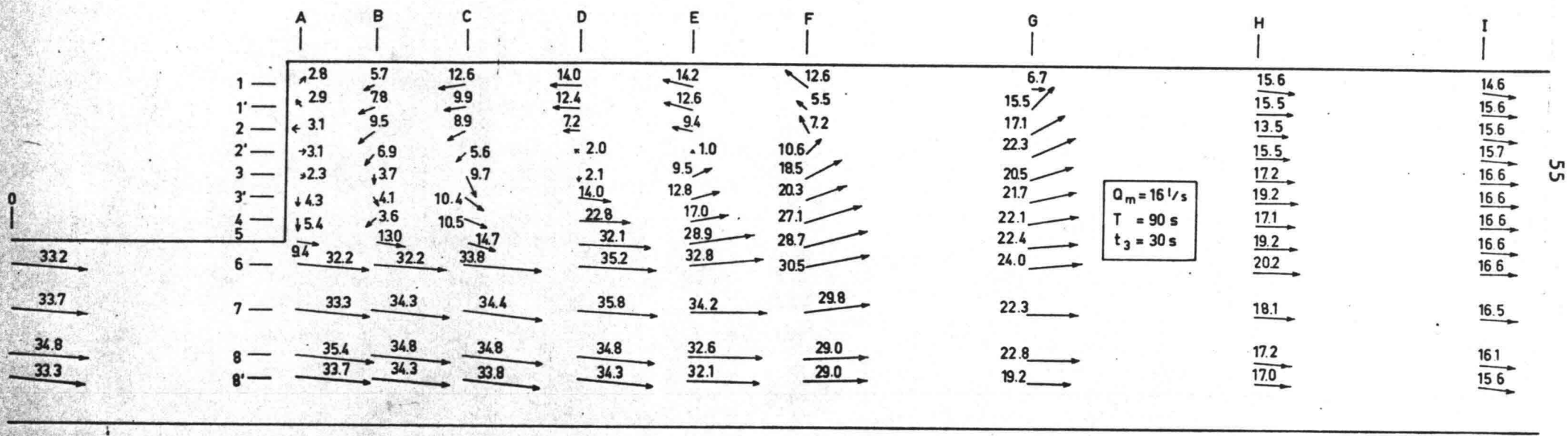

Fig. 4.22. Depth-averaged velocities (Q_m = 16 l/s, T = 90 s, T_3 = 30 s).

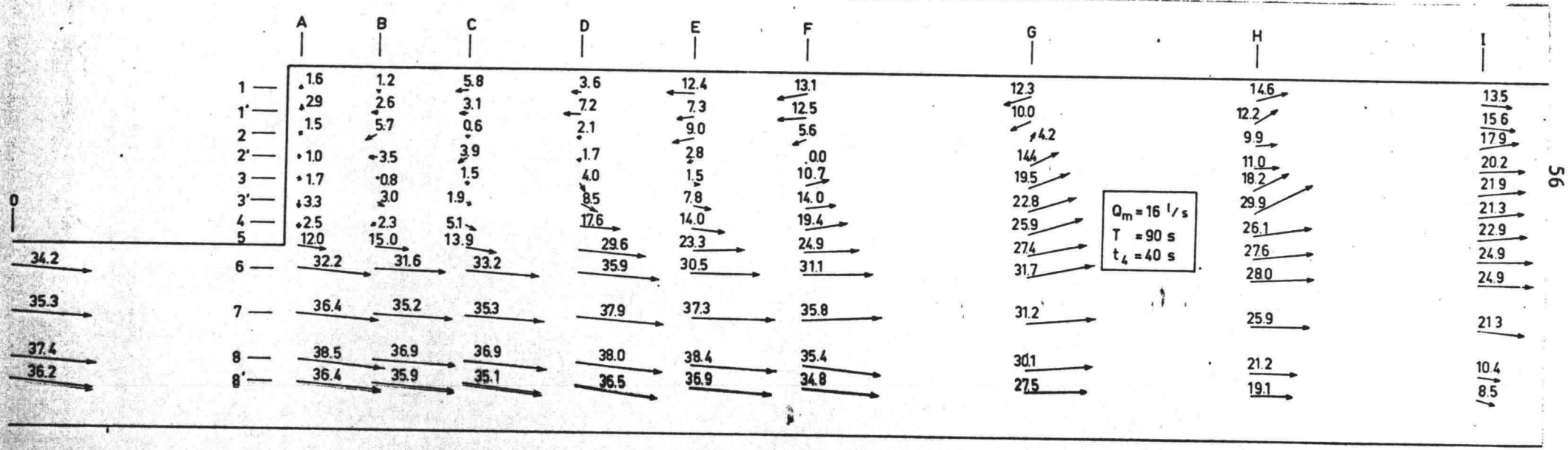

Fig. 4.23. Depth-averaged velocities (Q_m = 16 1/s, T = 90 s, t_4 = 40 s).

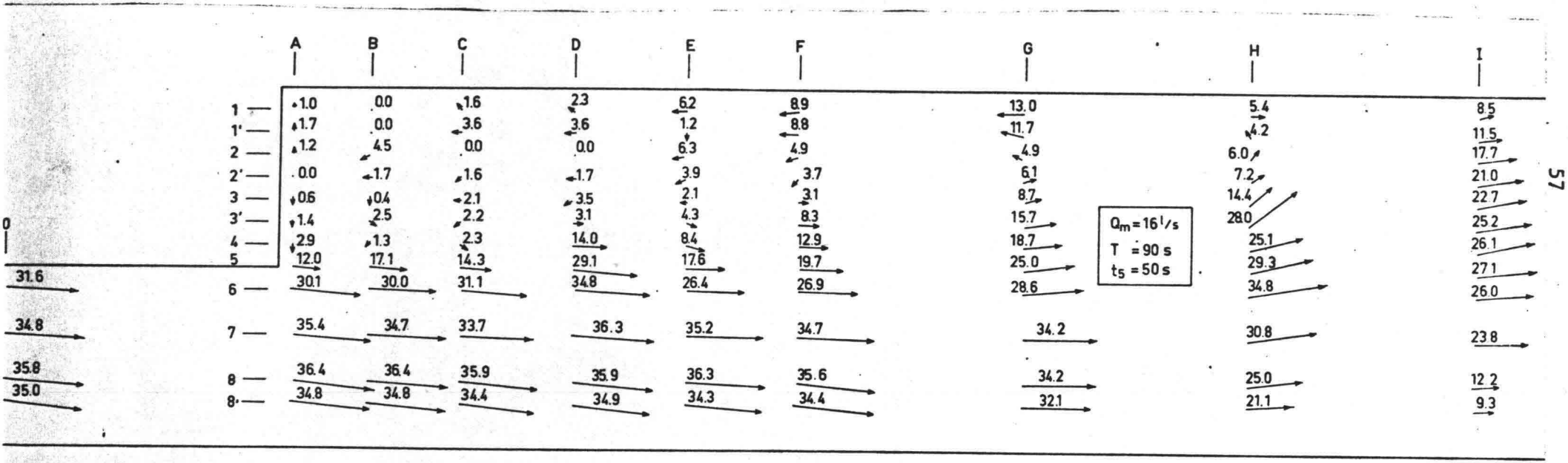

Fig. 4.24. Depth-averaged velocities (Q_m = 16 l/s, T = 90 s, t_5 = 50 s).

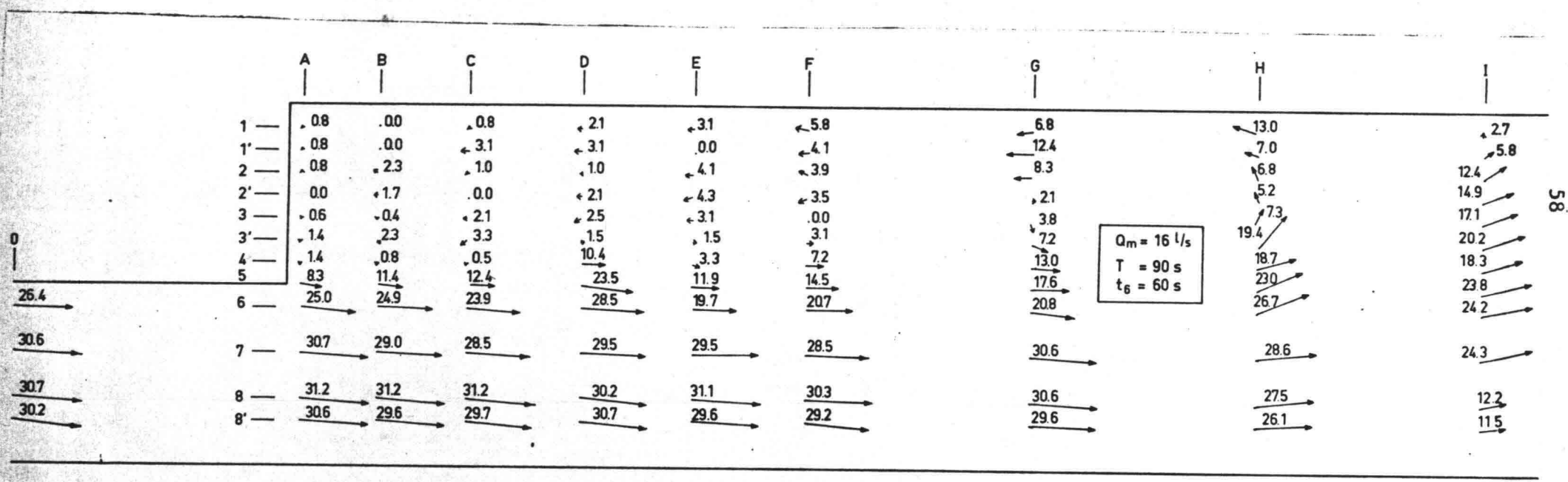

Fig. 4.25. Depth-averaged velocities (Q_m = 16 1/s, T = 90 s, t_6 = 60 s).

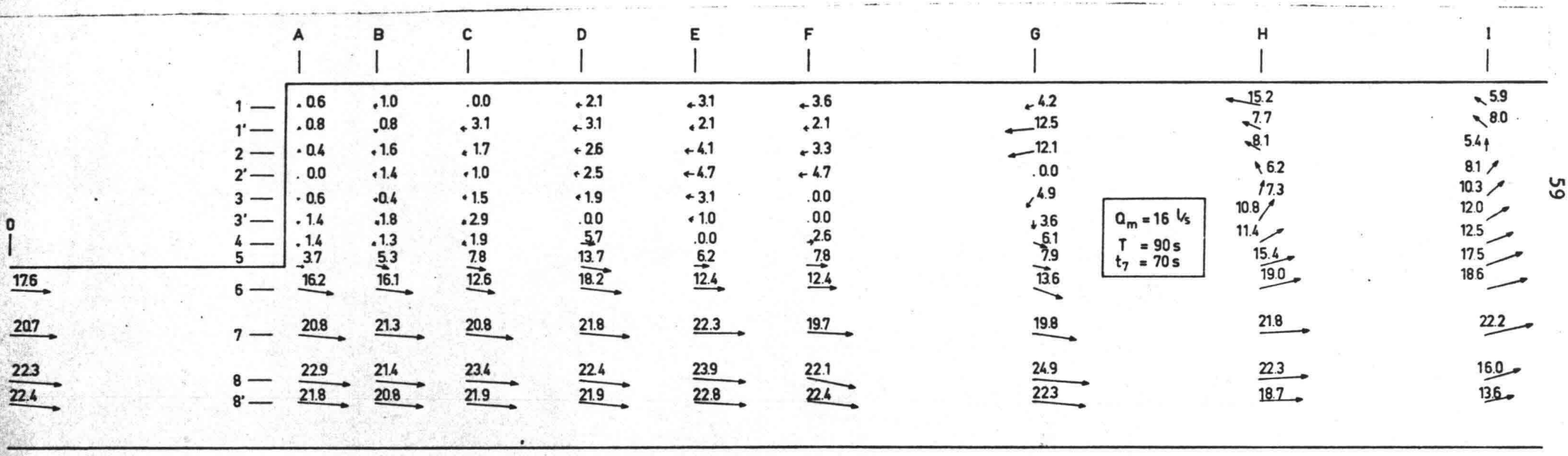

Fig. 4.26. Depth-averaged velocities (Q_m = 16 1/s, T = 90 s, t_7 = 70 s).

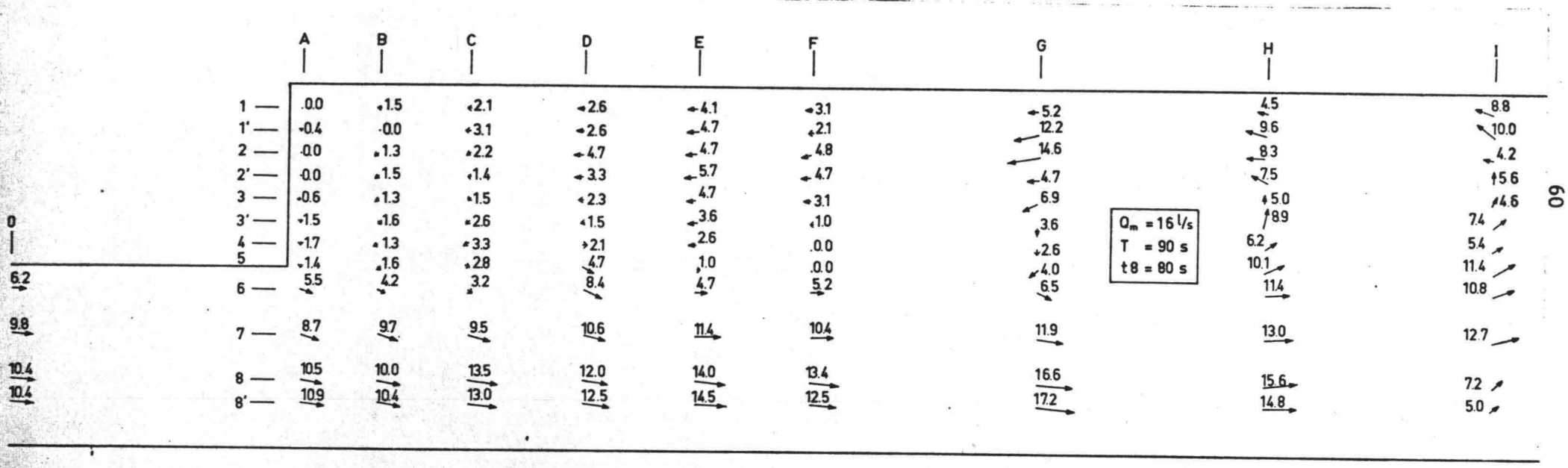

Fig. 4.27. Depth-averaged velocities (Q_m = 16 1/s, T = 90 s, t_8 = 80 s).

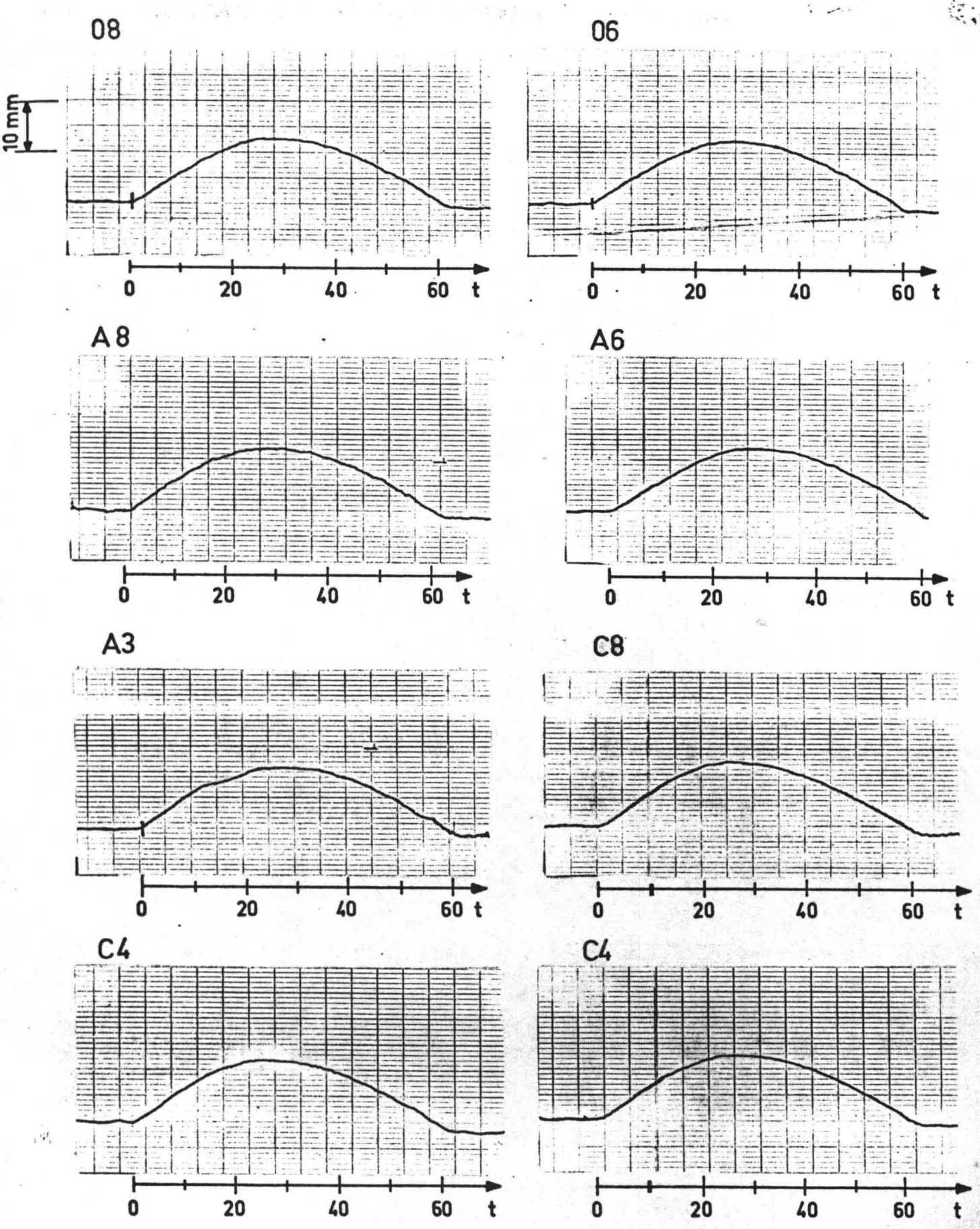

Fig. 4.28. Water-level variations (Q_m = 9 l/s, T = 60 s).

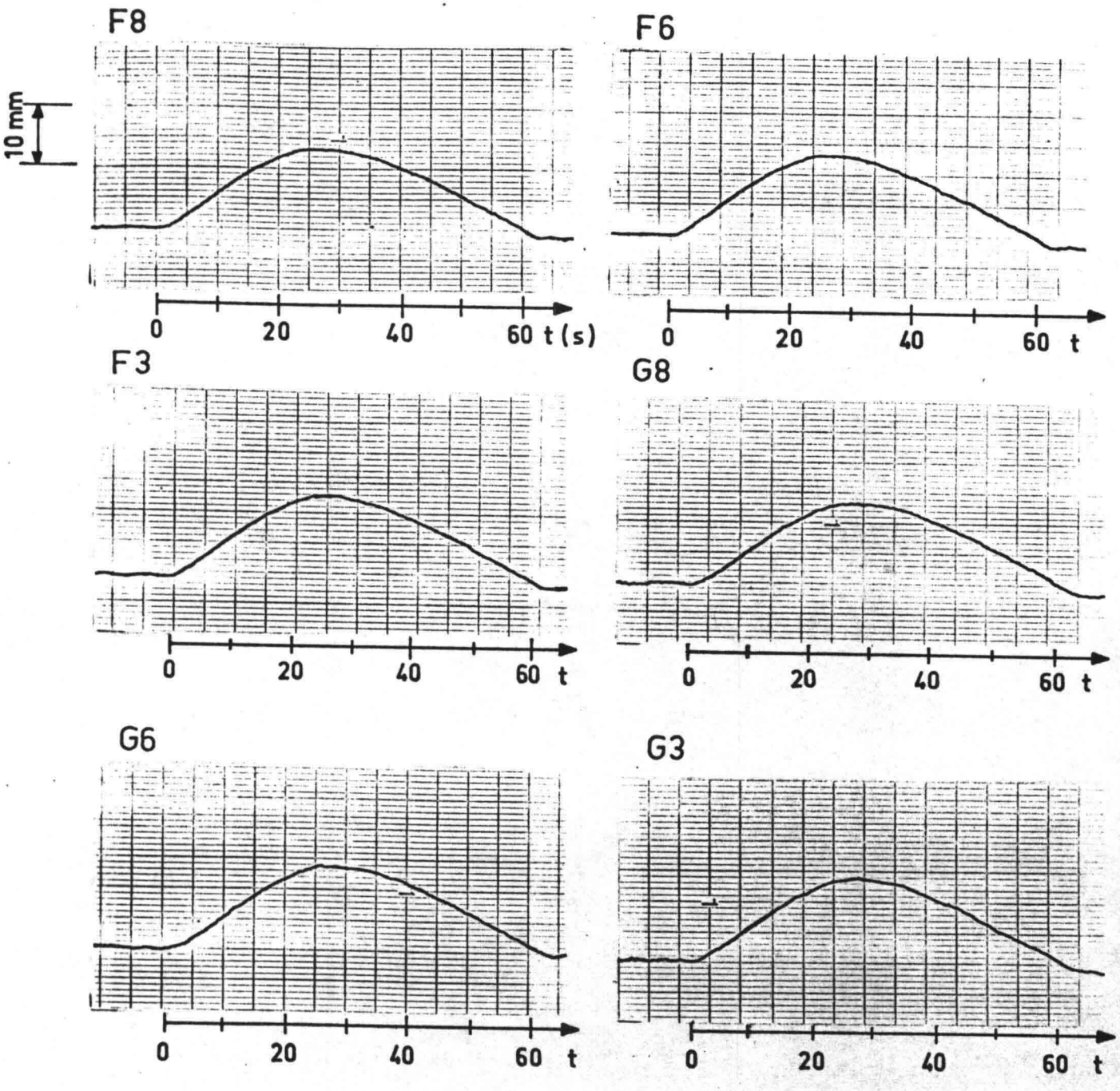

Fig. 4.29. Water-level variations (Q_m = 9 **l/s**, T = 60 s).

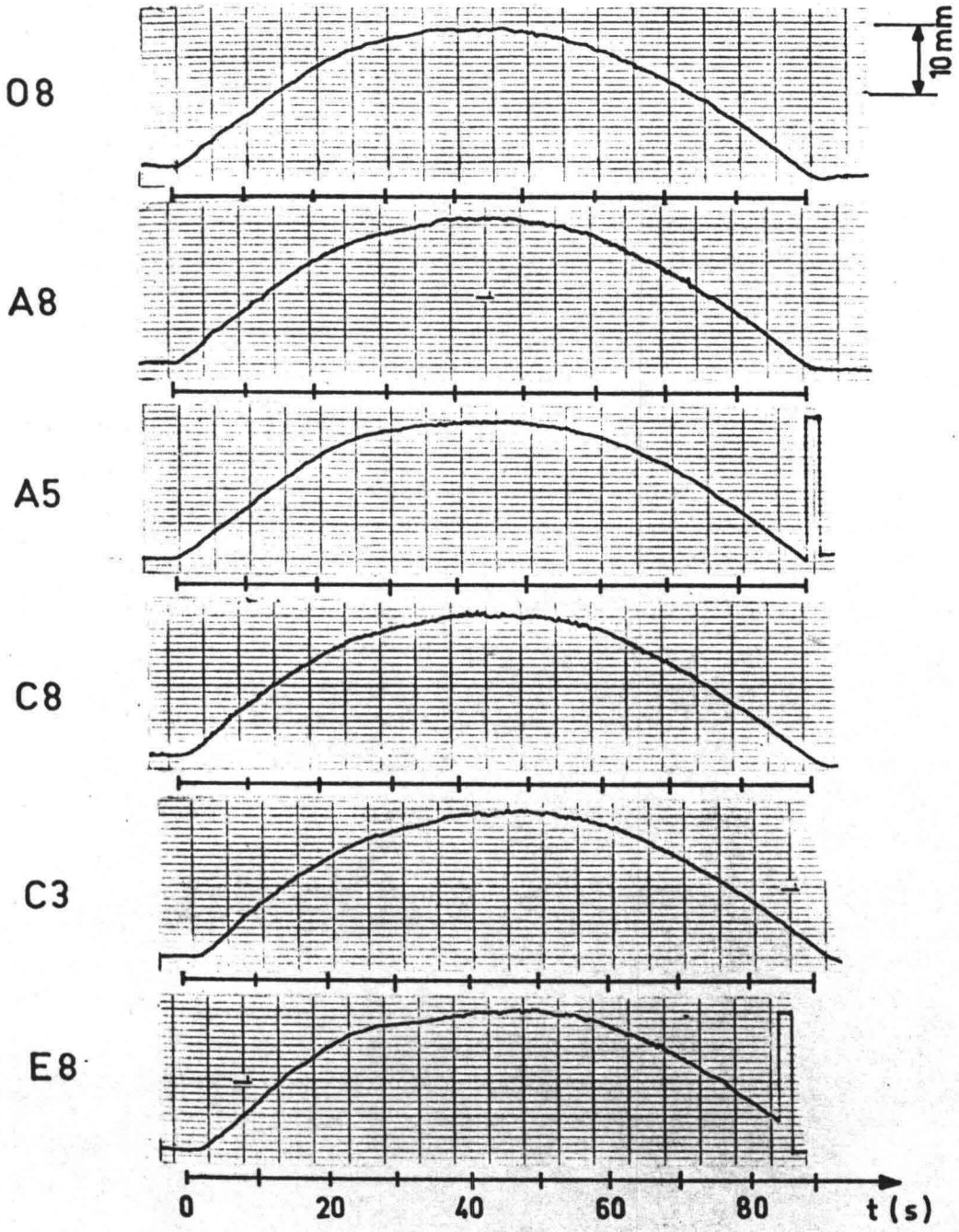

Fig. 4.30. Water-level variations (Q_m = 16 l/s, T = 90 s).

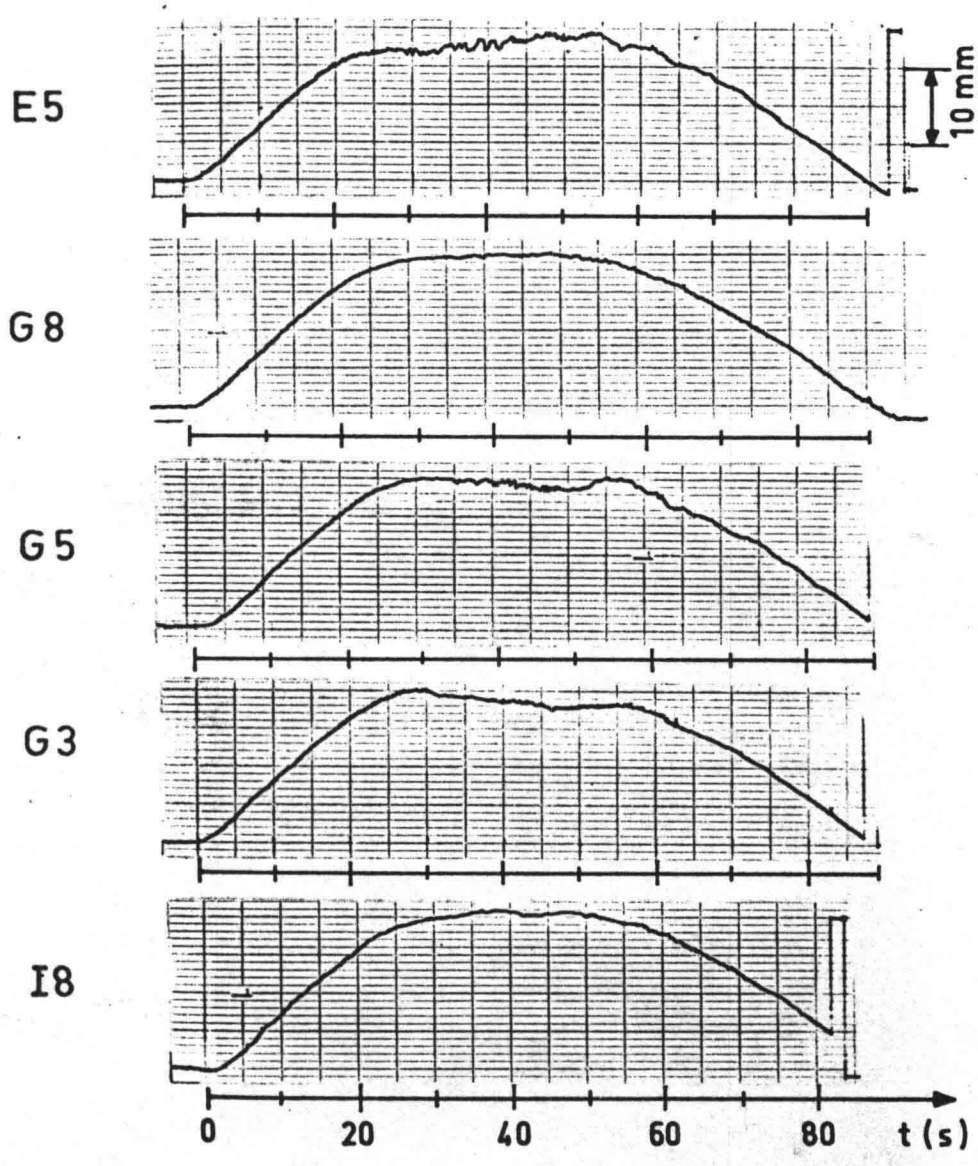

Fig. 4.31. Water-level variations (Q_m = 16 1/s, T = 90 s).

4.2. Turbulence measurements

It is difficult to obtain mean-velocities from a single measurement of the velocity in unsteady flow, not to speak of the characteristics of the turbulence. The main part of this investigation was concerned with the application of the ensemble-averaging technique to obtain the characteristics of the turbulence (see section 3.1). The main flow rate was Q_m = 9 l/s, but some measurements were made with Q_m = 16 l/s, especially in the mixing-layer between separation region and main flow.

Quantities shown in the following figures are:

- ensemble-averaged mean velocities u and v ;
- standard deviations of turbulence fluctuations σ_u and σ_v;
- Reynolds stresses $\overline{u'v'}$;
- a measure of the turbulence energy E calculated from

$$E = 1/2\ (\sigma_u^2 + \sigma_v^2)\ . \qquad (4.2)$$

The profiles of the mentioned characteristics in different measuring sections at a flow rate Q_m = 9 l/s are given in figures 4.32 to 4.40. Water-level changes were estimated also. The flow is quite complicated; the velocity is changing abruptly when the measuring point is affected by the moving vortex. We have also changes of sign of the velocity during development of the separation zone. All profiles are built up from measurements at three different depths. The possibility to measure close to the water surface was restricted, because of the influence on the flow of the plastic cover and the varying water-level. The profiles are drawn through the three measured values. This is inaccurate in some cases; profiles are then just extrapolated up to the free surface. At some moments the distributions of the turbulence characteristics are not drawn, because in the beginning of the experiments we have laminar flow.

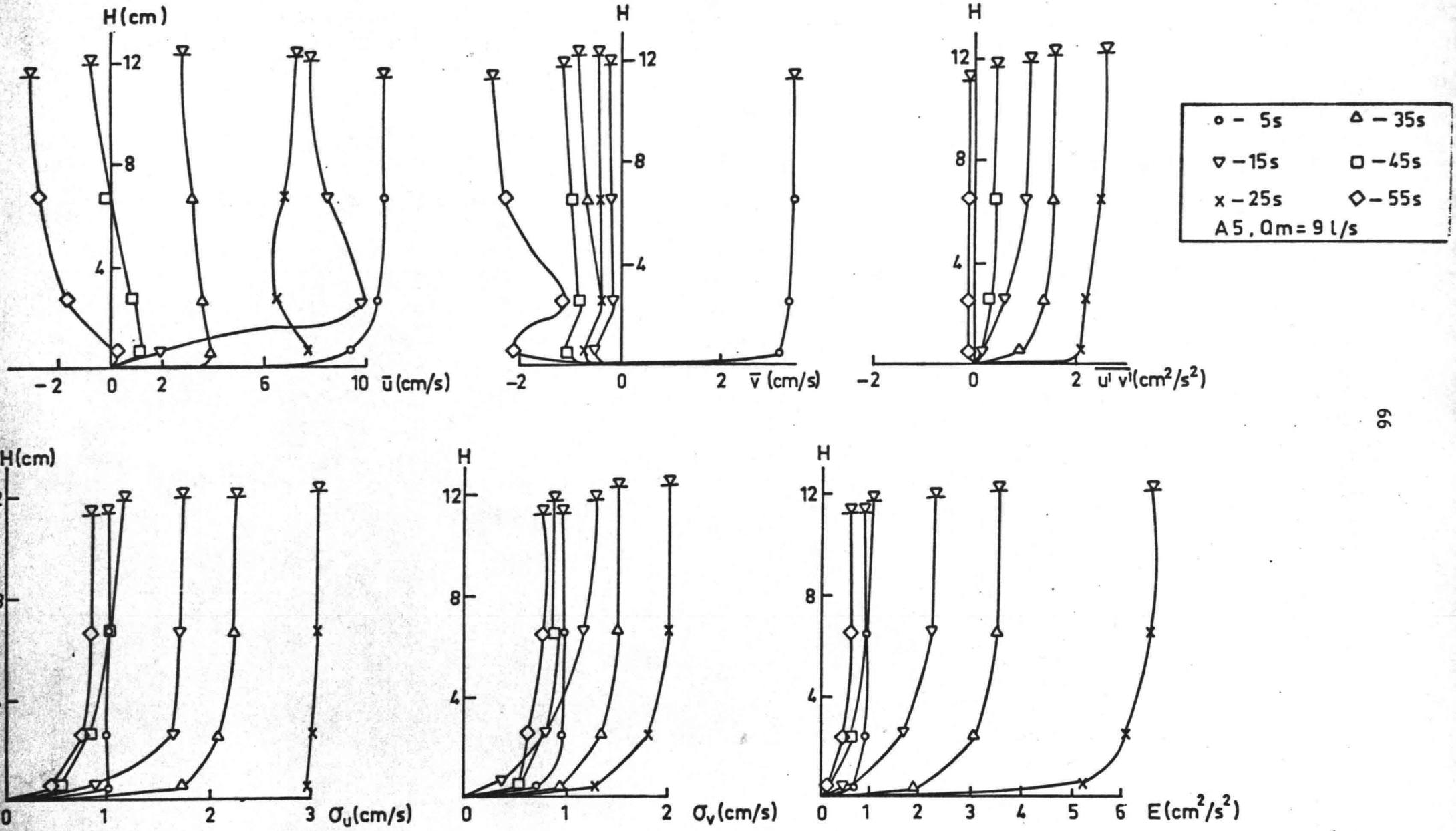

Fig. 4.32. Profile A 5, Q_m = 9 l/s.

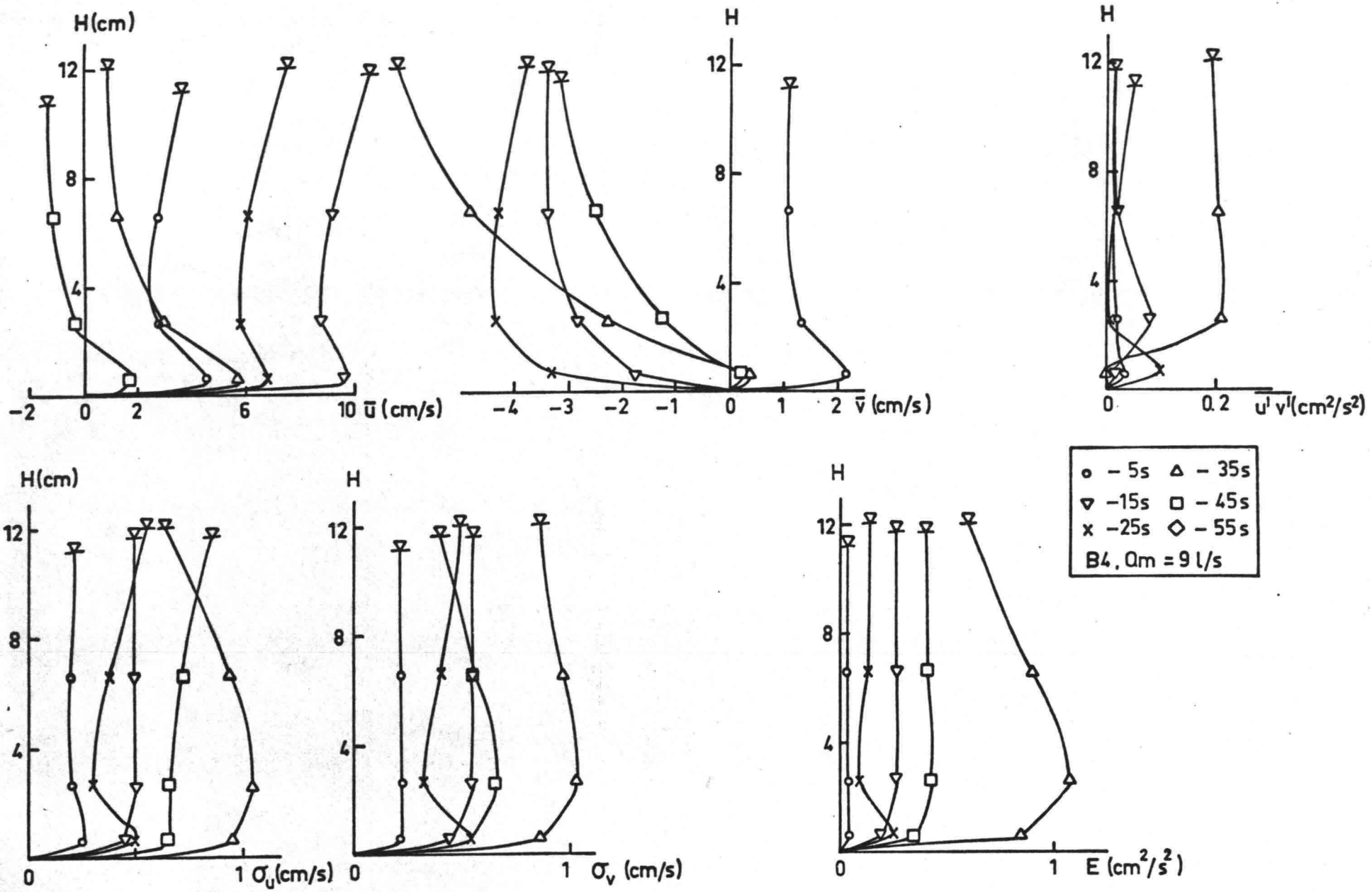

Fig. 4.33. Profile B 4, Q_m = 9 l/s.

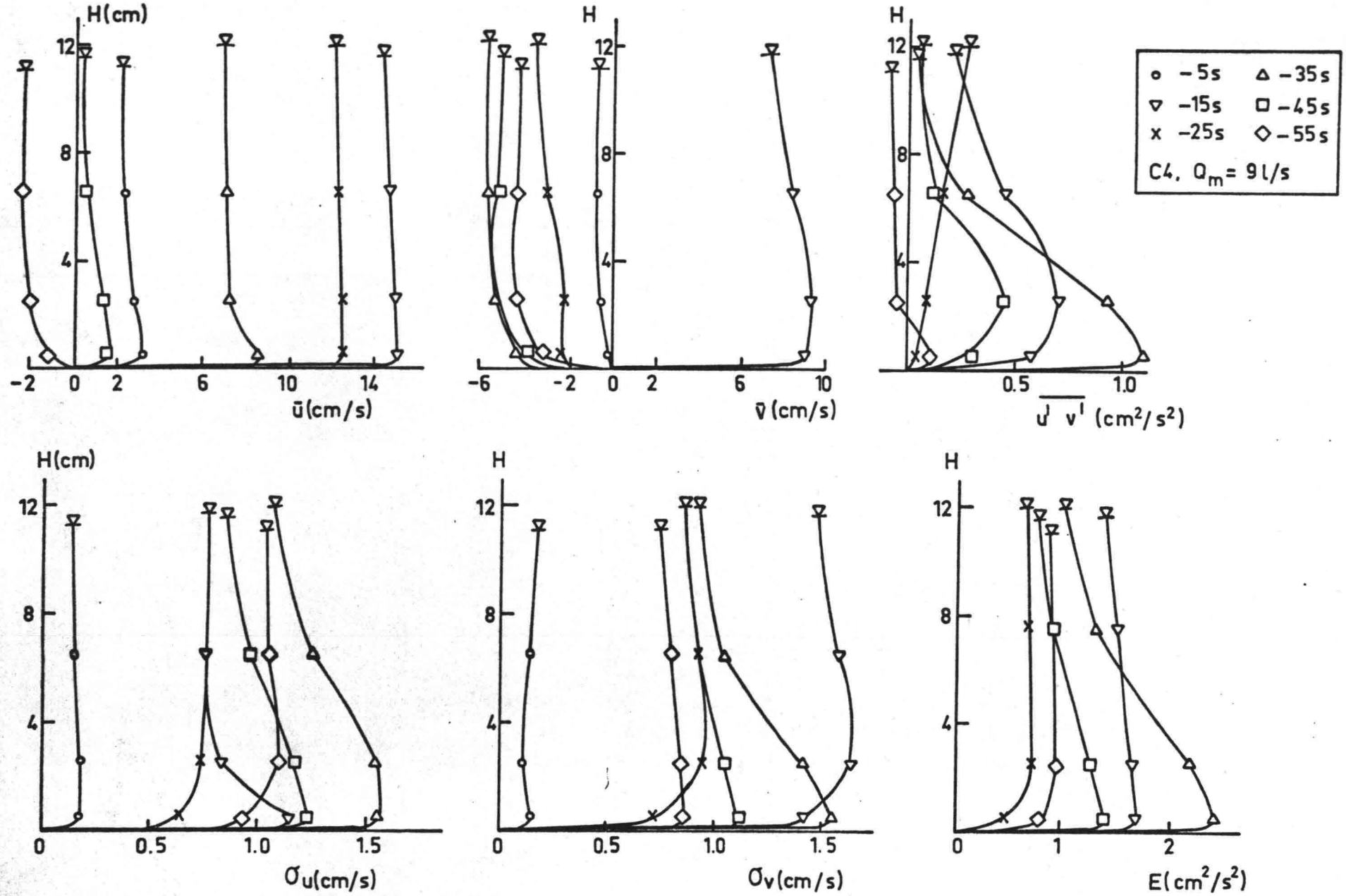

Fig. 4.34. Profile C 4, Q_m = 9 l/s.

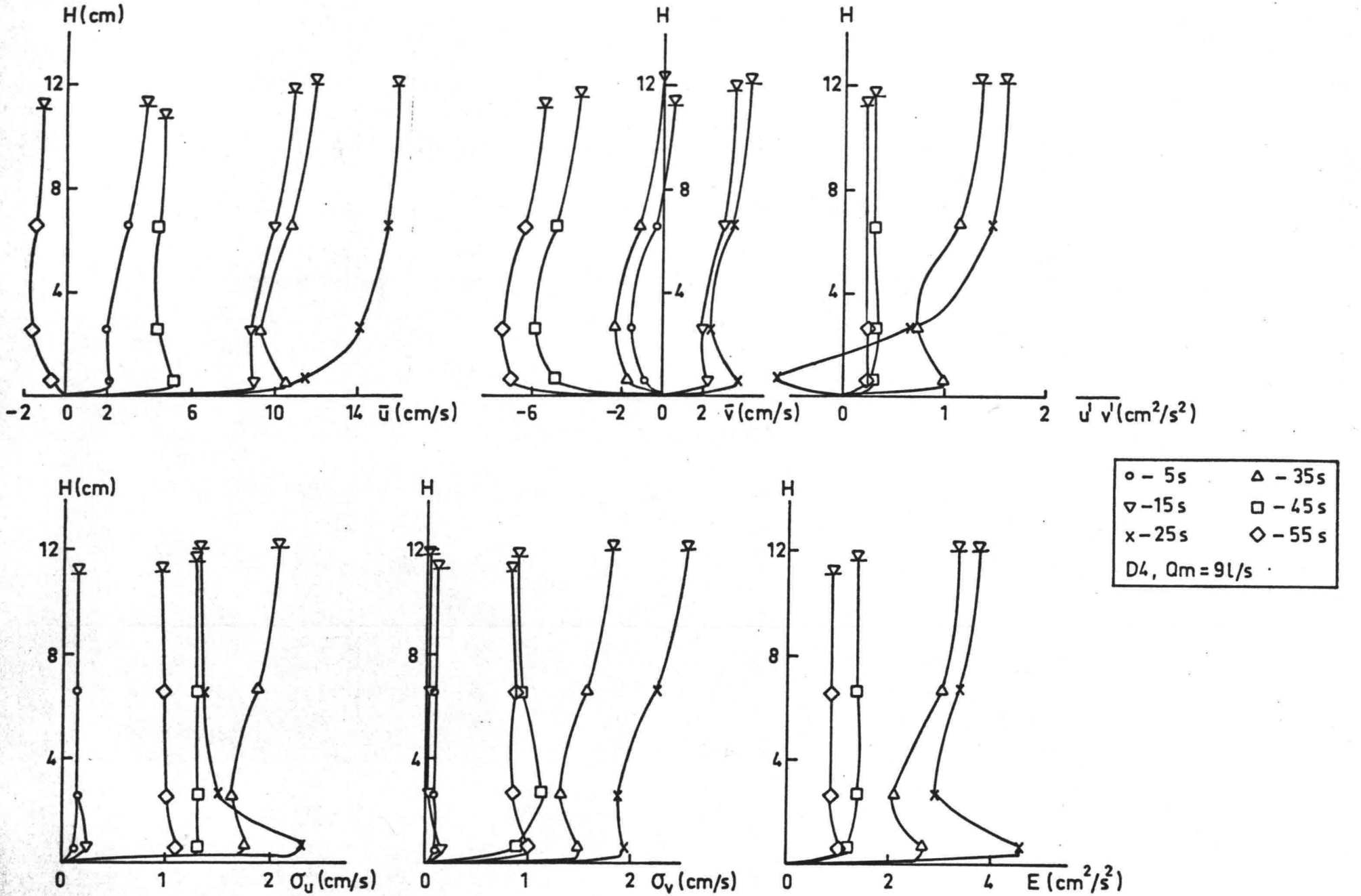

Fig. 4.35. Profile D 4, Q_m = 9 l/s.

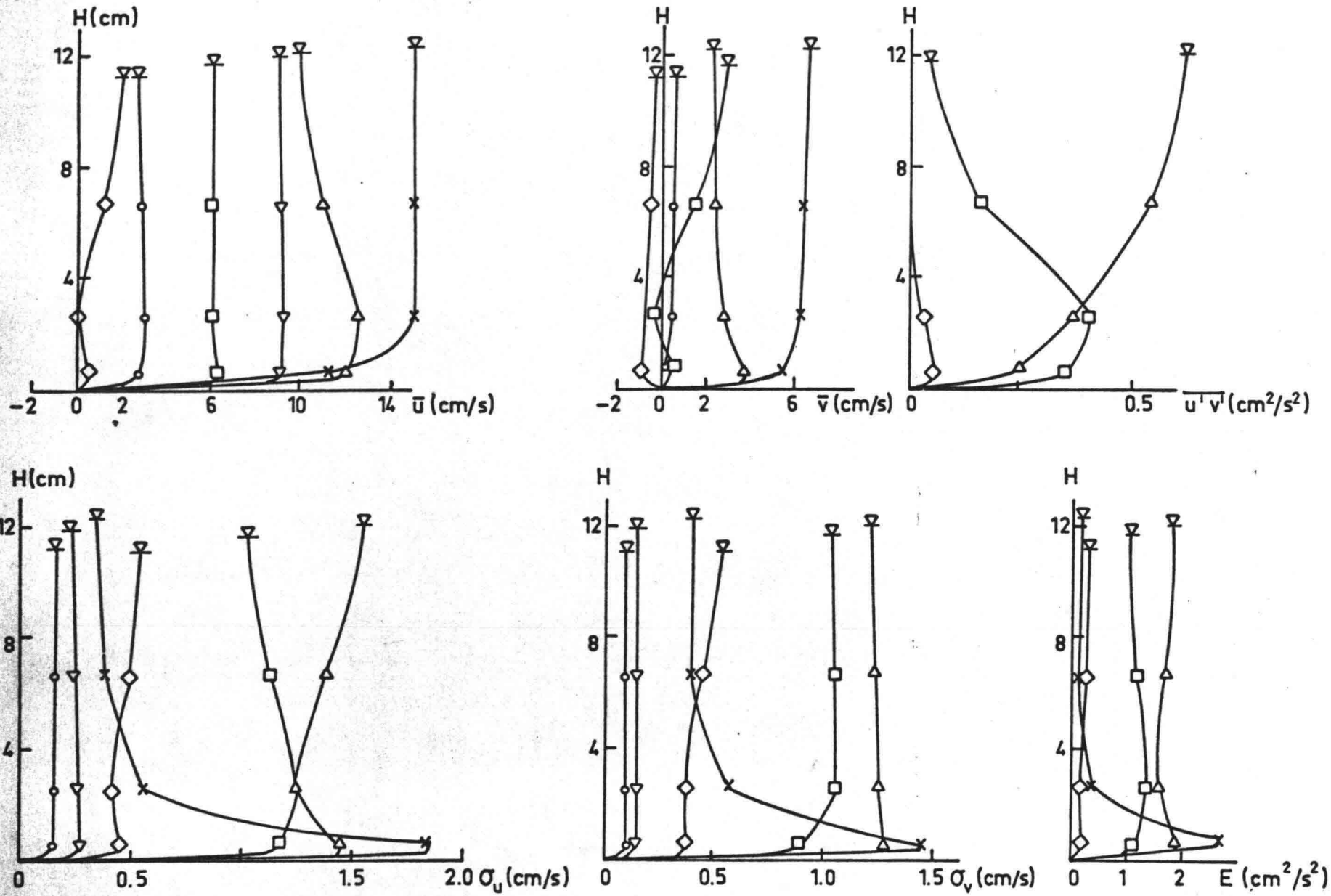

Fig. 4.36. Profile E 4, Q_m = 9 l/s.

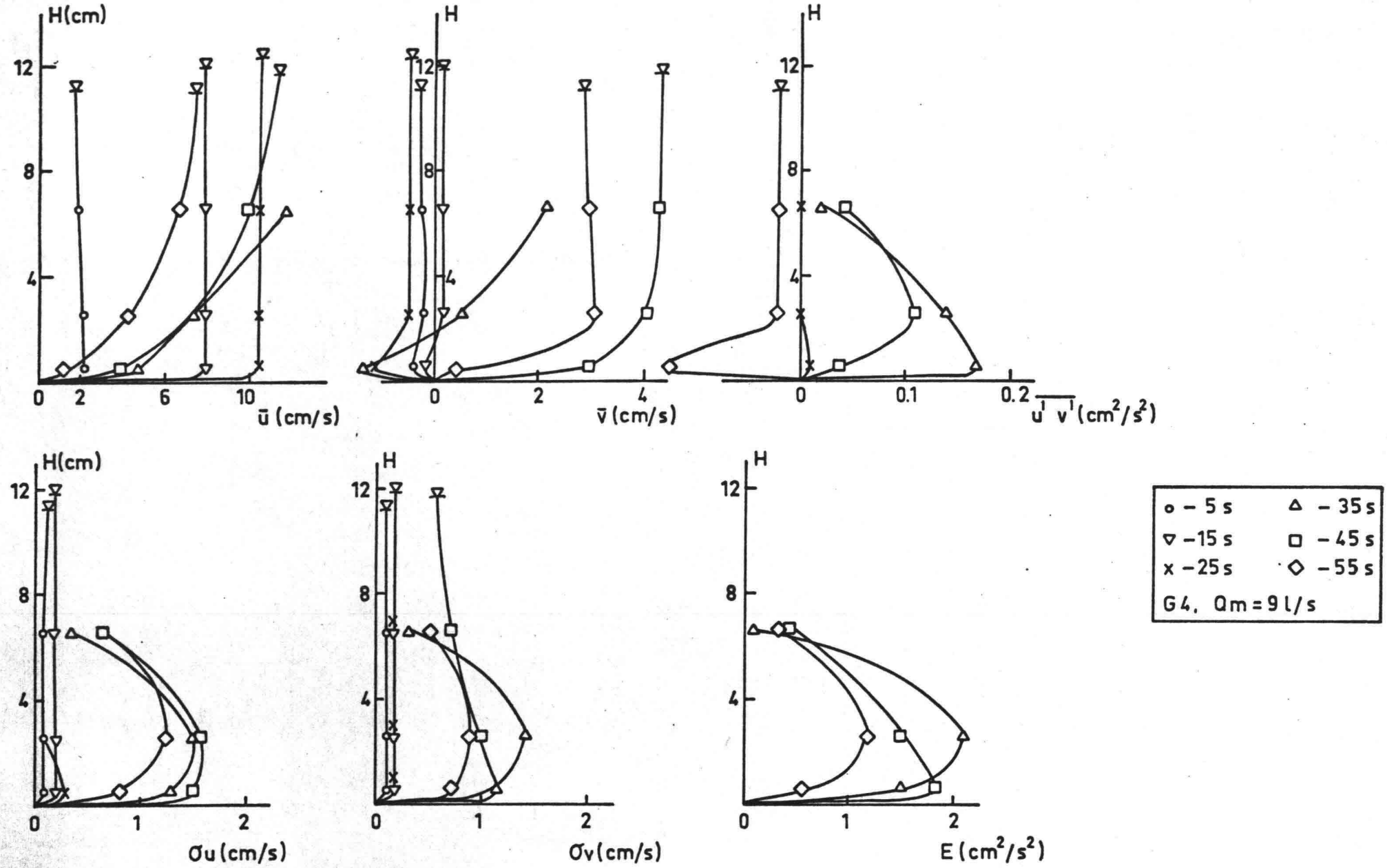

Fig. 4.37. Profile G 4, Q_m = 9 l/s.

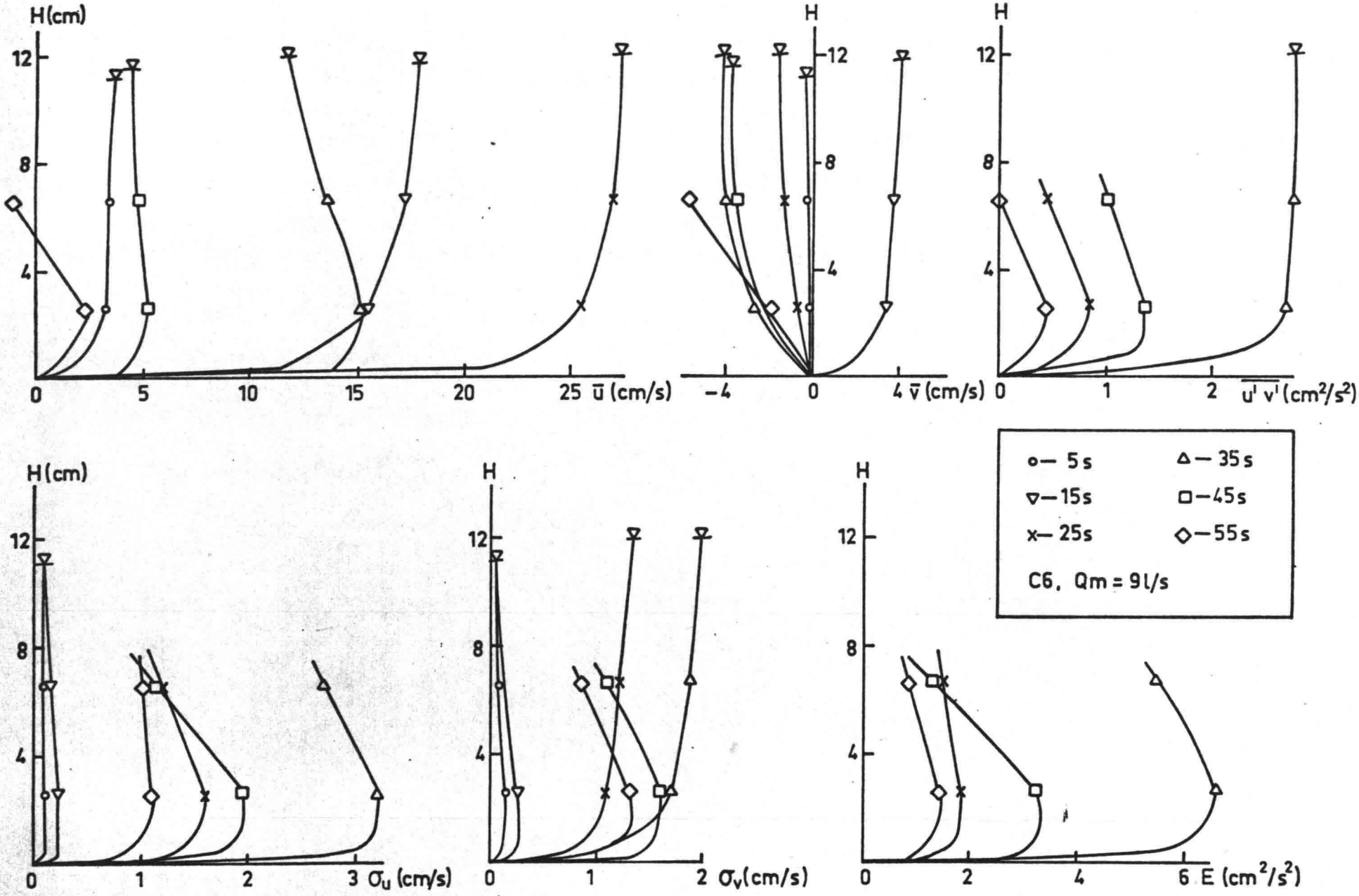

Fig. 4.38. Profile C 6, Q_m = 9 l/s.

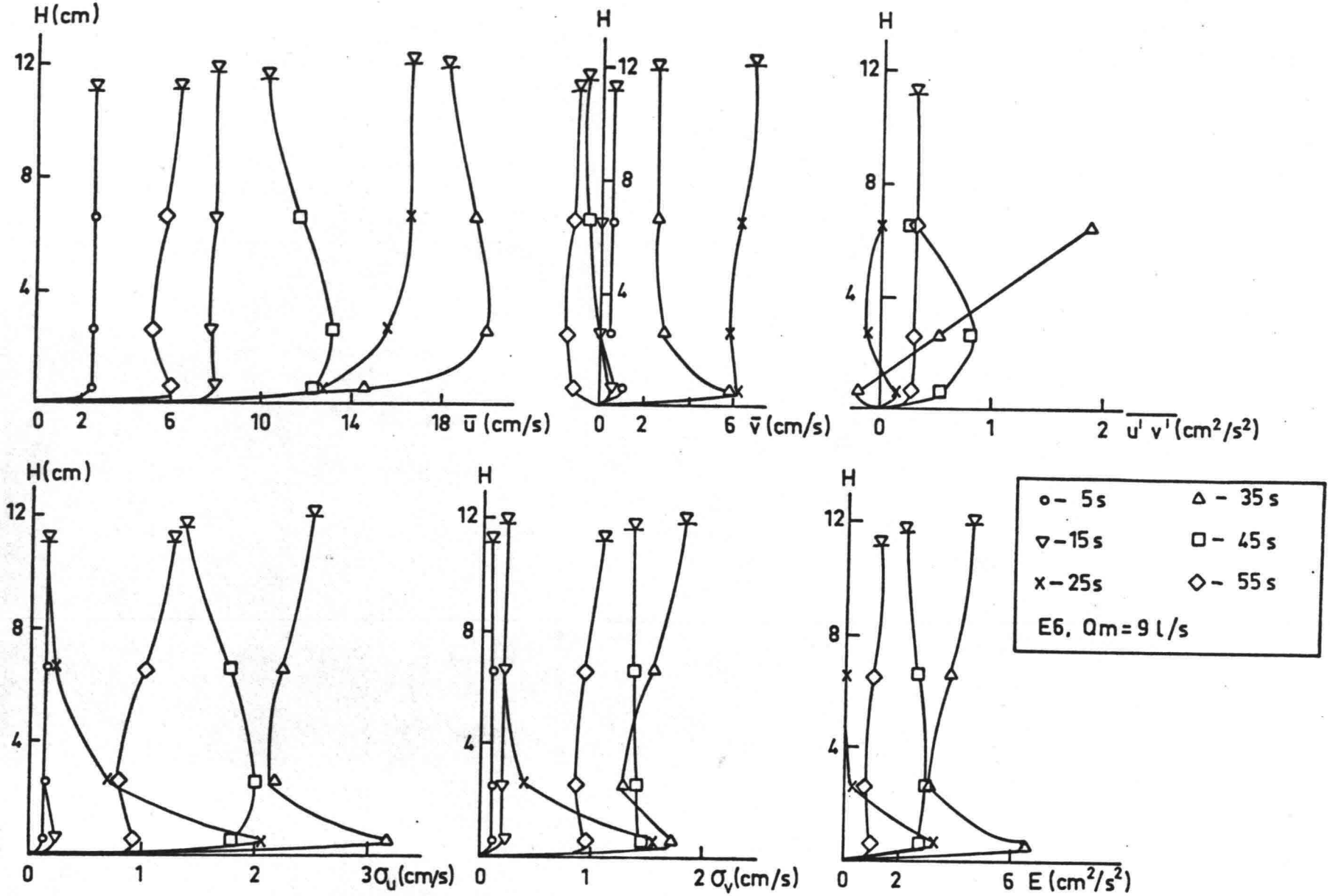

Fig. 4.39. Profile E 6, Q_m = 9 l/s.

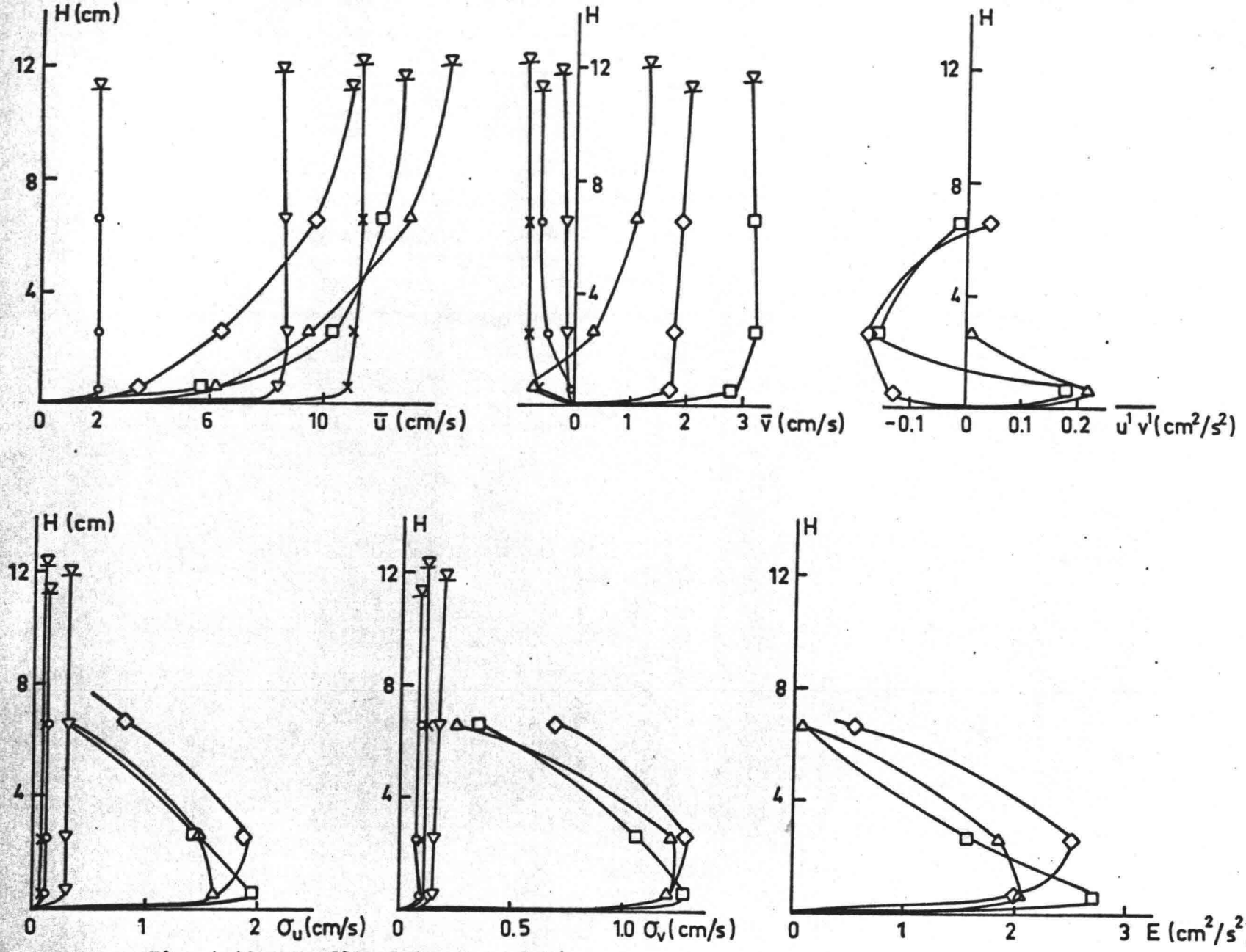

Fig. 4.40. Profile G 6, Q_m = 9 1/s.

The following conclusions could be drawn from these figures:

Flow-direction velocity $\bar{u}$. At the first moments the velocity distribution is quite uniform, only in the boundary layer we have development of the profile. Afterwards we can notice that the upper layers are moving at higher velocity, especially in the decelerating phase.

Cross-direction velocity $\bar{v}$. It is interesting that we can see from fig. 4.37 and 4.40 that the upper layers of the flow are affected first by changes in the velocity direction (the influence of the large vortex). This change takes place during a relatively short time and in other experiments we just did not catch this moment in the ensemble averaging process. The velocity $\bar{v}$ is changing sign in all measured profiles.

Reynolds stress $\overline{u'v'}$. In the first moments the flow is laminar. The turbulence is generated by two different sources, namely at the corner of the enlargement of the flow (separation taking place) and in the bottom boundary-layer. Profile A 5 is close to the corner of the enlargement and the value of $\overline{u'v'}$ is quite the same over the depth of the flow. Going in downstream direction the influence of the bottom boundary layer in generating the turbulence becomes noticeable (fig. 4.34 etc); in the upper layers $\overline{u'v'}$ is relatively small. The values of $\overline{u'v'}$ are decreasing with the decrease in velocity in downstream direction.

Turbulence intensities σ_u and σ_v. In profile A 5 the intensity of turbulence is related to the separation and it is quite constant over the flow depth. In profile B 4 (fig. 4.33) downstream of the corner, the intensity of the turbulence has already decreased and we can see some influence of the boundary layer. In profile C 4 (fig. 4.34) the influence of the boundary layer is more noticeable and also we can see the first moment of generation of the turbulence in the boundary layer at time $t = 15$ s; the same holds in profiles D 4, E 4, etc. at time moment $t = 25$ s. (these time moments are average values over a time period 2.56 s owing to the ensemble-averaging process). The intensity of turbulence is highest in the boundary layer and it takes time to develop turbulence in the upper layers. The development of the separating vortex with the turbulence inside can be seen in figs. 4.39 and 4.40 (the distance between the profiles E 6 and G 6 is 0.75 m); the time delay in the increase in the turbulence intensity between the profiles is 10 s.

The small intensity of the fluctuations at the first time moment (t = 5 s) are probably not connected with turbulence intensities, but mostly result from random influences on the laser signal. The intensities σ_u and σ_v are of the same order of magnitude in each measurement.
Turbulence energy E. The largest values are found at the separation corner and inside the mixing layer (profiles C 6, E 6). Initially, the turbulence-energy level in downstream profiles is very low, and only after some time the turbulence really develops.

It is to be expected that measurements closer to the bottom would give higher turbulence intensities.

Some ensemble-averaged measurements were made also inside the separation region in the points C 1/3, C 2/3 and E 1/3. The results are shown in figures 4.41, 4.42 and 4.43, respectively. All turbulence characteristics attain maximum values after time 25 s.

Some conclusions about the complex water movements inside the separation region could already be drawn using the visualization experiments. These were confirmed by the LDV measurements. All parameters of the flow are changing, even abruptly when the profile starts to be affected by the separating vortex.

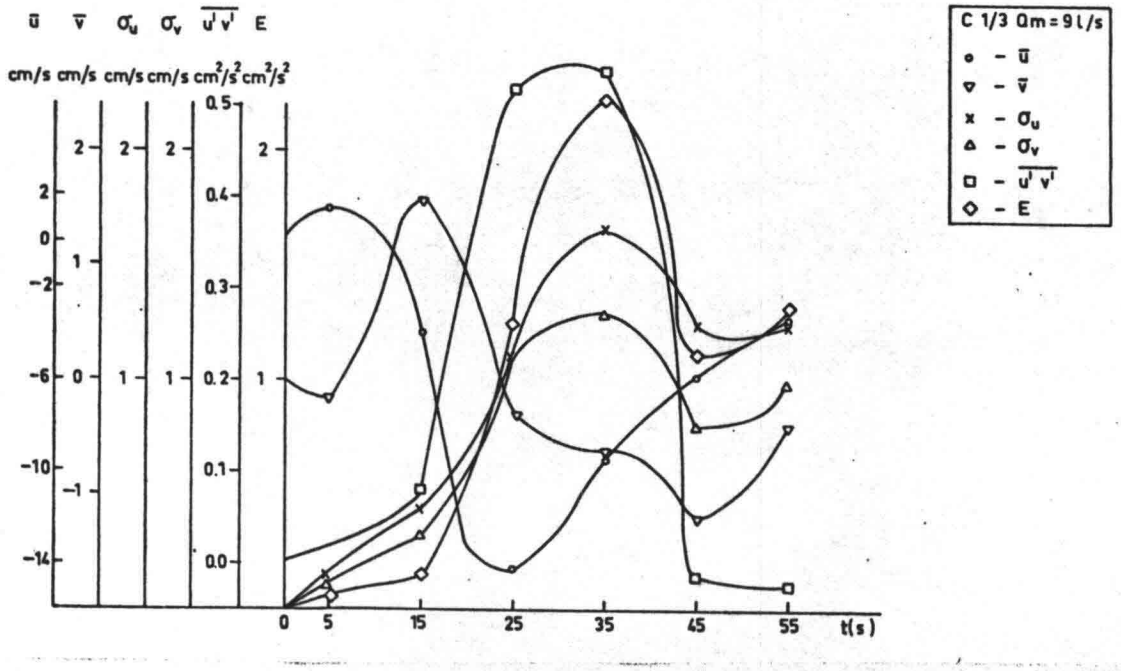

Fig. 4.41. C 1/3, Q_m = 9 1/s.

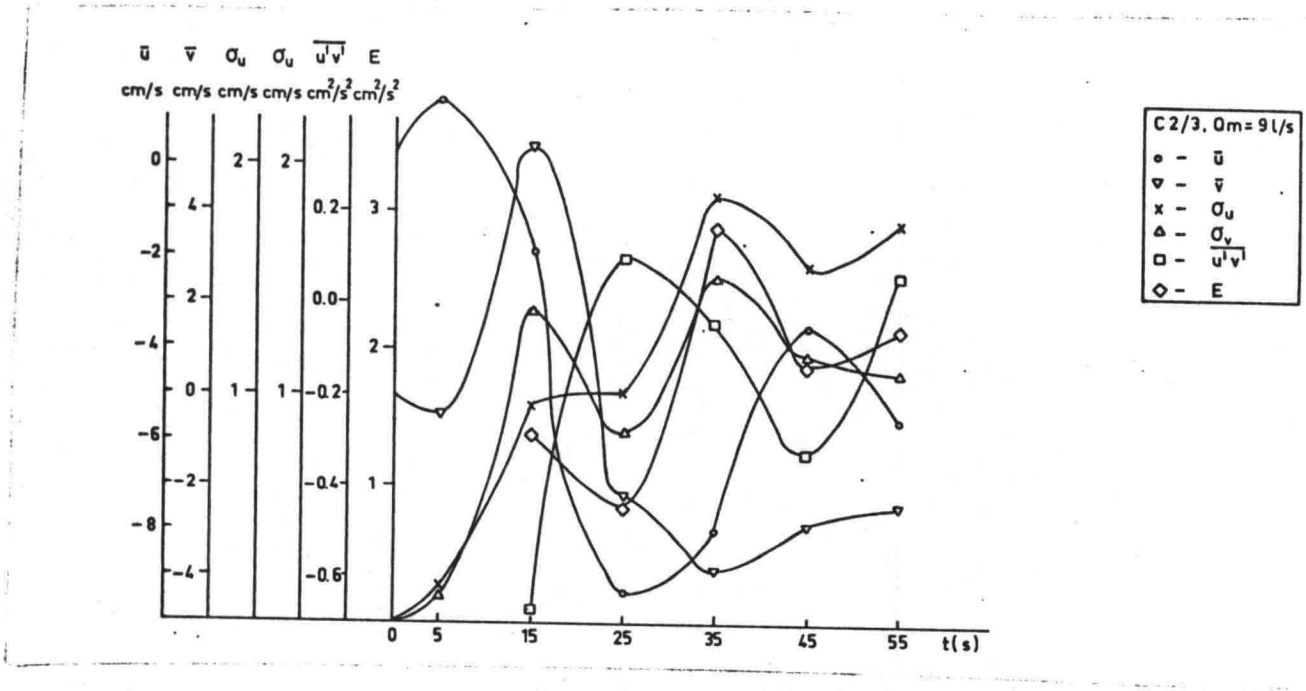

Fig. 4.42. C 2/3, Q_m = 9 1/s.

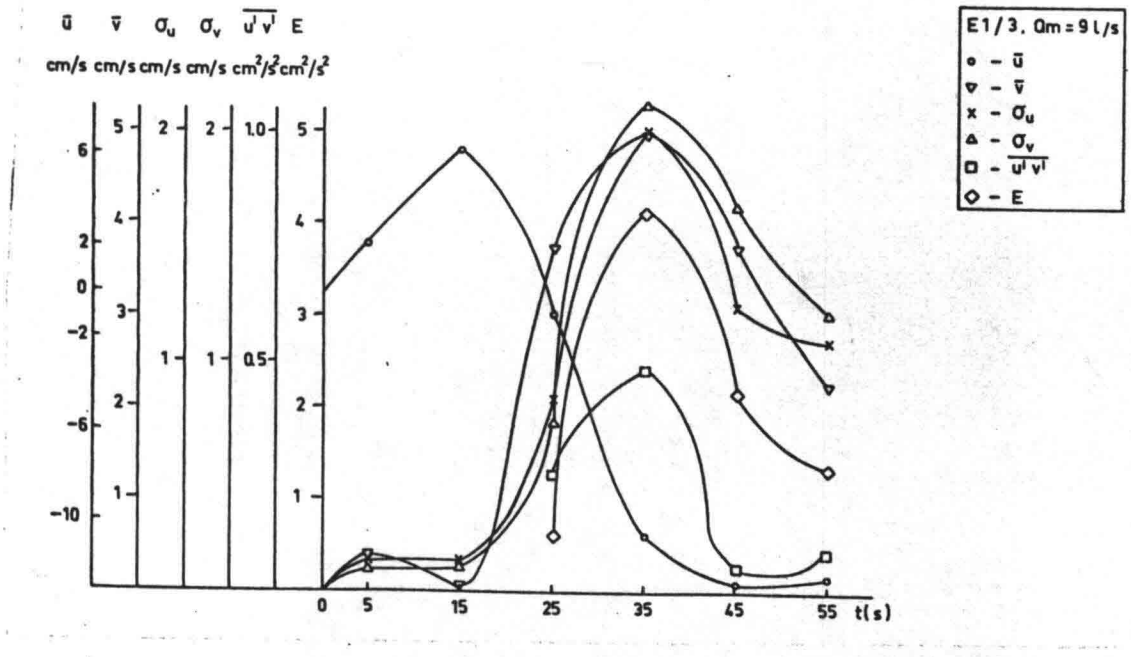

Fig. 4.43. E 1/3, Q_m = 9 1/s.

Measurements with the higher flow rate Q_m = 16 l/s, T = 90 s were also carried out, especially to obtain some information about the mixing layer. In this case higher turbulence levels were expected.

The results obtained in different points are collected in figures 4.44 to 4.51.

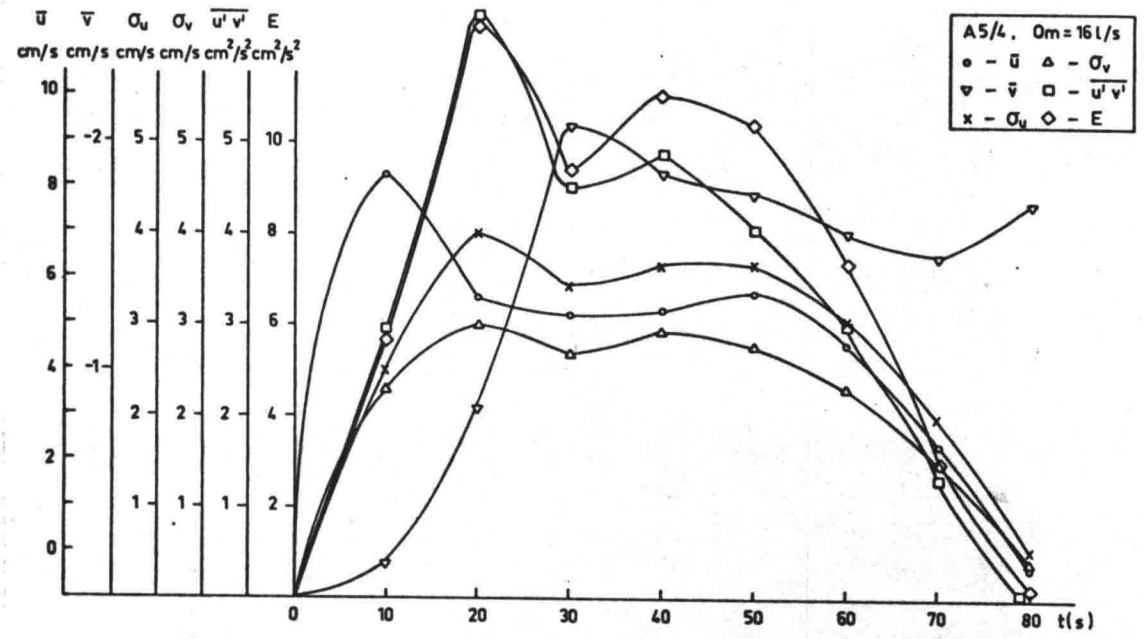

Fig. 4.44. A 5/4, Q_m = 16 l/s, T = 90 s.

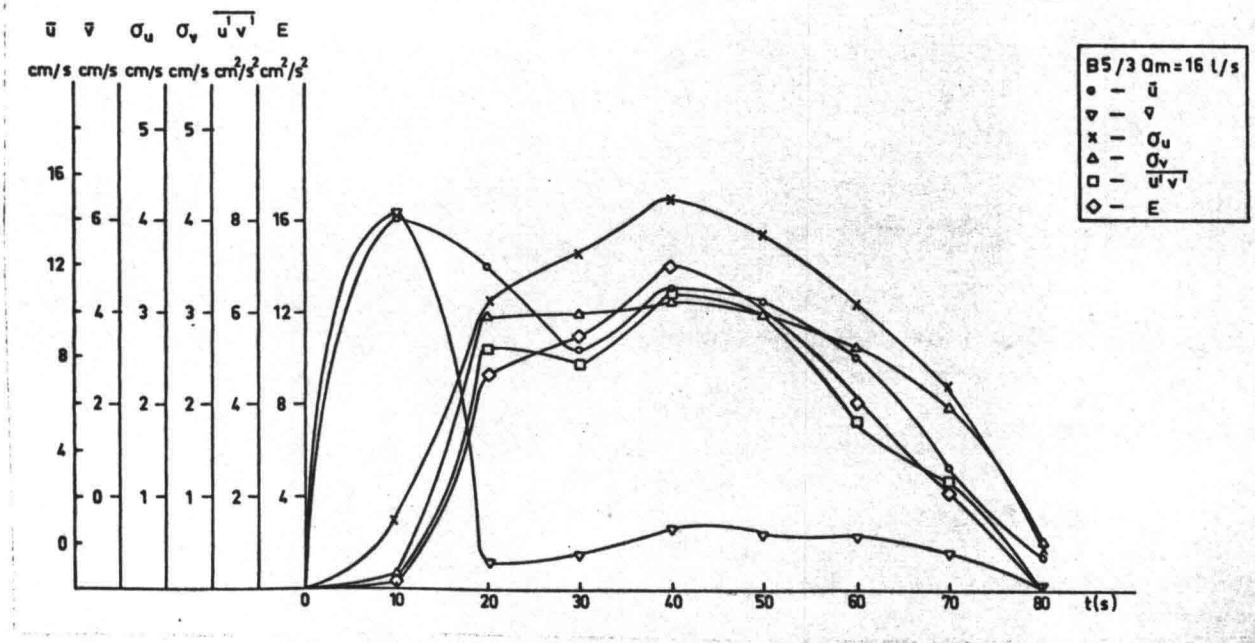

Fig. 4.45. B 5/3, Q_m = 16 l/s, T = 90 s.

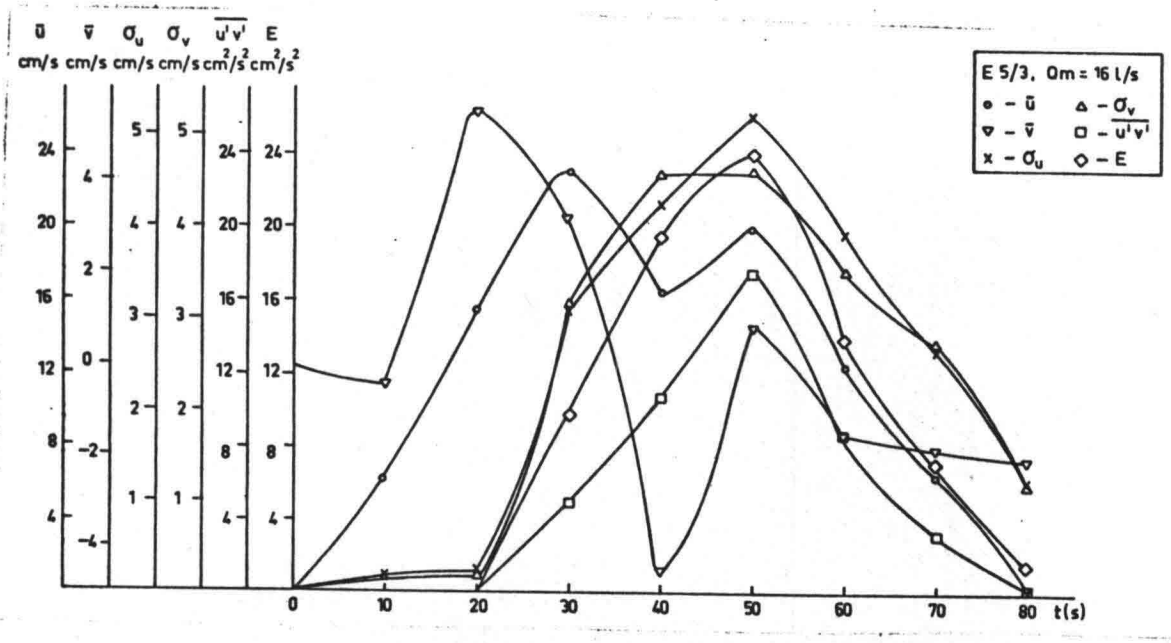

Fig. 4.48. E 5/3, Q_m = 16 1/s, T = 90 s.

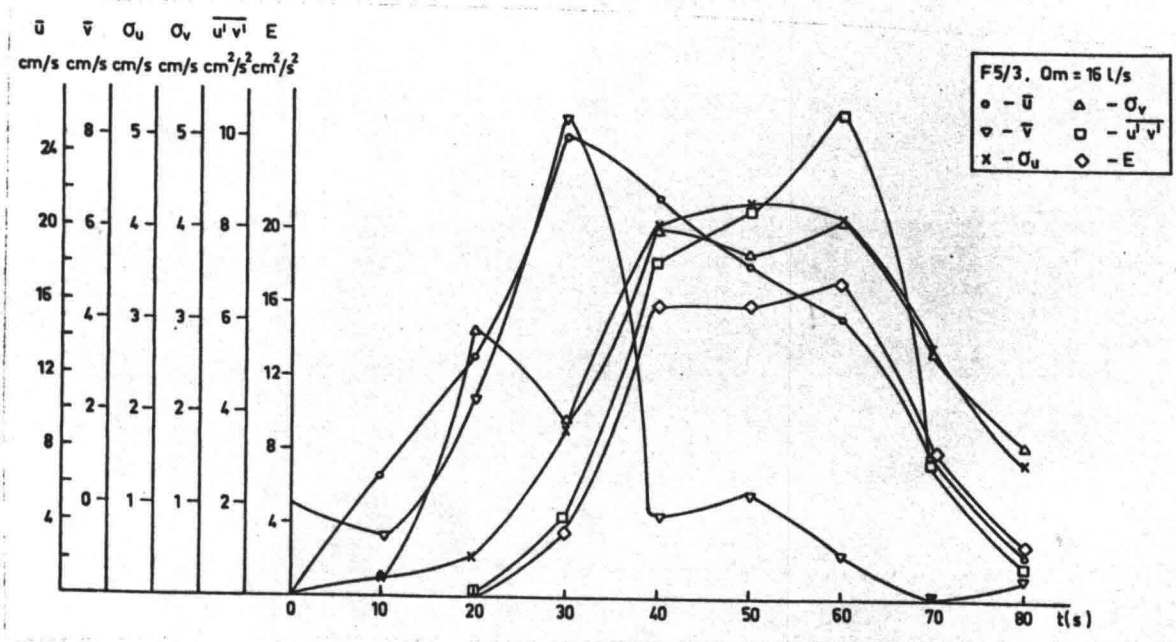

Fig. 4.49. F 5/3, Q_m = 16 1/s, T = 90 s.

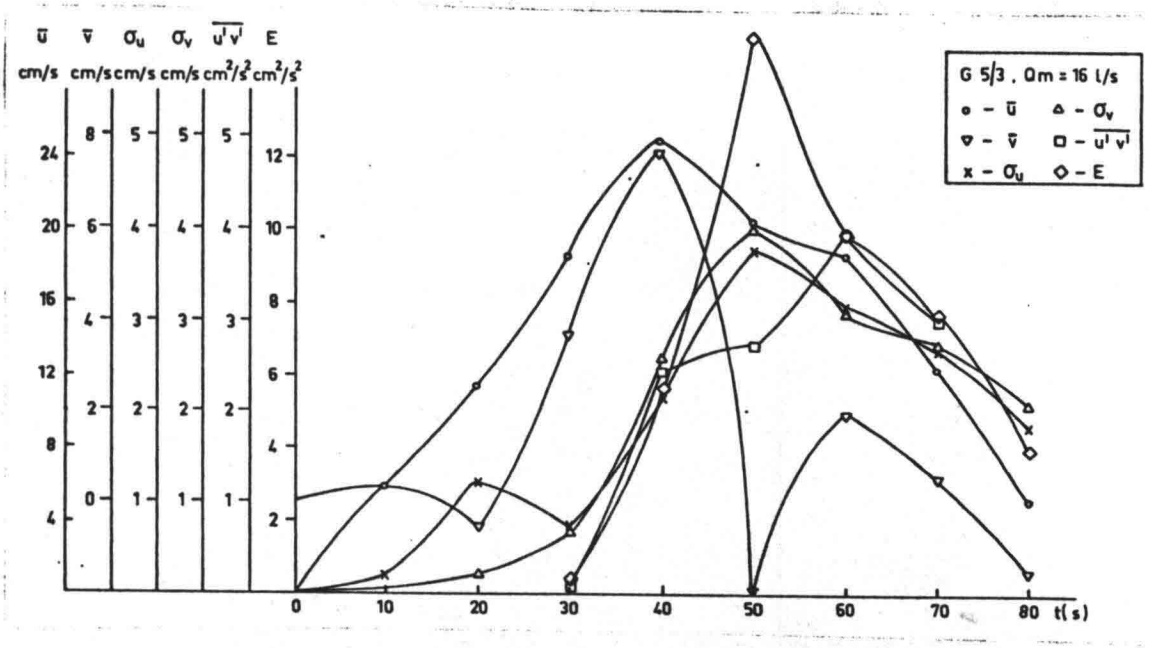

Fig. 4.50. G 5/3, Q_m = 16 1/s, T = 90 s.

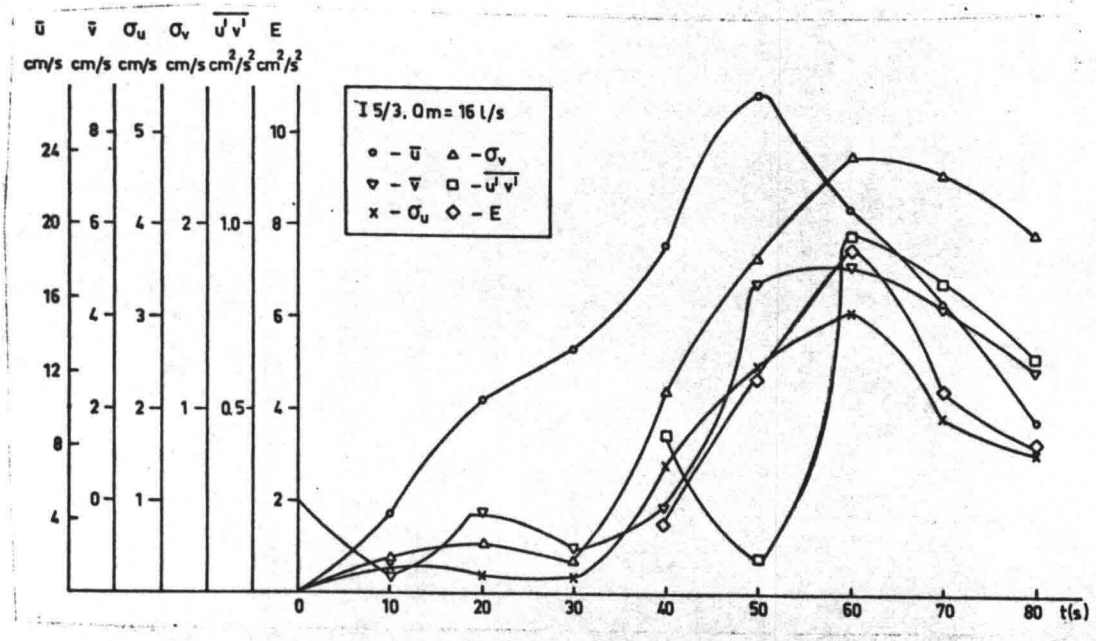

Fig. 4.51. I 5/3 , Q_m = 16 1/s, T = 90 s.

All measurement points are on line 5 (fig.4.13) in downstream direction. The u-component of the velocity does not have the half-sine shape in time, but is affected by the motion in cross-direction. The turbulence parameters correspond better with the half-sine relation in time. They increase in the accelerating phase and decrease in the decelerating phase. From the increase of turbulence parameters we can follow how the separation region grows in downstream direction when it affects the measuring point. In the last figure (4.51) of this series the turbulence parameters increase after 40 seconds from the start of the flow. The absolute values of the intensities of velocities u and v are of the same order of magnitude.

The values of $\overline{u'v'}$ increase during the development of the separation region in downstream direction, but from profile F 5 (1.15 m from corner) they start to decrease.This fact probably indicates that in the mixing layer $\overline{u'v'}$ increases during development of the separation and that inside the separation region $\overline{u'v'}$ is less. Profile F 5 is not affected so much by mixing-layer turbulence in the accelerating phase. We can conclude this from fig. 4.52, where the development of $\overline{u'v'}$ in downstream direction during the experiment is given.

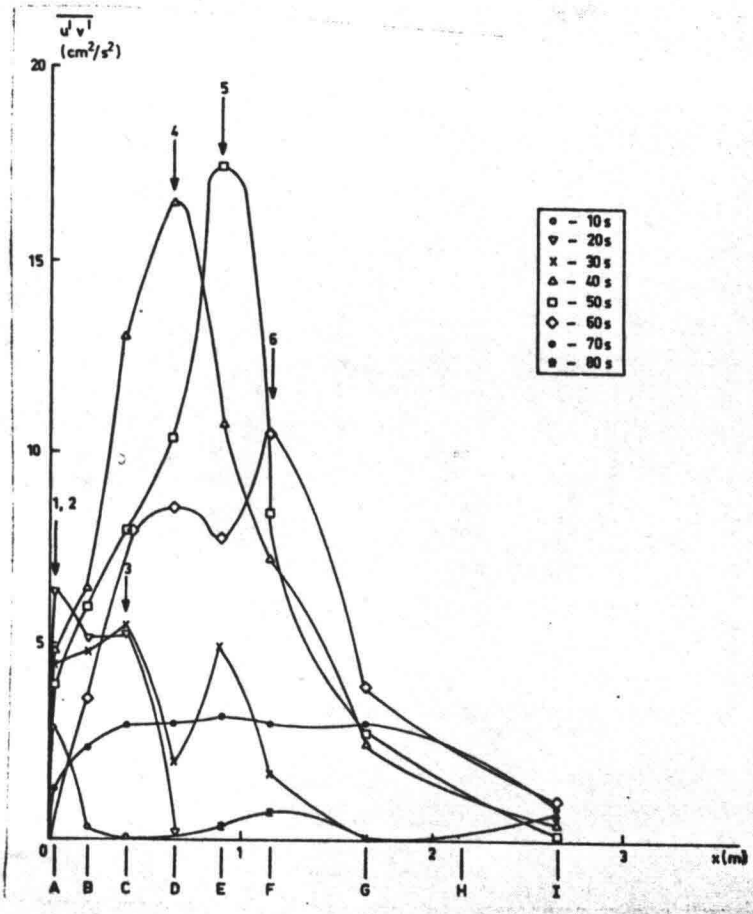

Fig. 4.52. Development of $\overline{u'v'}$ in downstream direction (Q_m= 16 1/s,T = 90 s).

The peak value of $\overline{u'v'}$ moves in downstream direction. In the accelerating phase this peak value increases and it decreases in the decelerating phase (the peak values are numbered according to the time moments). The maximum value of the normalised Reynolds stress occurs at the end of the experiment (fig. 4.53).

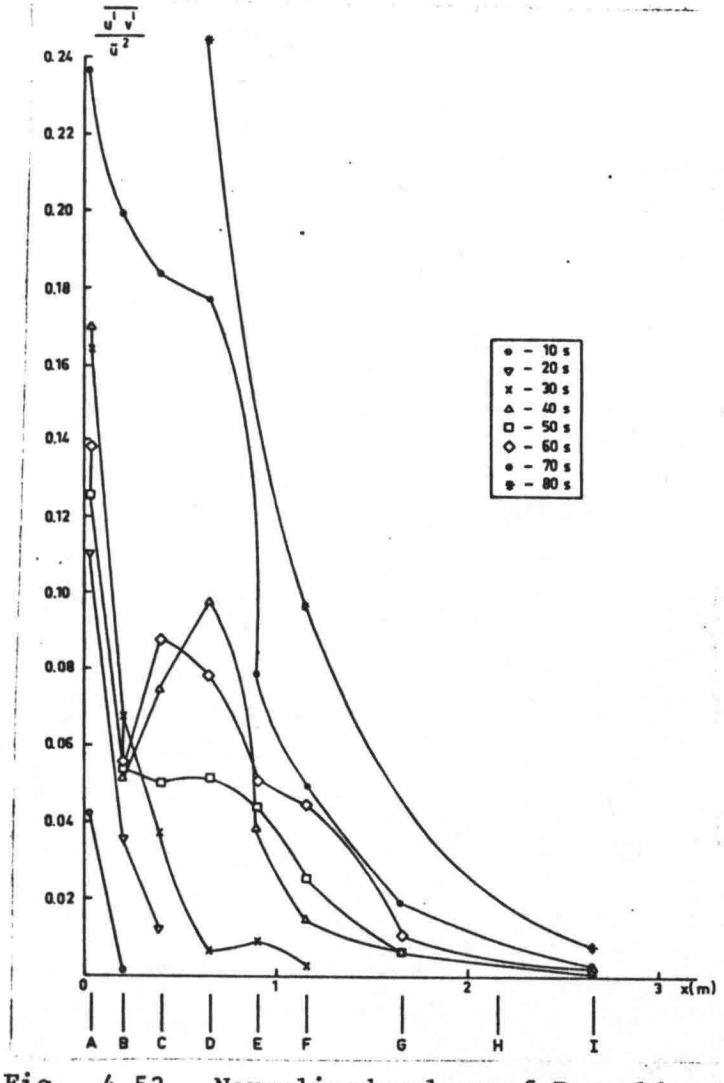

Fig. 4.53. Normalised values of Reynolds stress (Q_m = 16 1/s, T = 90 s).

The normalised intensity $\sigma_u/\bar{u}$ is given in figure 4.54 (Q_m = 16 1/s, T = 90 s). The relative intensity increases during the development of the flow and has its maximum value at the end of the decelerating phase. In downstream direction the value of $\sigma_u/\bar{u}$ is decreasing at every time moment.

Finally, the ensemble-averaged velocities and intensities in profile 0.7 (see fig. 4.13) in front of the enlargement are given in fig.4.55. The intensity is maximum always close to the bottom. In the accelerating phase it increases and it decreases in the decelerating phase. In the beginning (t_1 = 10 s and t_2 = 20 s) the turbulence is generated very close to the bottom; afterwards it develops also in the upper layers of the flow.

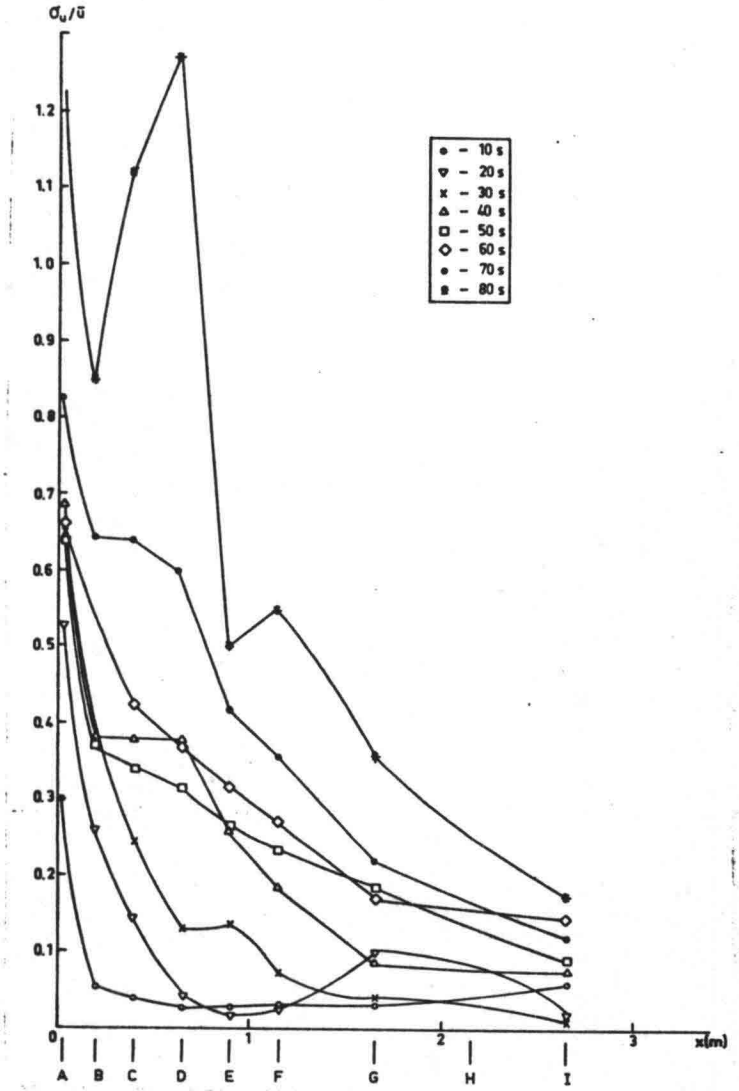

Fig. 4.54. Normalised intensity (Q_m = 16 1/s, T = 90 s).

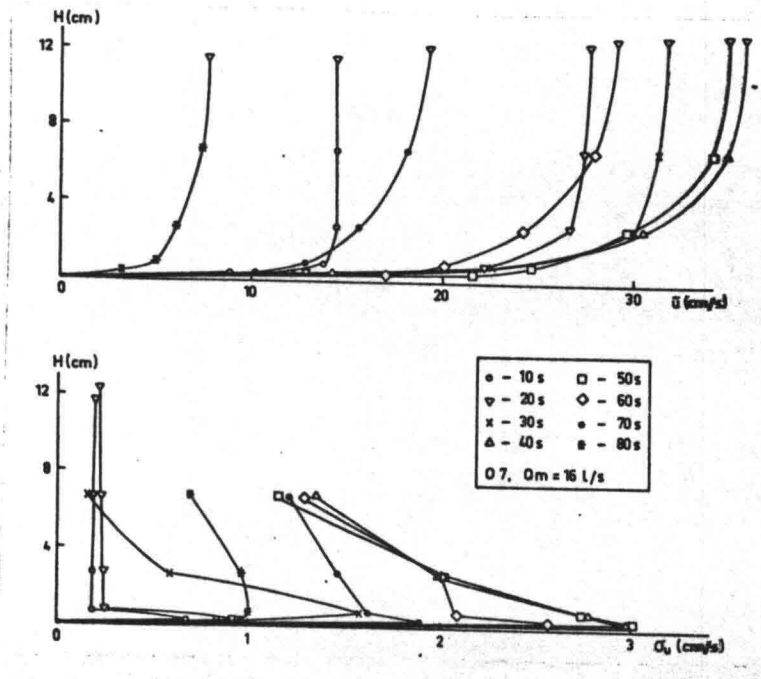

Fig. 4.55. Profile 0 7 (Q_m = 16 1/s, T = 90 s).

4.3. Spectral analysis and statistical distributions

It was planned to carry out spectral analyses of the turbulent energy during the development of the separation. The methods of computation are given in section 3.2. Unfortunately, the spectral computations could not be finished so that only some spectral estimates can be presented.

The use of discrete FFT computations implies some kind of estimate of power spectra. The estimate usually depends on the computation algorithm used. It also depends on the type of data window used to reduce the leakage of energy. Experience suggests that the IMSL library subroutine FTFPS for two time series is not the best choice. It is recommended to select another subroutine for turbulence computations, especially when an integral of the spectra is required. Some influence of the unsteadiness of the flow can also make the spectral estimates unacceptable, but experiences in the past (using a different algorithm) indicate that the power spectra estimates can give interesting qualitative information in the case of unsteady flow in pipes.

As an example, the unscaled power spectra estimates (logarithmic scale) for two velocity components in measuring point D 5/3 (Q_m = 16 1/s, T = 90 s) at different time moments are given in figs. 4.56 to 4.62.

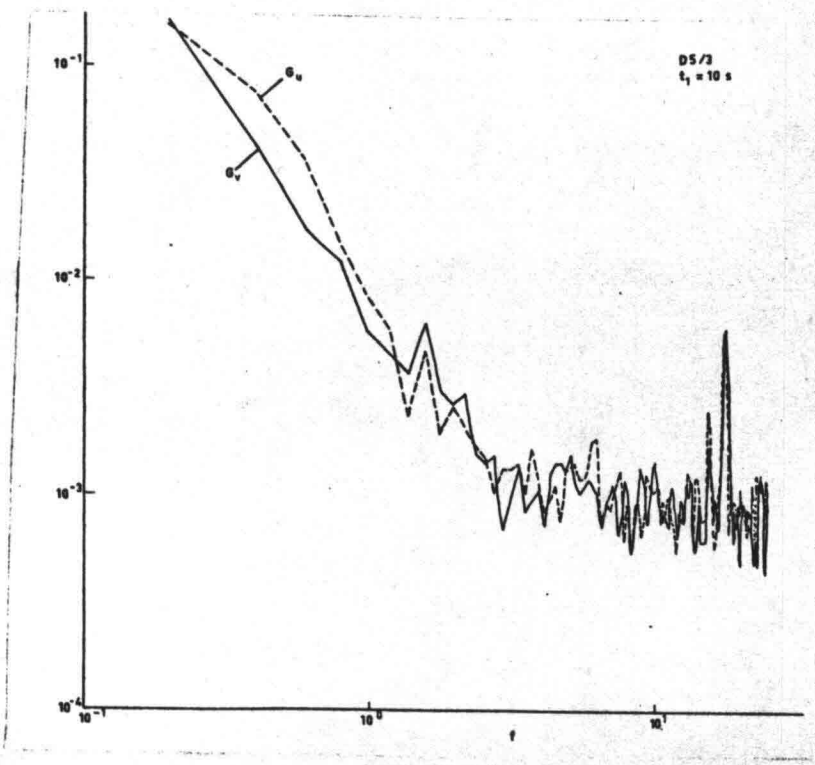

Fig. 4.56. Power spectra in point D 5/3 at t_1 = 10 s.

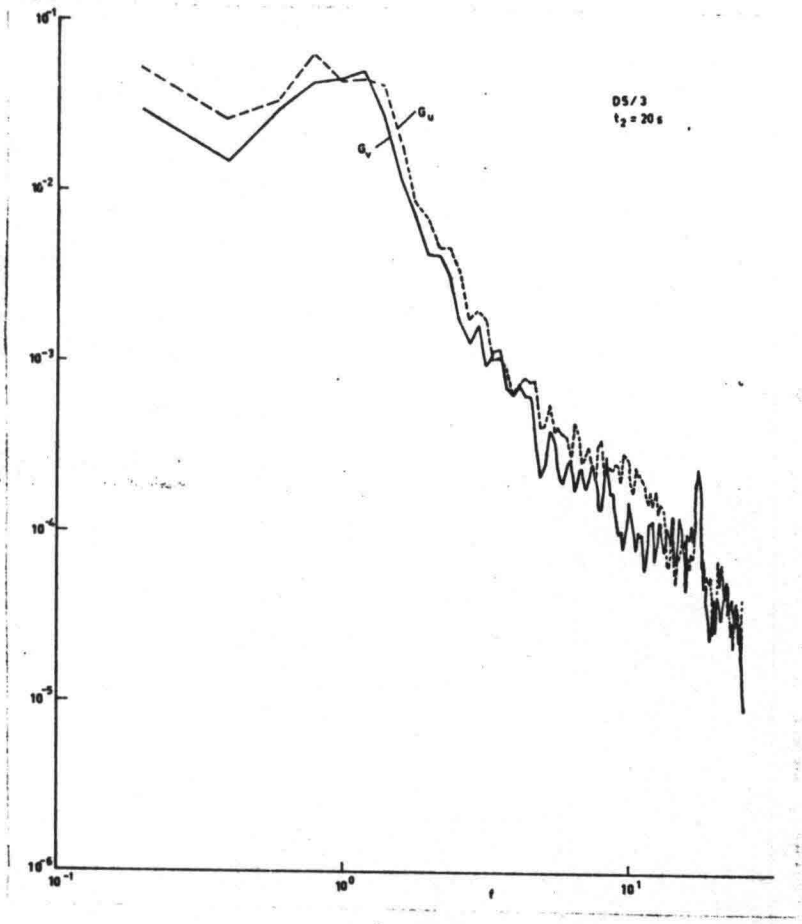

Fig. 4.57. Power spectra in point D 5/3 at t_2 = 20 s.

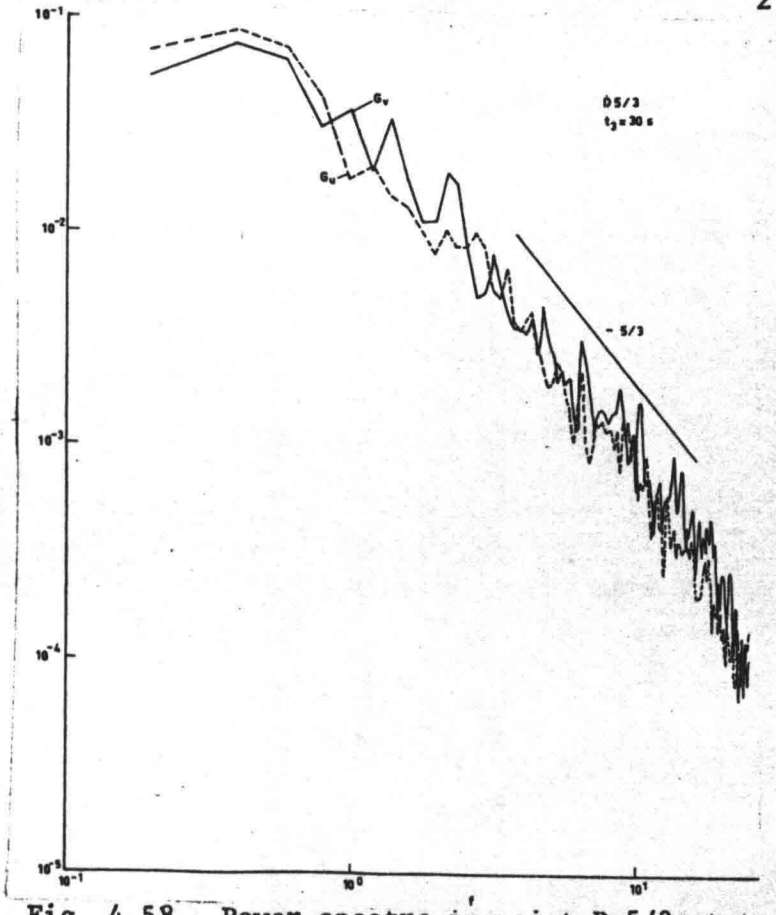

Fig. 4.58. Power spectra in point D 5/3 at t_3 = 30 s.

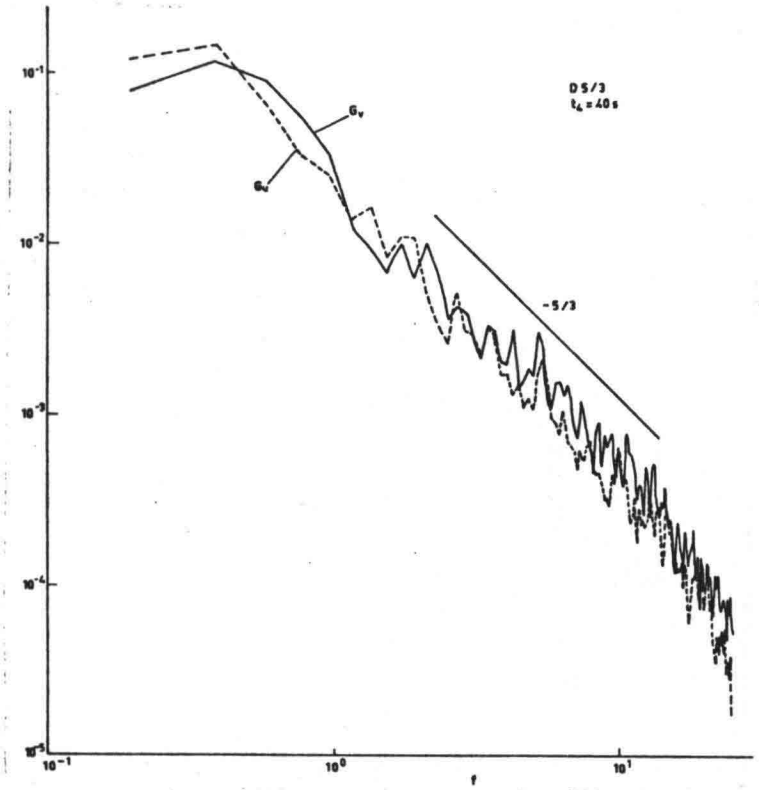

Fig. 4.59. Power spectra in point D 5/3 at t_4 = 40 s.

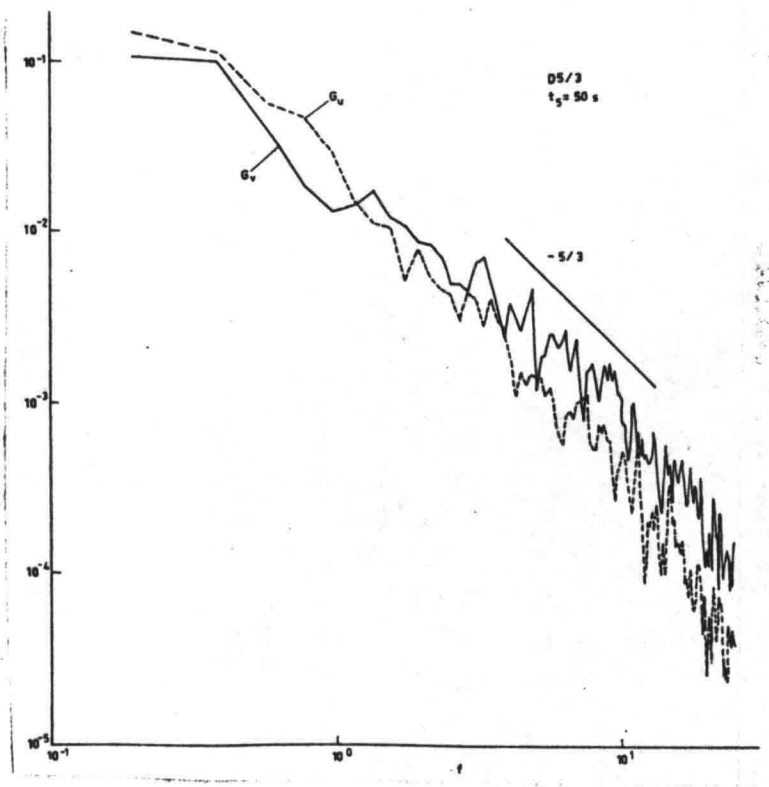

Fig. 4.60. Power spectra in point D 5/3 at t_5 = 50 s.

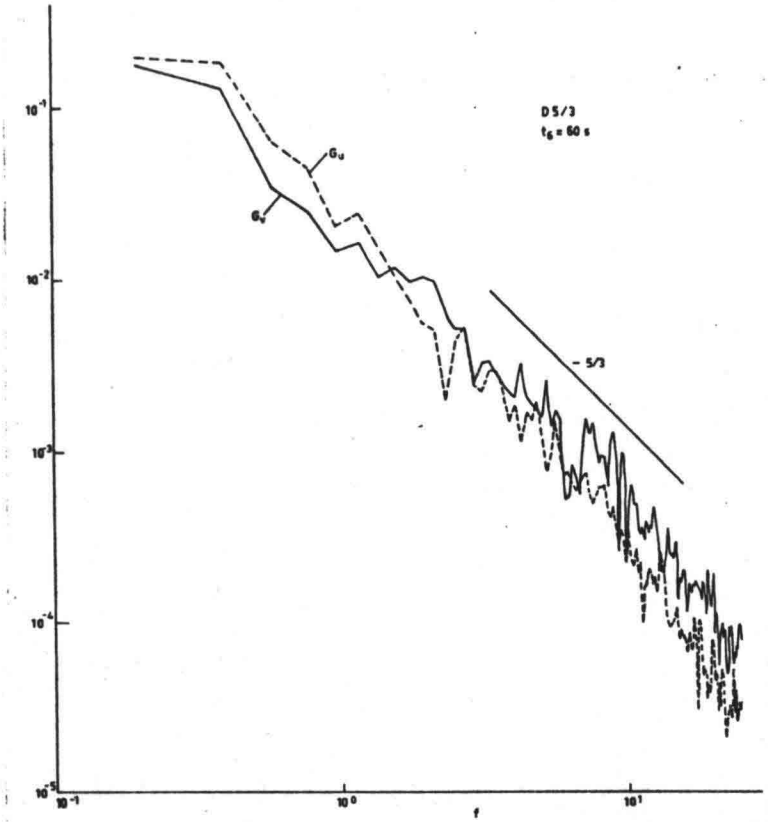

Fig. 4.6 1. Power spectra in point D 5/3 at t_6 = 60 s.

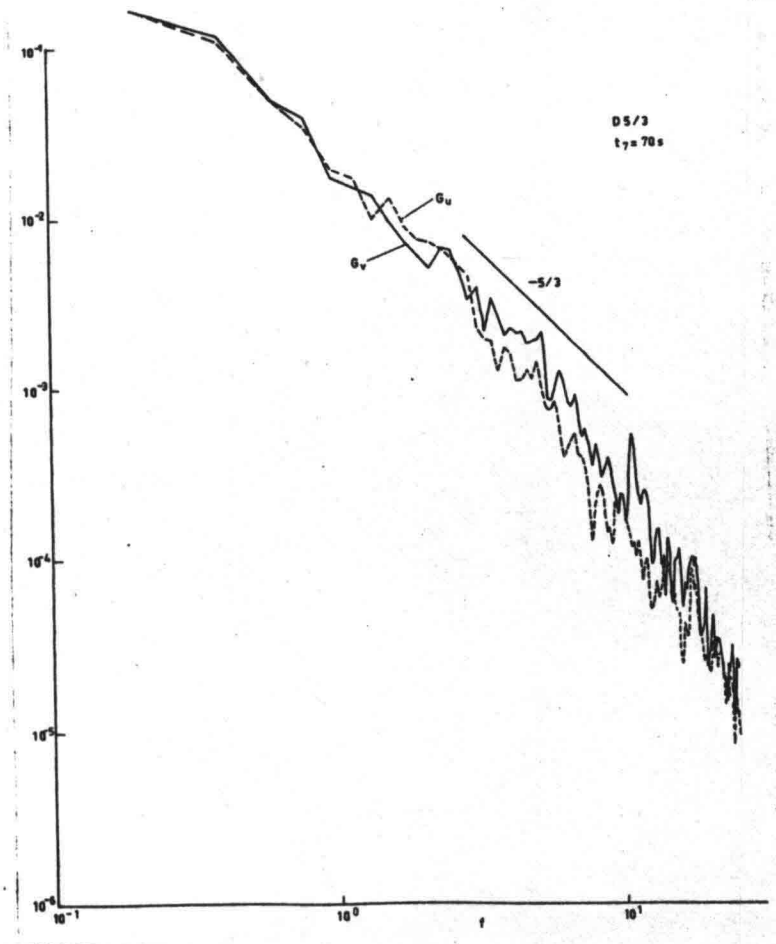

Fig. 4.6.2. Power spectra in point D 5/3 at t_7 = 70 s.

It is not yet possible to calculate turbulence scales from these power spectra estimates, but some qualitative conclusions can be drawn. In the beginning of the experiment (t_1 = 10 s and t_2 = 20 s) low-frequency components are dominating. Afterwards the turbulence energy will be distributed more as usual. In fig. 4.47 we notice also that at time t = 30 s the turbulence intensity was increasing.

To obtain some information about the statistical distribution of the turbulent fluctuations, some histograms were calculated (see section 3.3). Mostly, the statistical distributions were close to the normal distribution. This conclusion is drawn from the calculated values of the skewness (eq. 3.29). Only when the mixing layer of the main vortex affected the measuring point and the velocity components were large, the distributions are more peaked and the skewness is larger (fig. 4.64). As an example the statistical distributions in point D 5/3 are given in fig. 4.63 to 4.69. The experiment was the same as that relating to figs. 4.56 to 4.62.

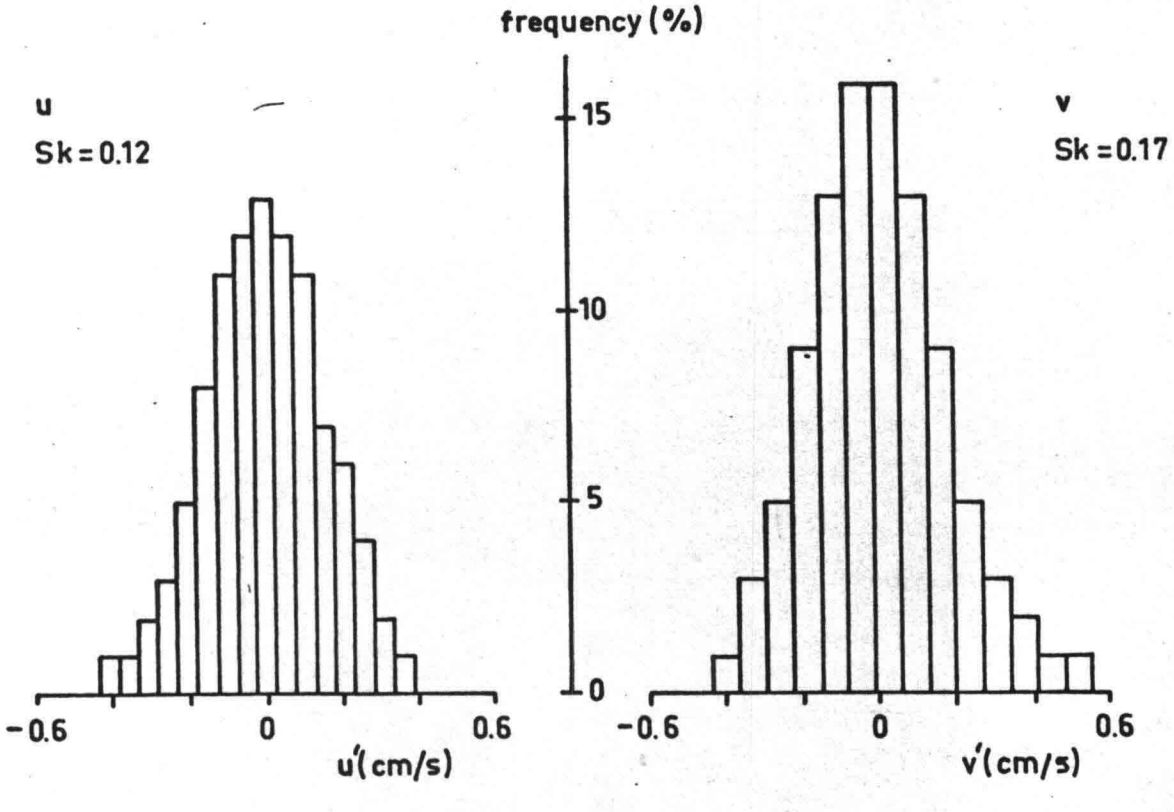

Fig. 4.63. Statistical distributions in point D 5/3 at time t_1 = 10 s. (Q = 16 1/s, T = 90 s).

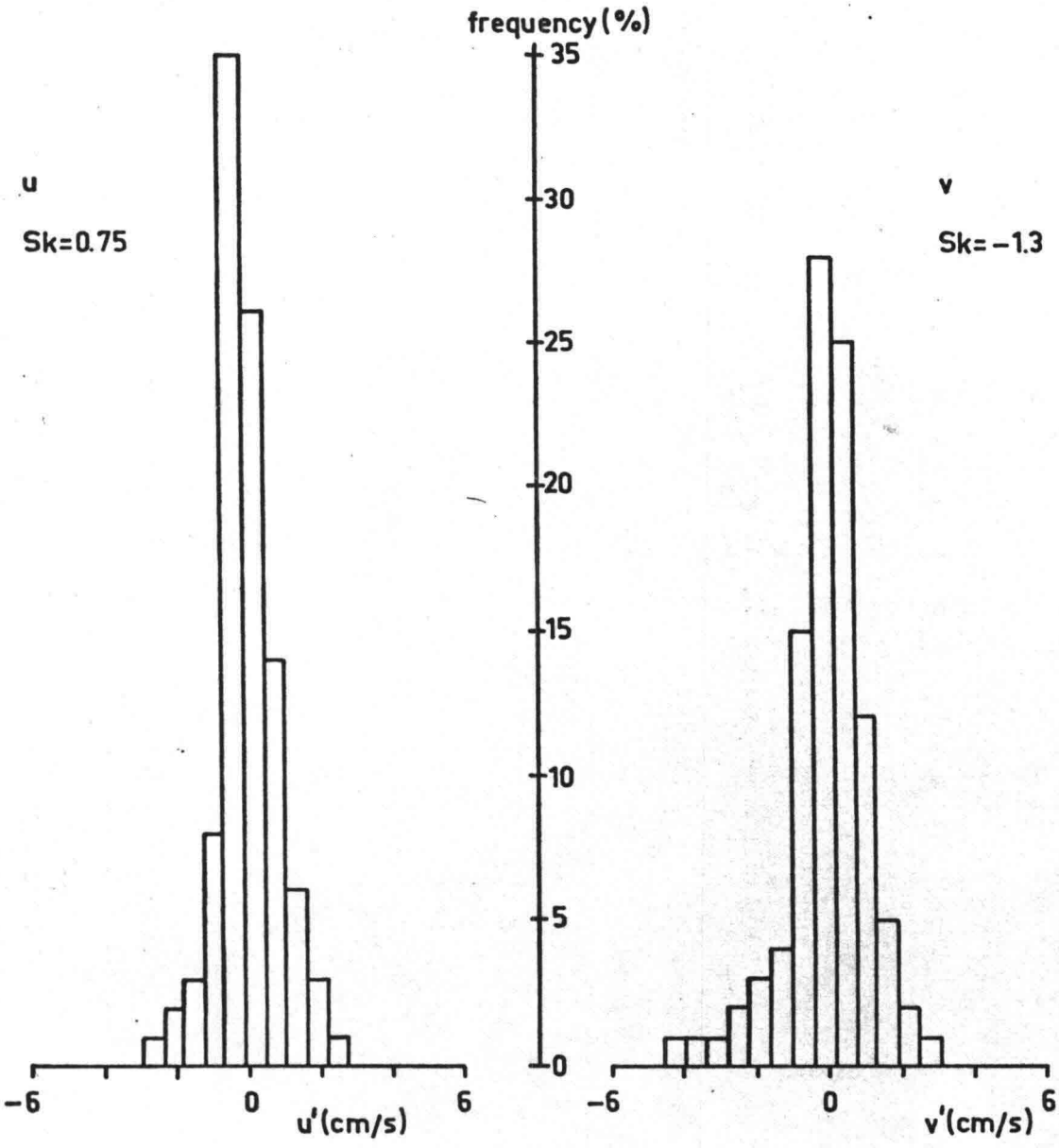

Fig. 4.64 Statistical distributions in point D 5/3 at time t_2 = 20 s.

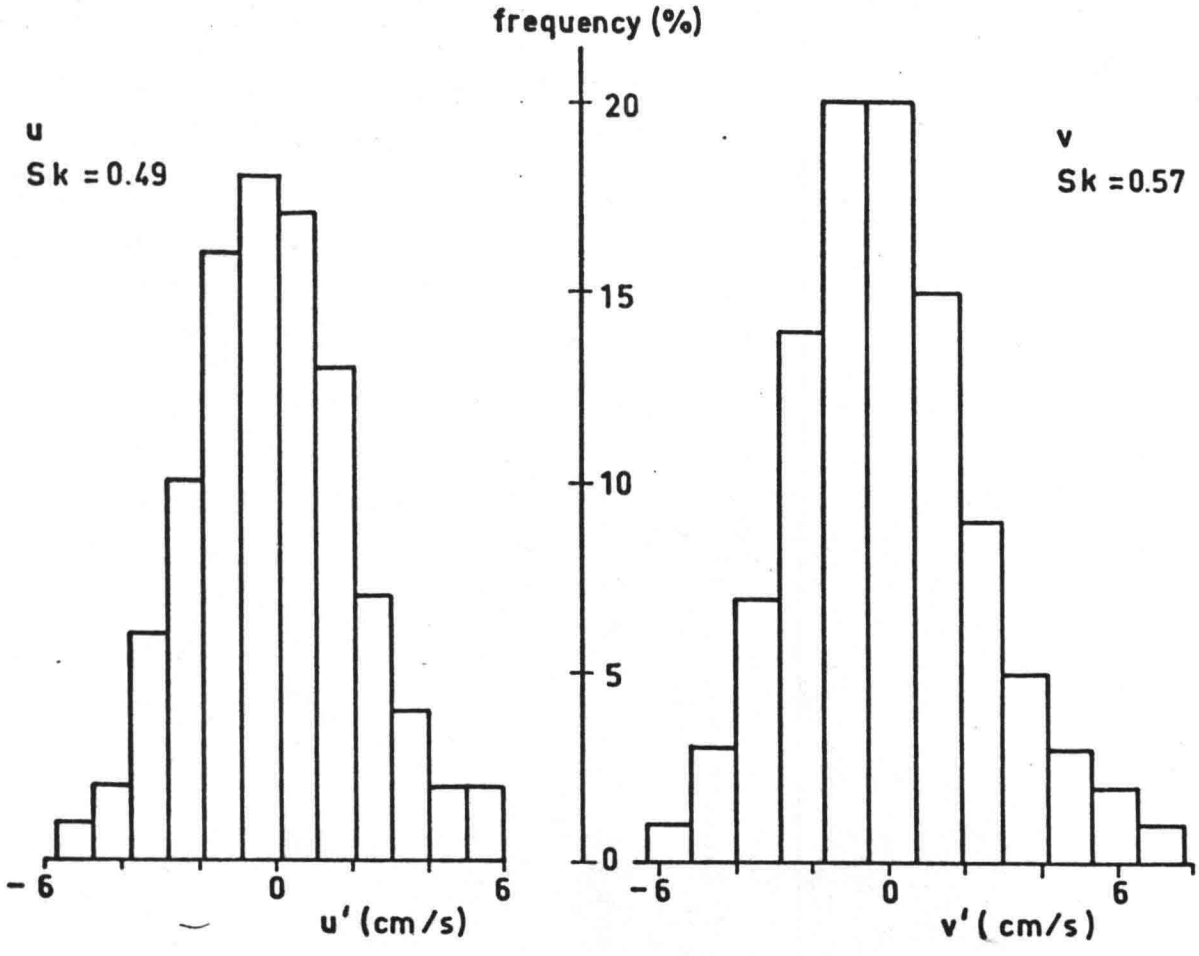

Fig. 4.65. Statistical distributions in point D 5/3 at time t_3 = 30 s.

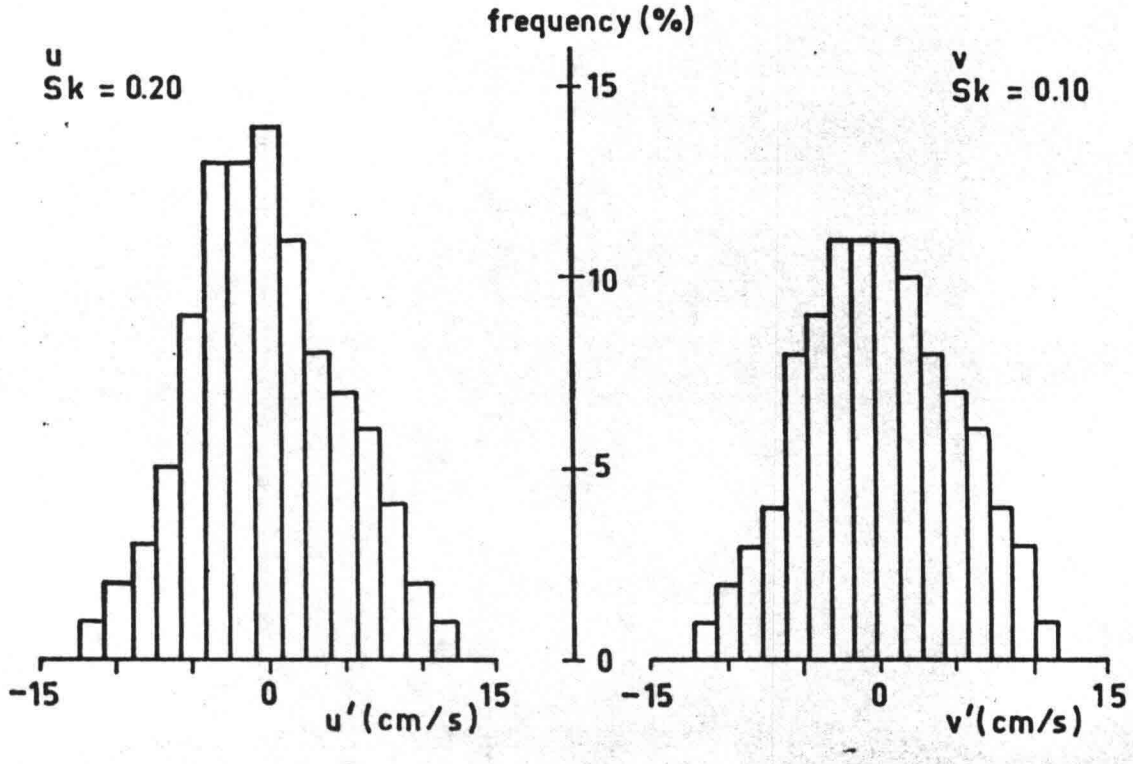

Fig. 4.66. Statistical distributions in point D 5/3 at time t_4 = 40 s.

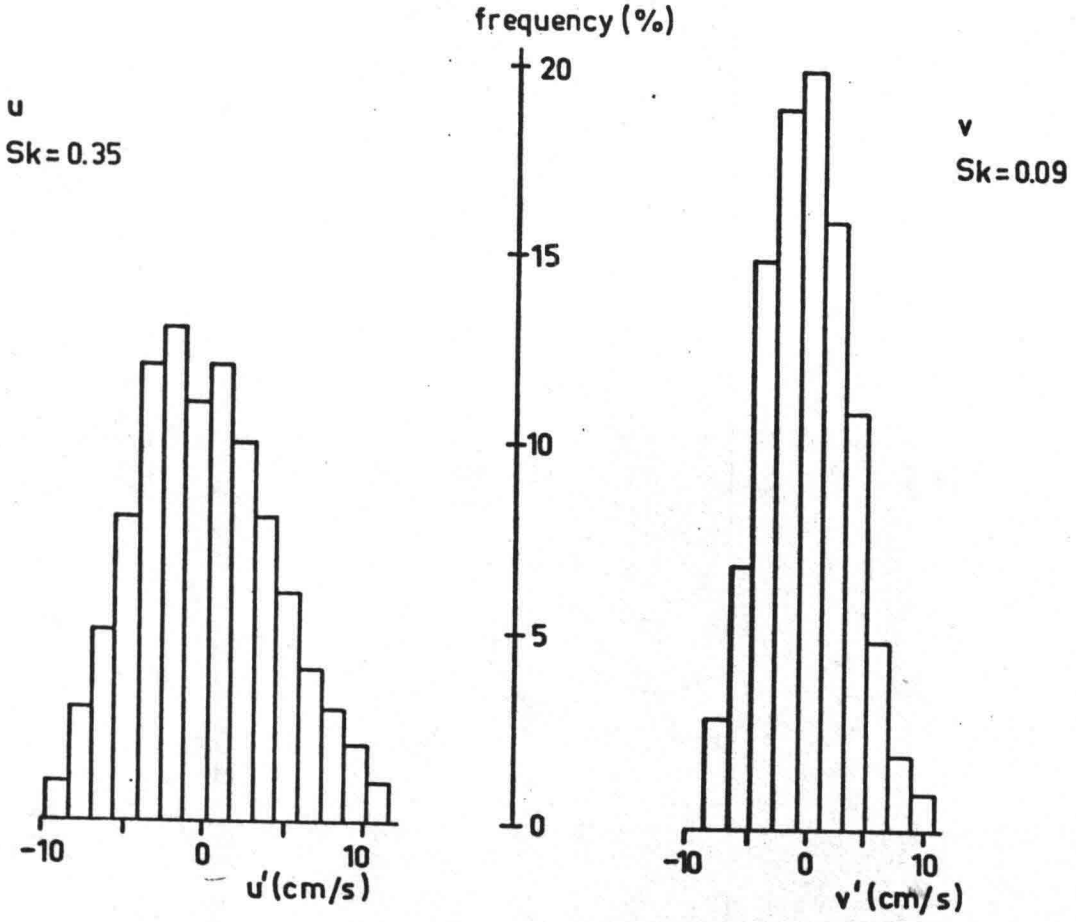

Fig. 4.67. Statistical distribution in point D 5/3 at time t_5 = 50 s.

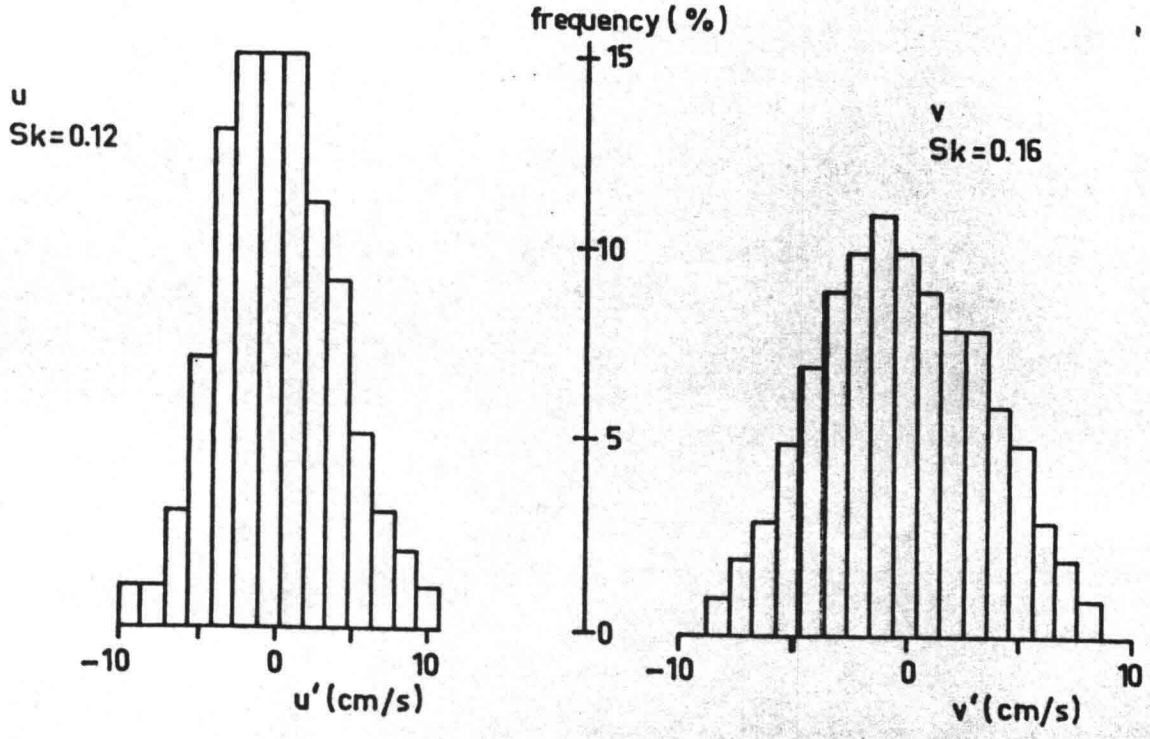

Fig. 4.68. Statistical distributions in point D 5/3 at time t_6 = 60 s.

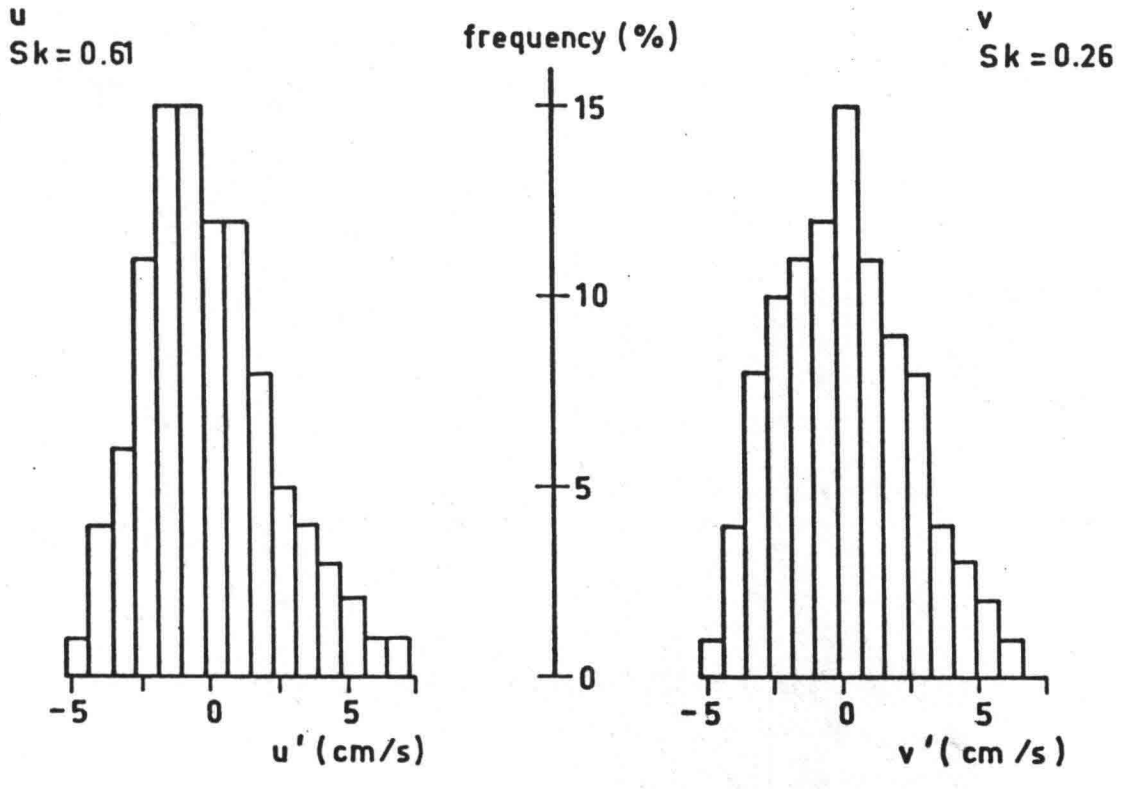

Fig. 4.69. Statistical distributions in point D 5/3 at time t_7 = 70 s.

5. Conclusions

- Separation of the flow takes place at the enlargement of the flow. At small flow rates this vortex is more stable during the development of the flow than at higher flow rates, when small vortices are observed inside the separation vortex. These vortices affect each other.
- The LDV measurements indicate that inertia forces influence all parameters of the turbulence.
- During the development of the separated flow turbulence was generated by the separation process and by boundary-layer instability. Downstream of the separation region boundary-layer turbulence is dominating. In the turbulent mixing layer between separation region and main flow coherent structures develop.
- This investigation should be continued by developing a mathematical model of the flow. Also further experiments would be useful to increase the understanding of the various transfer processes.

Acknowledgements

The writer expresses his gratitude to prof. M. de Vries for the possibility to stay in the Delft University of Technology, and to prof. dr. J.P.Th. Kalkwijk and dr. C. Kranenburg for the interesting research program in the Laboratory of Fluid Mechanics. Many thanks go to dr. Kranenburg for his help in preparing this report.
Several members of the University helped me during my stay. I would like to express my gratitude to S. de Boer and H. Klaasman for their help in the data processing, to A.W.J. van Rijswijk and A.M. den Toom for their help with the visualization experiments and to L.E.A. Calle for handling DAS and other equipment. I am thankful to Mrs. T. Capel for typewriting the report.

REFERENCES

1. AINOLA, L.J. KOPPEL, T.A. LIIV. U.R.
An investigation of turbulence generation and wall shear stress spectral analysis during unsteady flow in tubes.
XVIII Congress IAHR, Proc., vol.3, Cagliari, Italia, 1979, p. 165.
2. ATKINS, D.J. MASKELL, S.J. PATRICK. M.A.
Numerical prediction of separated flows.
Int. J. for Numerical Methods in Eng., vol.15, 1980, p. 129.
3. BEARMAN, P.W. GRAHAM, J.M.R.
Vortex shedding from bluff bodies in oscillatory flow:
A report on Euromech. 119.
J.F.M., v. 99, p. 2, 1980, p. 225.
4. BENDAT, J.S. PIERSOL, A.G.
Random data: analysis and measurement procedures.
Wiley - Interscience, 1971.
5. BERMAN, N.S. DUNNING, J.W.
Pipe flow measurements of turbulence and ambiguity using Laser-Doppler velocimetry. J.F.M. vol.61, p.2, 1973, p. 289.
6. BERNARDINIS, B. de. GRAHAM, J.M.R. PARKER, K.H.
Oscillatory flow around disks and through orifices.
J.F.M., v. 102, 1981, p. 279.
7. BIEN, F. PENNER, S.S.
Phys. of Fluids, v.13, 1970.
8. BOER, S. de
Private communication, 1981.
9. BONARD, R. CONTANCEAU, M.
The early stage of development of the wake behind an impulsively started cylinder for $40 < Re < to^4$,
J.F.M., v. 101, p. 3, 1980, p. 583.
10. BUCHHAVE, P.
Transducer techniques. DFC - 78, p.427.
11. CHATTERTON, N.E. et al.
Two-dimensional Laser-Doppler velocimetry in turbulent flows. Proc. of Symposium on Turbulence Measurement in Liquids, University of Missouri-Rolla, sept. 1969.
12 CHERDRON, W. DURST, F. WHITELAW, J.H.
Asymetric flows and instabilities in symmetric ducts with sudden expansions.
J.F.M., vol. 84, p. 1, 1978, p.13.
13. DISSELHORST, T.H.M. WIJNGAARDEN, L. van
Oscillatory flow around the edge of a flat plate.
J. Eng. Math., v. 13, p.3, 1979, p. 271.
14. DURST, F. MELLING, A. WHITELAW, J.H.
Principles and practices of Laser-Doppler anemotery,
Academic Press, 1976.
15. EDWARDS, R.V. ANGUS, J.C. MORROW, D.L.
Flow measurements with Doppler shifted laser light.
Advances in Instrumentation, v.23, ISA-Conference, p. 868.
16. ETHERIDGE, D.W. KEMP, P.H.
Measurements of turbulent flow downstream of a rearward-facing step.
J.F.M. v. 86, p. 3, 1978, p. 545.

17. FALCO, R.E.
Combined simultaneous flow visualization/hot-wire anemometry for the study of turbulent flows.
Trans. ASME, J.F. Eng., v. 102, no. 2, 1980, p. 174.
18. Flow visualization. International symposium, Tokyo, oct. 1977, proc., ed: Tsuyoshi Asanuma. Washington, Hemisphere, 1979, 413 p.
Series in thermal and fluids engineering.
19. FRIEHE, C.A.
Vortex shedding from cylinder at low Reynolds numbers.
J.F.M., v. 100, p.2, 1980, p. 237.
20. GEORGE, W.K.
Limitations on the measurement of unsteady flow velocities with a Laser-Doppler velocimeter, DISA Conference Proceedings, Leicester, 1972.
21. GODEFROY, H.W.H.E.
Application of the Laser-Doppler velocity measurements method in open and closed conduits. Flomeko 1978.
22. GOLOVKIN, V.A. GOLOVKIN, M.A.
Numerical solution for unsteady separated inviscid incompressible flow past an arbitrary body.
Sixth Int. Conf. Numerical Methods in Fluid Dynamics, Tbilisi, 1978.
Berlin, Springer, 1979, lect.notes in Physics no. 90, p. 254.
23. GRAHAM, T.M.R.
The forces on sharp-edged cylinders in oscillating flow at low Keulegan-Carpenter numbers.
J.F.M. v. 97, p. 2, 1980, p. 331.
24. GRASS, A.J.
Structural features of turbulent flow over smooth and rough boundaries.
J.F.M., v. 50, p.2, 1971, p. 233.
25. HUSSAIN, A.K.M. CLARK, A.R.
On the coherent structure of the axi-symmetric mixing layer: a flow-visualization study.
J.F.M., v.104, 1981, p. 263.
26. IBRAGIMOV, M.H. et al.
Structure of the turbulent flow and heat-transfer mechanism in channels.
Moscow, 1978. (In Russian).
27. JÖNSSON , L.
Laser velocity meter for water flow.
Institution för vattenbyggand. Tekniska Högskolan i Lund.
Bulletin Series A nr. 32, Lund 1974.
28. KARAHAN, M.E. PETERSON, A.W.
Visualization of separation over sand waves.
J. of the Hydr. Div., ASCE, HY8, 1980, p. 1345.
29. KIM, J. KLINE, S.J. JOHNSTON, J.P.
Investigation of a reattaching turbulent shear layer:
Flow over a backward facing step.
Trans. ASME, J.F. Eng., v. 102, no. 3, 1980, p. 302.
30. KOPPEL, T.A. LIIV, U.R.
An experimental investigation of starting of the flow in pipes.
Mechanics of Fluids and Gases, Proc. of Academy of Science of U.S.S.R., No. 6, 1977, p. 79 (In Russian).
31. KOROMILAS, C.A. TELIONIS, D.P.
Unsteady laminar separation: an experimental study.
J.F.M. , v. 97, p. 2, 1980, p. 347.

32. KOVASZNAY, L.S.G.
Measurement in intermittent and periodic flow.
DFC-78, p. 133.
33. LAKSHMANA GOWDA, B.H. ASWATHA NARAYANA, P.A.
An experimental investigation of separating flow on a convex surface.
Appl. Sci. Res., v. 36, no. 4, 1980, p. 271.
34. LEE, L.H.J. CLARU, J.A.
Flow visualization in complex turbulent flows.
Proc. ASCE, J. Hydr. Div., v.106, 1980, p. 247.
35. MULLIN, T. GREATED, C.A. GRANT, J.
Pulsating flow over a step.
Phys. of Fluid, v. 34, no. 4, 1980, p. 669.
36. ORLOFF, K.L.
Laser Doppler anemometer diagnostics in unsteady flow.
DFC-78, p. 514.
37. Proceedings of the Dynamic Flow Conference 1978.
Dynamic Measurements in Unsteady Flows. Sijthoff & Noordhoff, 1979.
38. PULLIN, D.I. PERRY, A.E.
Some flow visualization experiments on the starting vortex.
J.F.M., vol. 97, p. 2, 1980, p. 239.
39. RESTIVO, A. WHITELAW, J.H.
Turbulent characteristics of the flow downstream of a symmetric, plane sudden expansion.
Trans. ASME, ser. I, J. Fluids Eng., v. 100, no. 3, 1978, p. 308.
40. REYNOLDS, A.J.
Turbulent flows in engineering.
John Wiley and Sons, 1974.
41. TA PHUOC LOC
Numerical analysis of unsteady secondary vortices generated by an impulsively started circular cylinder.
J.F.M., v. 100, p. 1, 1980, p. 111.
42. TAYLOR, G.I.
The statistical theory of isotropic turbulence.
J. Aeronaut. Sci, v. 4, no. 8, 1937, p. 311.
43. THOMSON, H.D. STEVENSON, W.H. (eds.)
Laser velocimetry and particle sizing.
Hemisphere Publ. Corp., 1979.
44. TPD. Beschrijving van de Laser Doppler Snelheidsmeter.
Rapport, 1977.
45. VEN TE CHOW
Open channel hydraulics.
International student edition, 1959.